LIPID-PROTEIN INTERACTIONS AT INTERFACES

- Many functions crucial to life are carried out by membrane proteins bound to or embedded in lipid bilayers
- A wide variety of diseases results from deficient or abnormal lipid-protein interactions

Interface between biological and physical sciences

elucidate the normal functions of these proteins
mechanism by which toxicity is introduced in disease

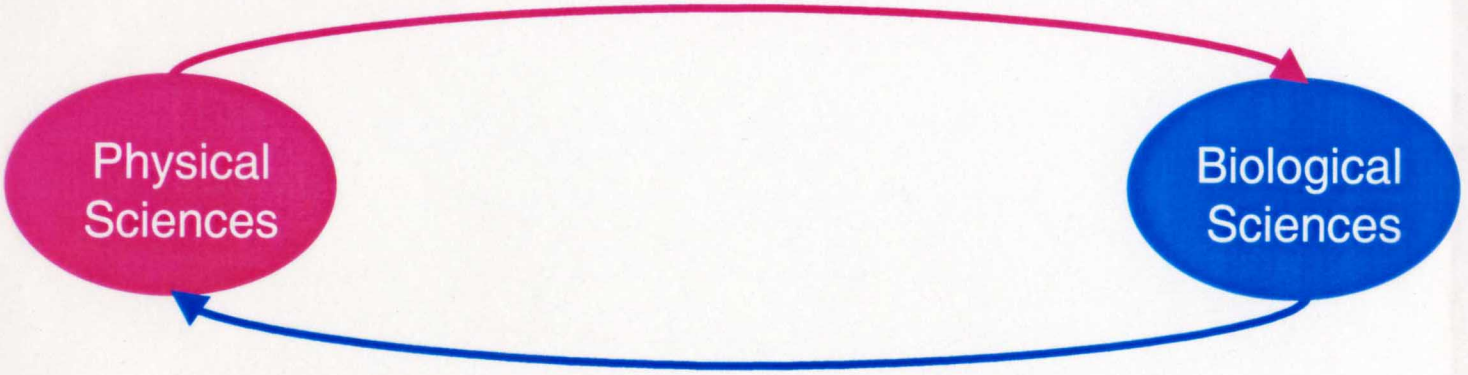

uncover and understand new physical phenomena
basis for new materials

LOSS OF MEMBRANE STRUCTURAL INTEGRITY

Electrically shocked cells suffer a loss of structural integrity.

Electrically shocked cell

COPOLYMER SURFACTANT AS MEMBRANE SEALANT

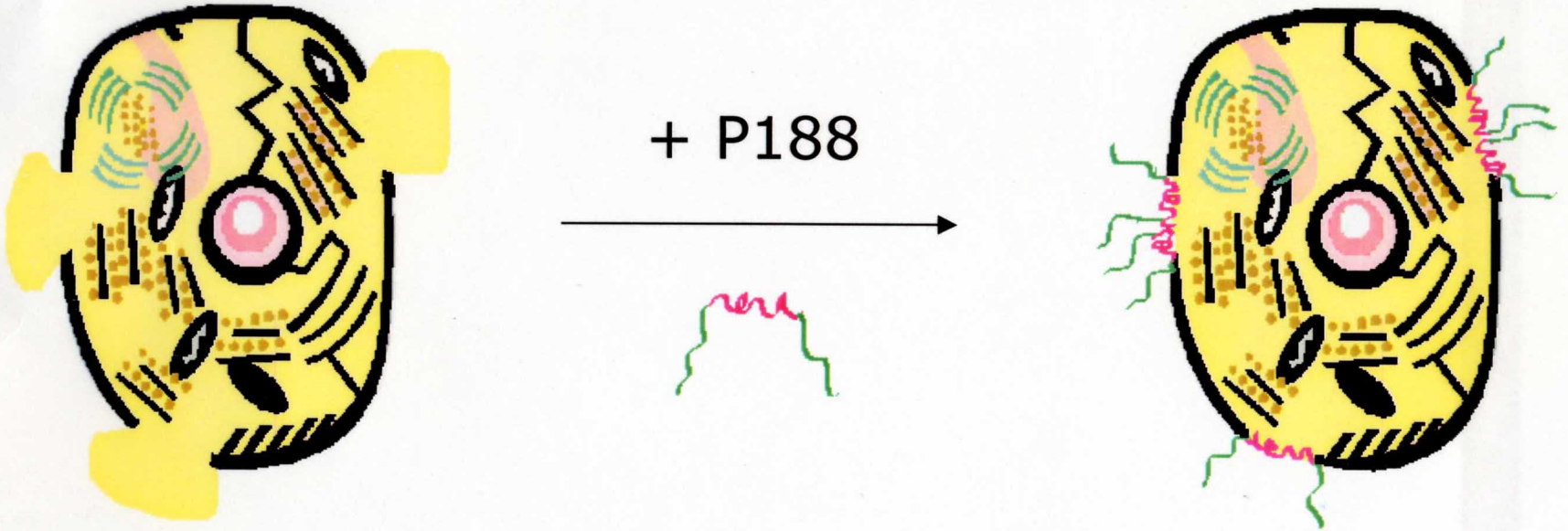

Lee, R.C.; River, L.P.; Pan, F.; Ji, L.; Wollmann, R. L. Proc. Natl. Acad. Sci. USA May 1992, 89, 4524-4528.

QUESTIONS TO BE ADDRESSED

- How does P188 interact with the cell membrane?
- Does P188 insertion affect membrane morphology?
- Is the sealing effect localized?
- What happens to the polymer as the cell heals?
- Effective treatment strategies? Designer polymers?

- How membrane packing regulates P188 insertion
- How lipid electrostatics influence P188 insertion
- Morphological changes using FM
- High resolution imaging using AFM

Lipid monolayers as models for outer leaflet of bilayer

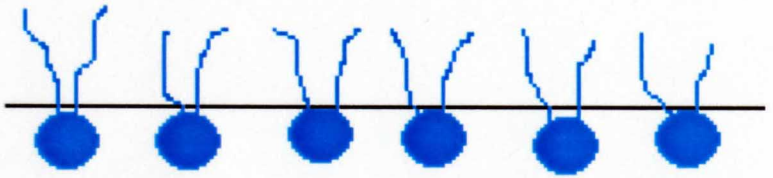

Lipid monolayer
at air-water interface

TRIBLOCK COPOLYMER P188

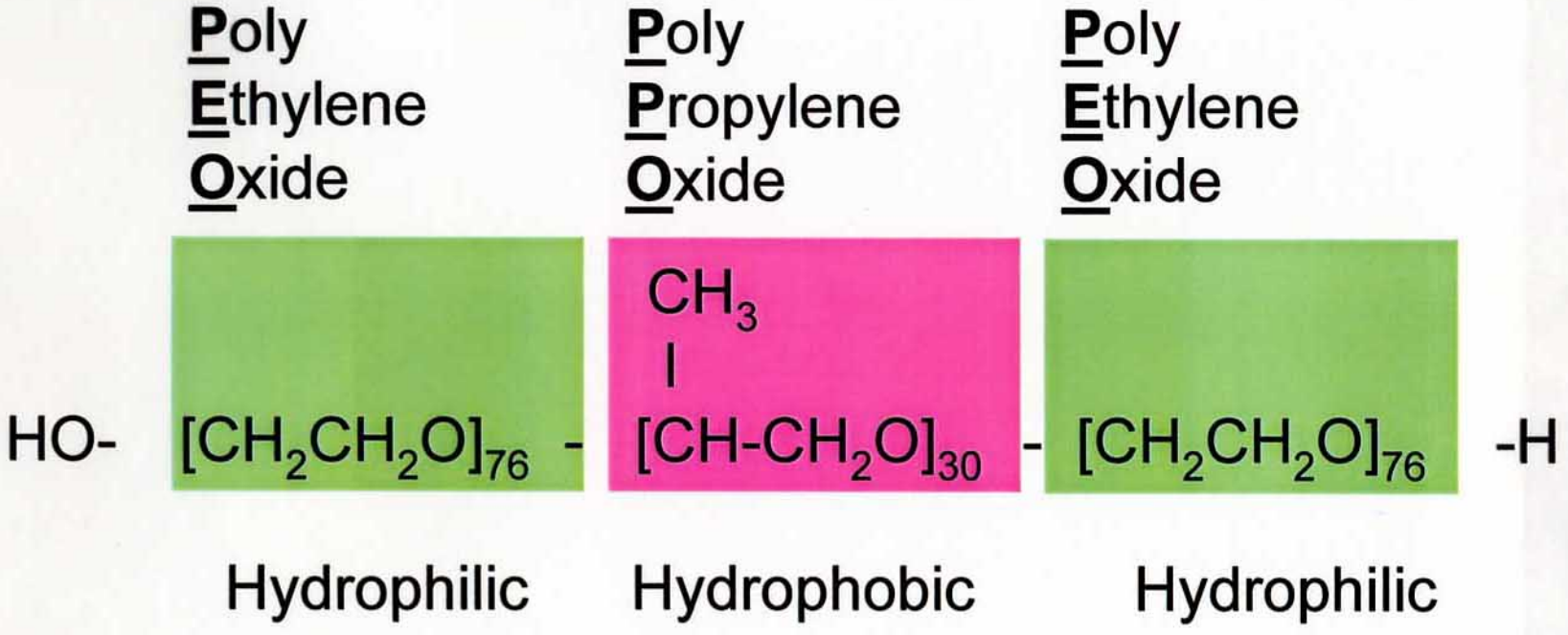

INJECTION EXPERIMENTS

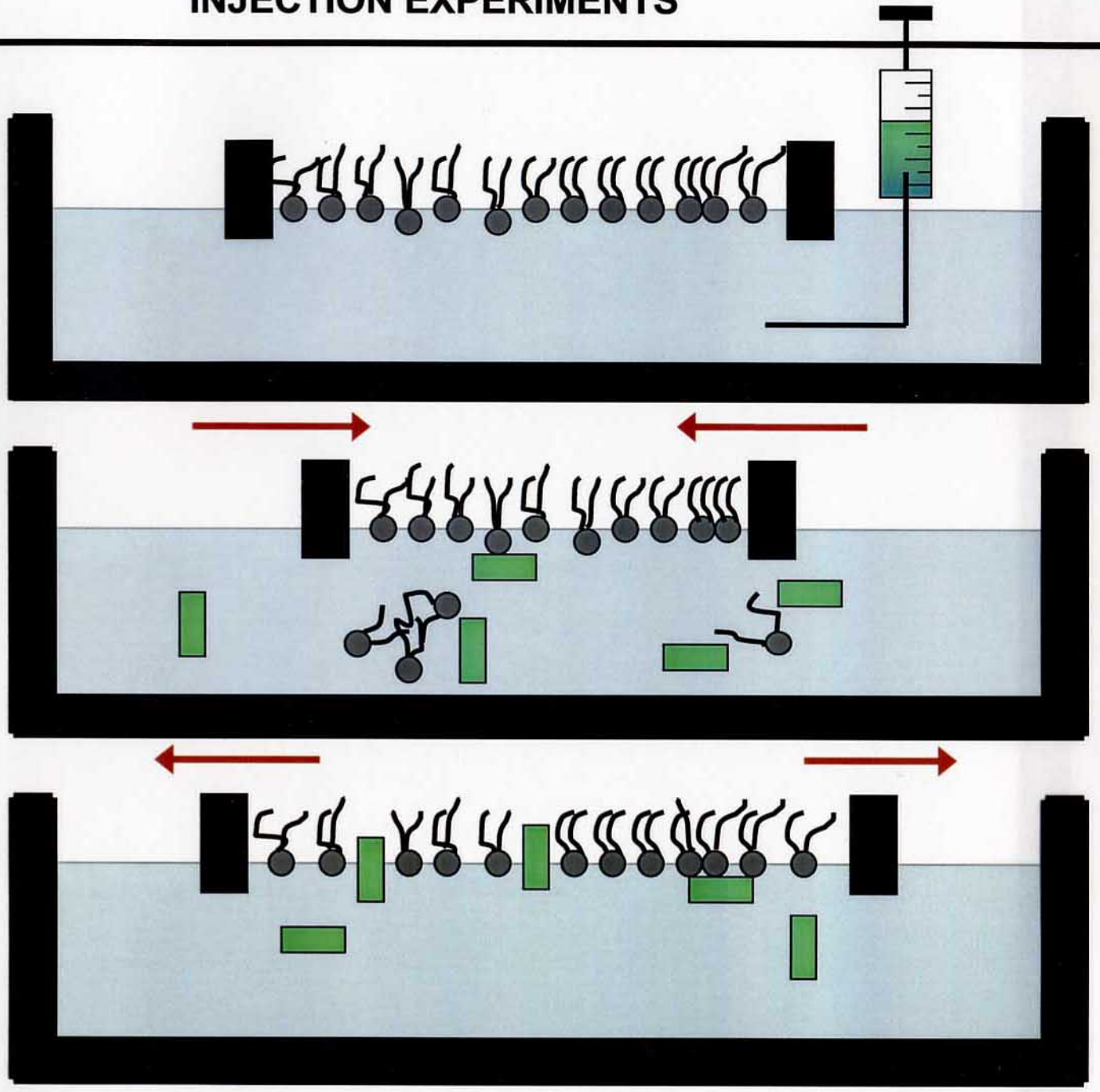

P188 INSERTION REGULATED BY LIPID PACKING DENSITY

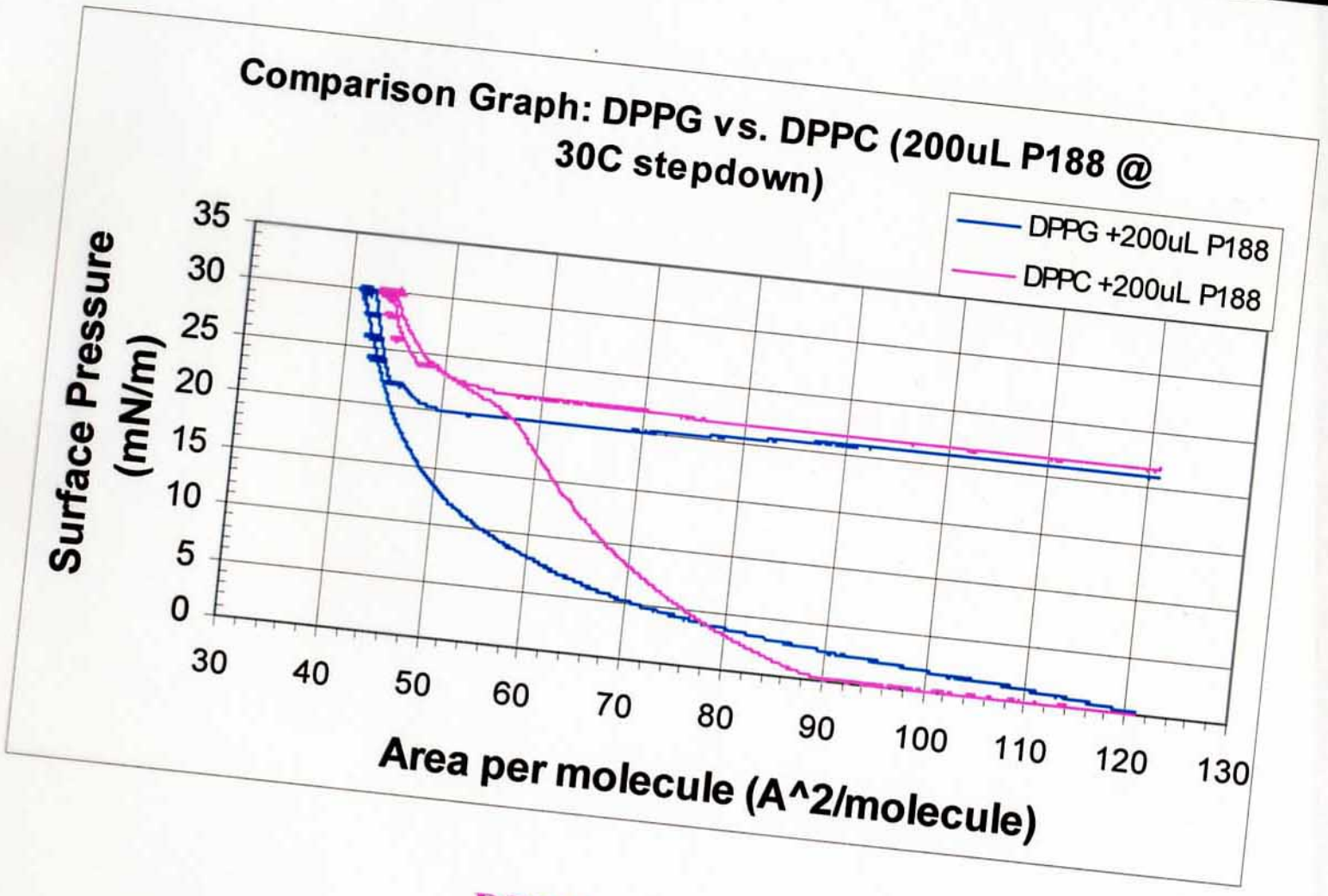

DPPC + P188

DPPG + P188

P188 INSERTION INTO DPPG MONOLAYERS

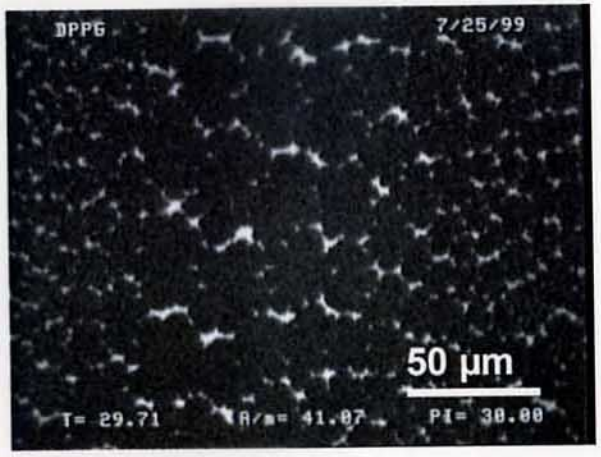

Pure **DPPG** at 30 mN/m
before P188 injection

DPPG + P188 at 20 mN/m
Area/ PG molecule = 78 $Å^2$

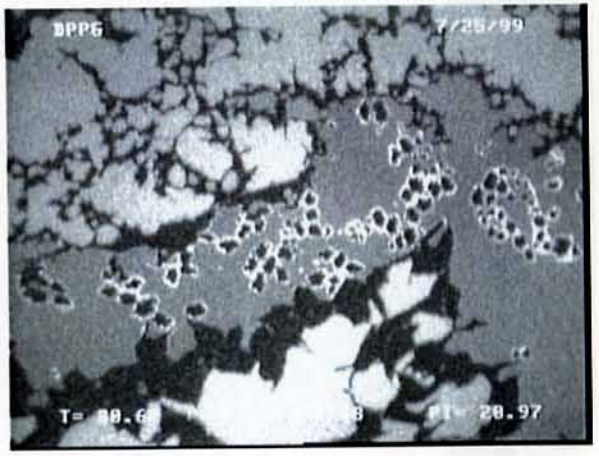

DPPG + P188 at 20 mN/m
Area/ PG molecule=120 $Å^2$

PRETREATMENT EXPERIMENTS WITH DPPG MONOLAYERS

P188 is added before the lipid monolayer is compressed

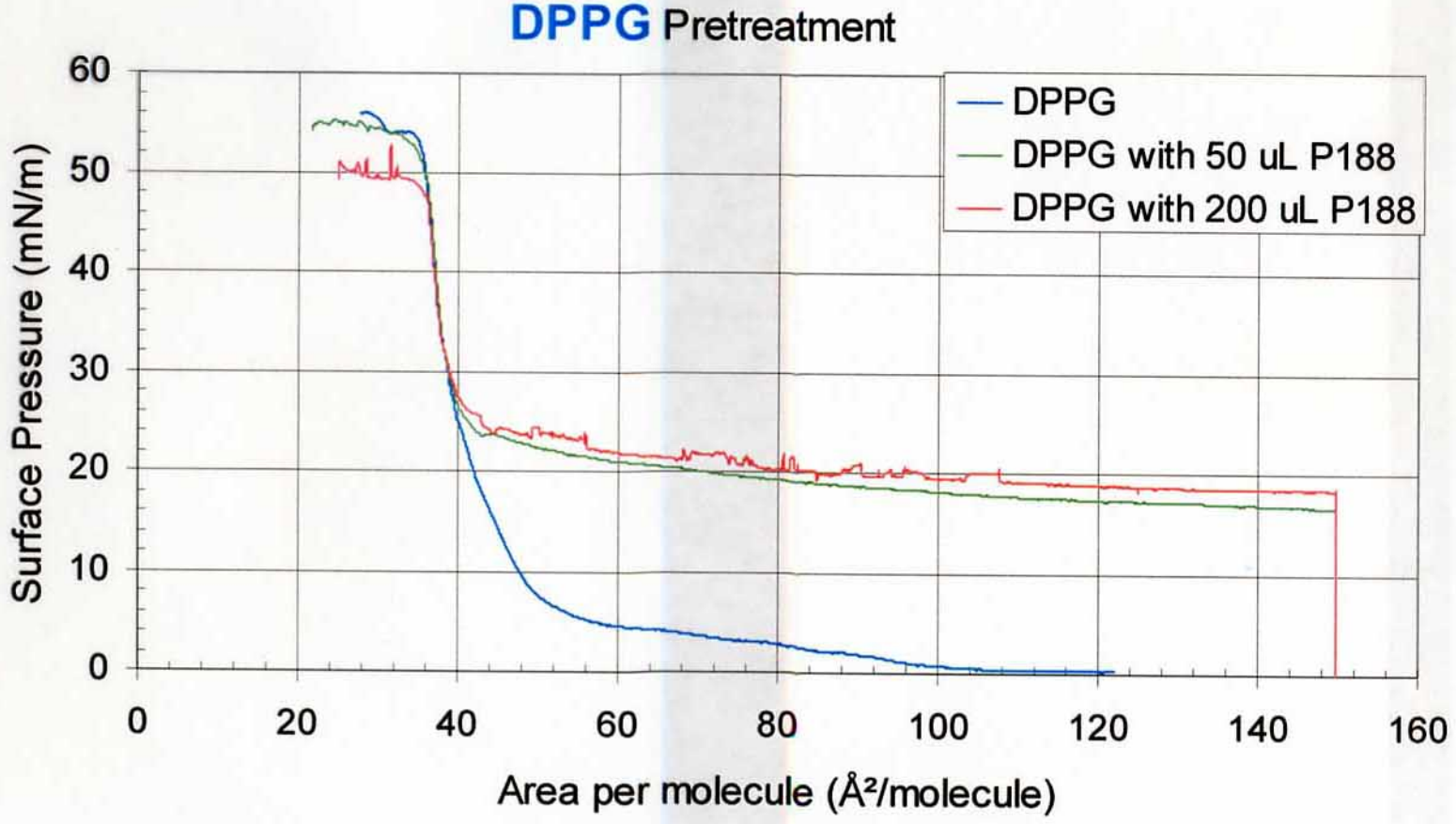

Biophys. J., submitted

EFFECT OF INCREASED MOLECULAR WEIGHT

Poloxamer 238 (P238)

Same Hydrophobic (20% PPO): Hydrophilic (80% PEO) weight ratio as P188

MW (P238) = 10,600 g/mol

MW (P188) = 8400 g/mol

P238 INJECTED INTO DPPC AND DPPG MONOLAYERS AT 30 mN/m

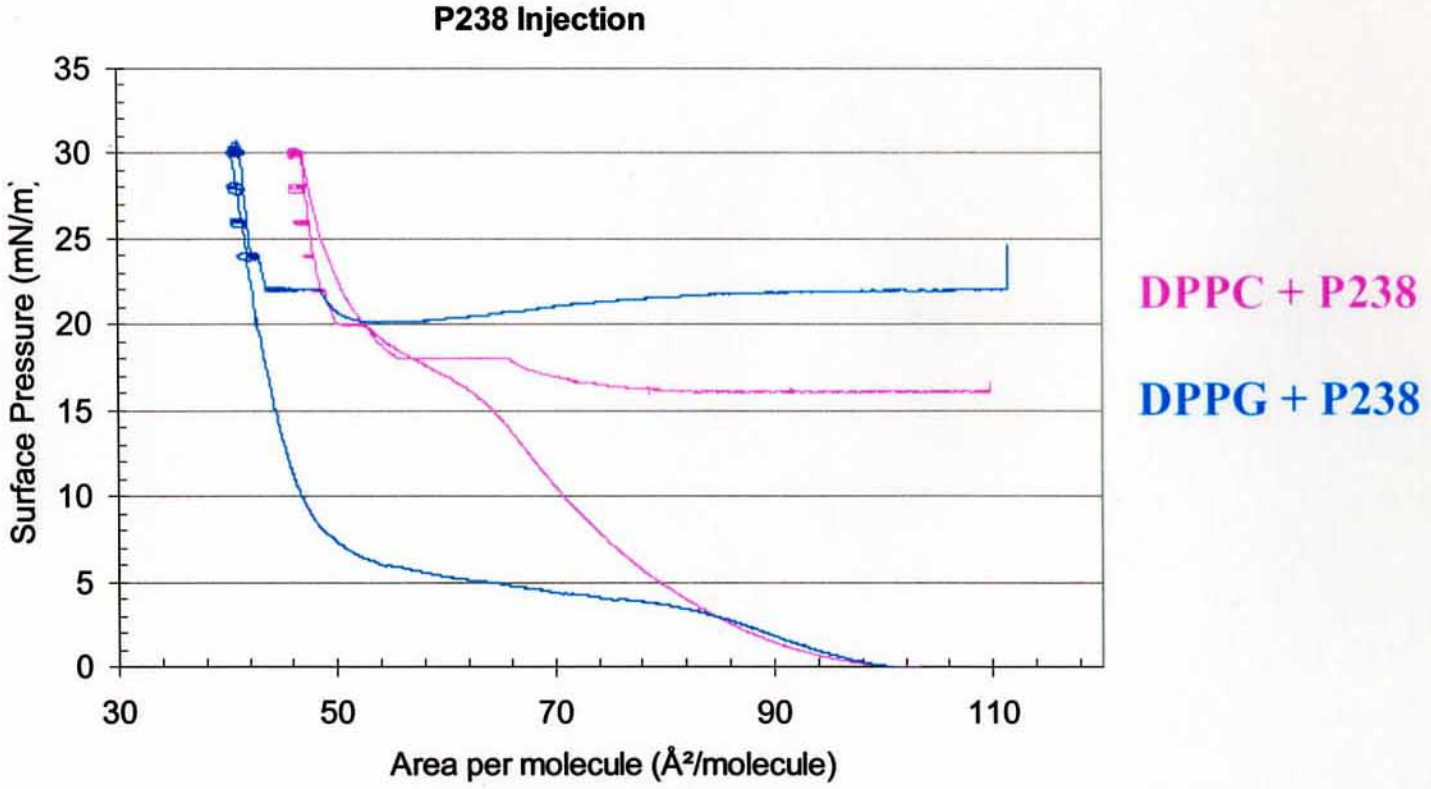

PRETREATMENT EXPERIMENTS WITH DPPC MONOLAYERS

P188 is added before the lipid monolayer is compressed

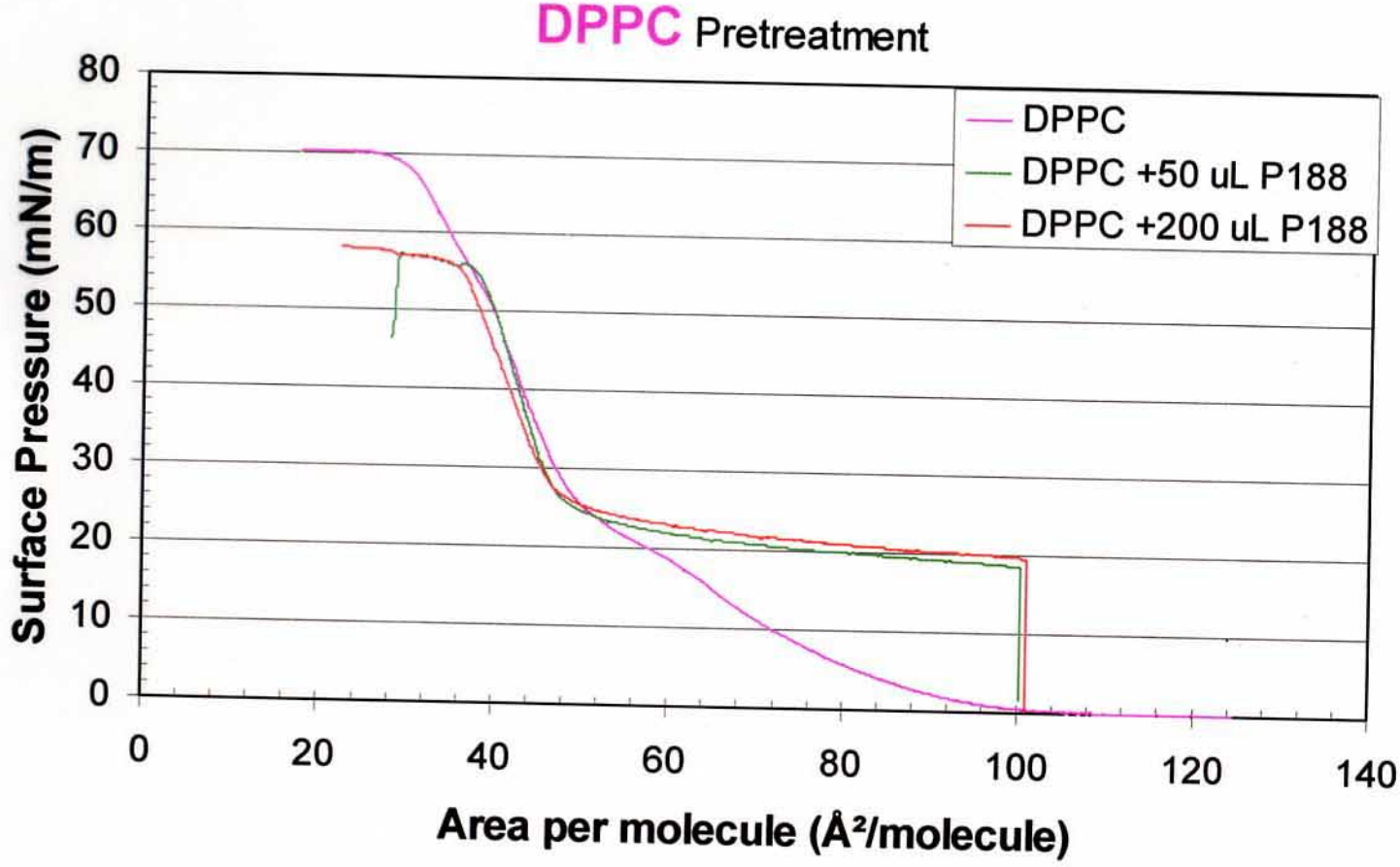

Poloxamer 338 (P338)

Same Hydrophobic (20% PPO): Hydrophilic (80% PEO) weight ratio as P188

MW (P338) = 14,100 g/mol

MW (P188) = 8400 g/mol

P338 INJECTED INTO DPPC AND DPPG MONOLAYERS AT 30 mN/m

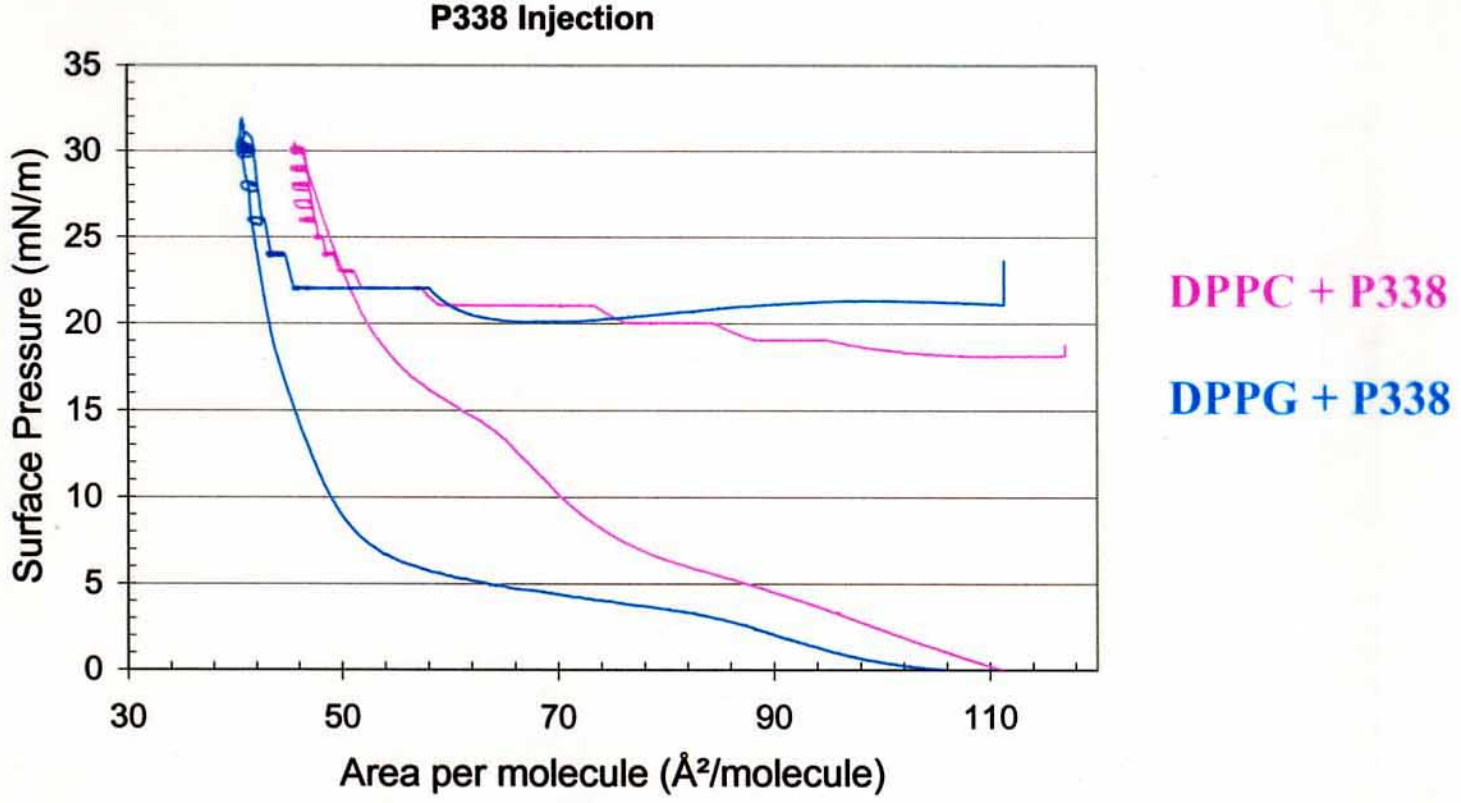

EFFECT OF INCREASED HYDROPHOBICITY

Poloxamer 217 (P217)

<u>P217 weight percentages</u>
30 % PPO (hydrophobic)
70 % PEO (hydrophilic)

versus

<u>P188 weight percentages</u>
20 % PPO (hydrophobic)
80 % PEO (hydrophilic)

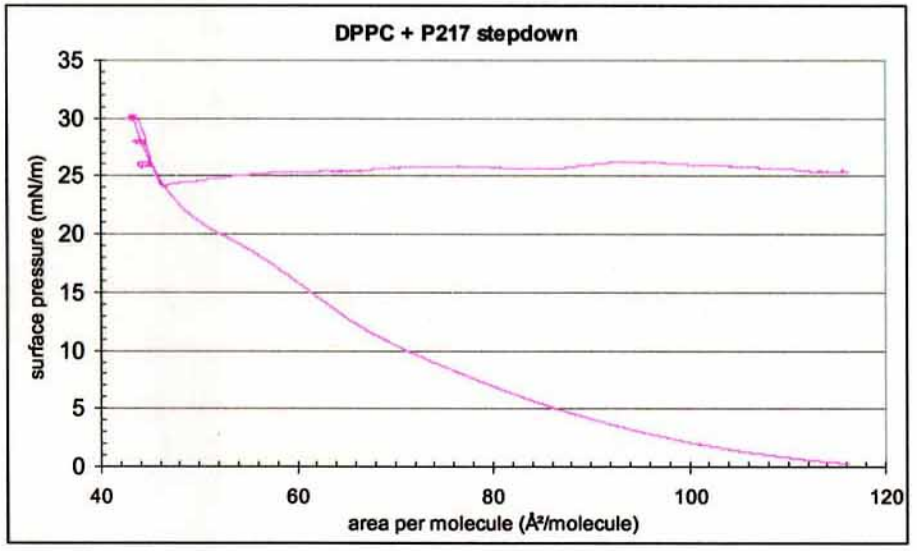

DPPC + P217 Stepdown at 30°C

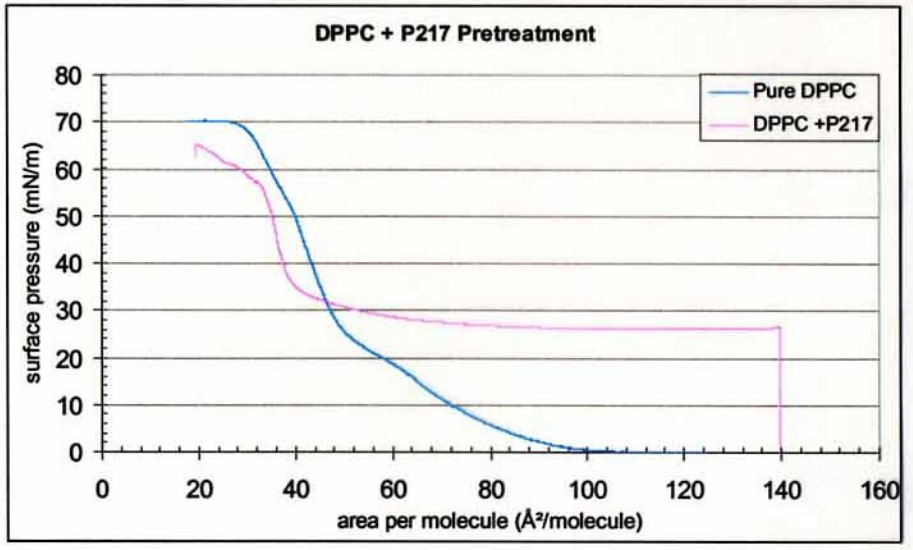

DPPC + P217 Pretreatment at 30°C

DEPOSITION OF MONOLAYERS ONTO SOLID SUBSTRATES

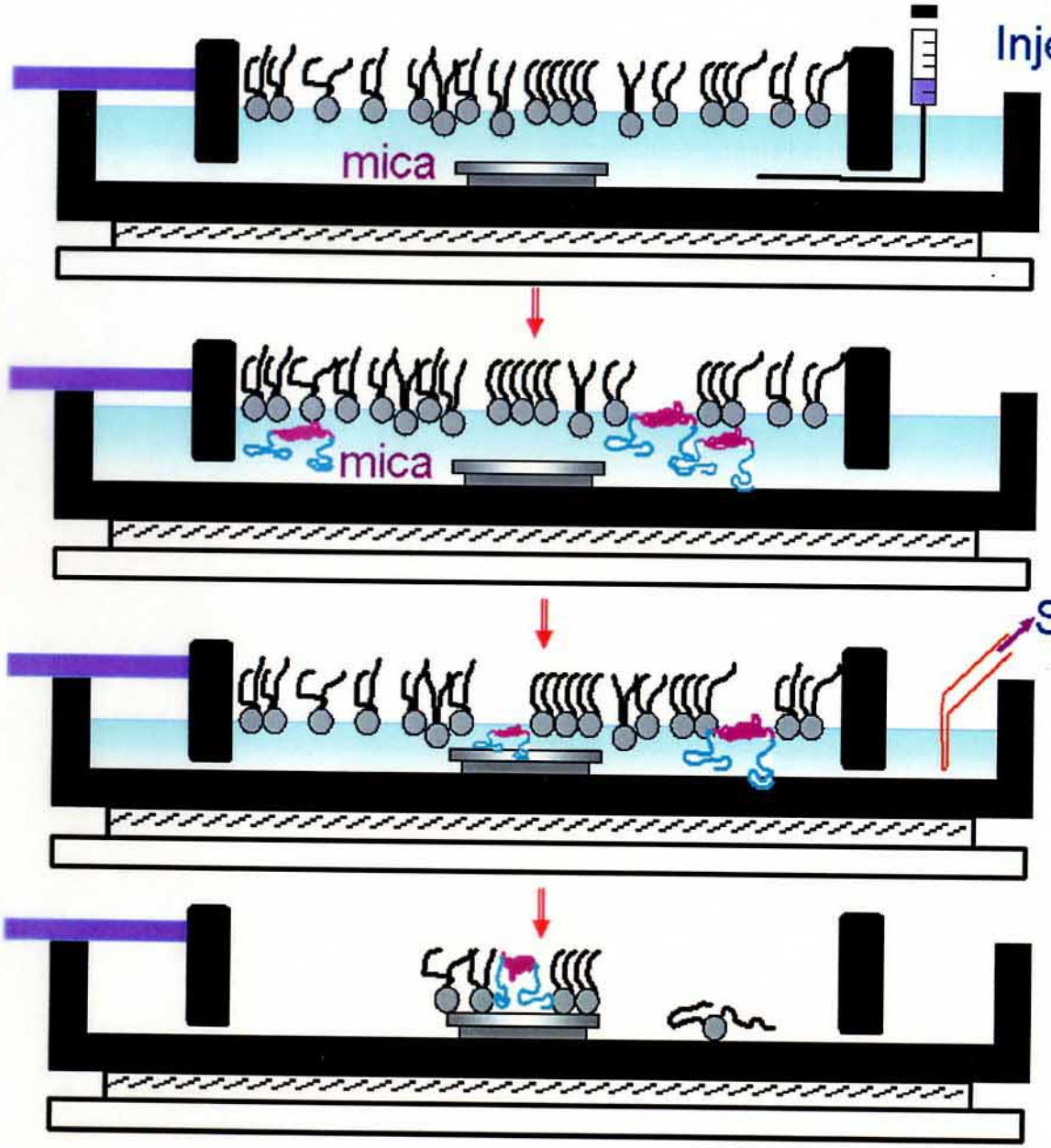

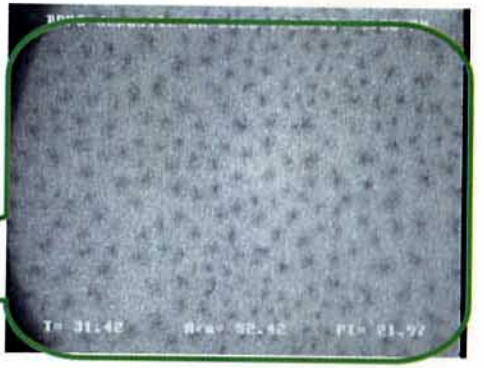

Before deposition

After Deposition

AFM HEIGHT IMAGES - SUPPORTED DPPC FILM AT 24 mN/m

π = 24 mN/m

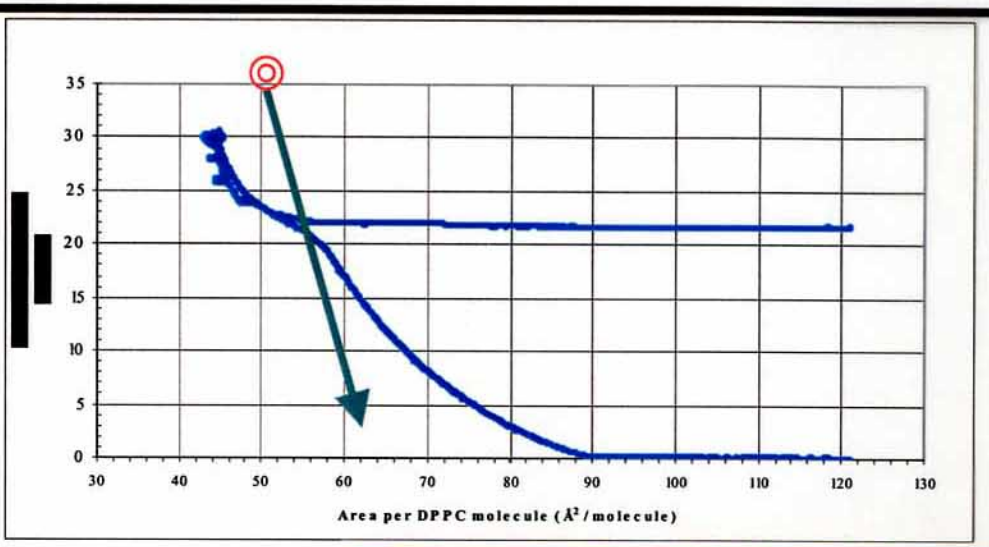

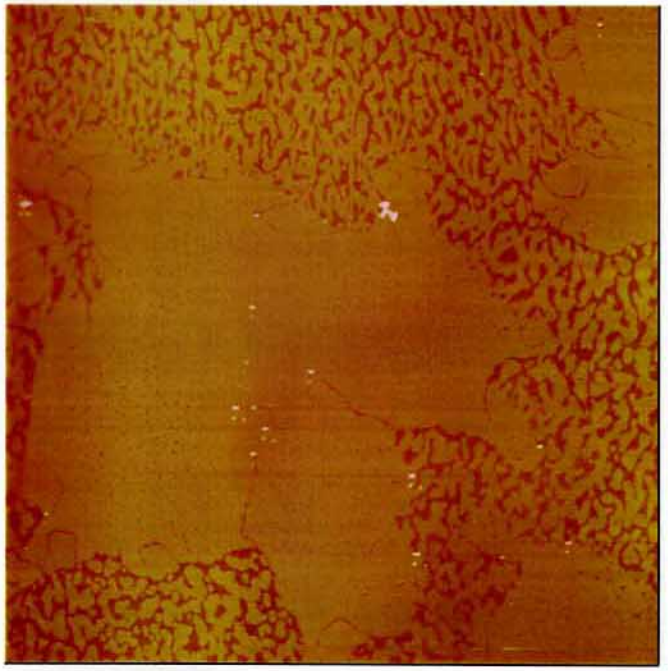

DPPC 15 µm

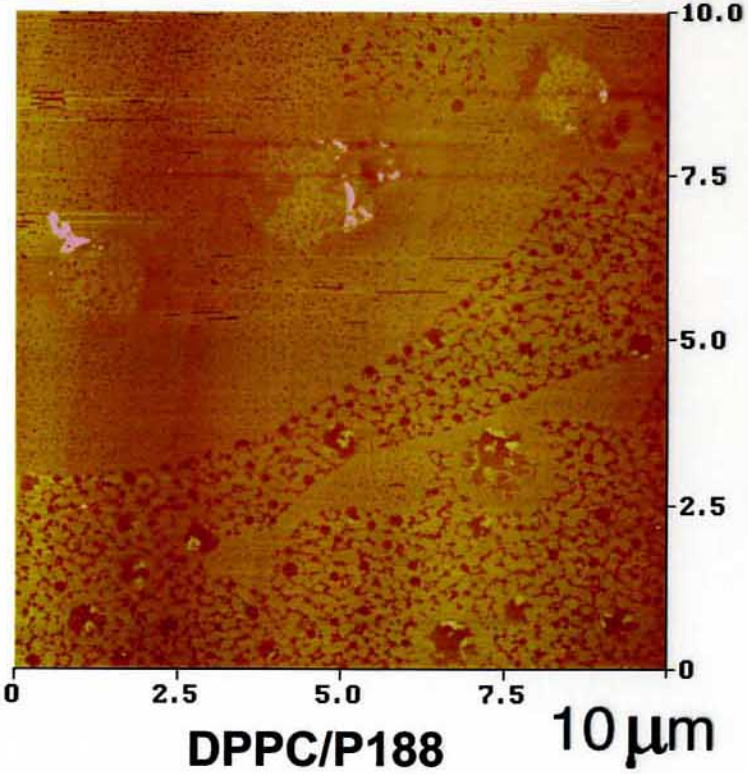

DPPC/P188 10 µm

AFM HEIGHT IMAGES - SUPPORTED DPPC FILM AT 22 and 20 mN/m

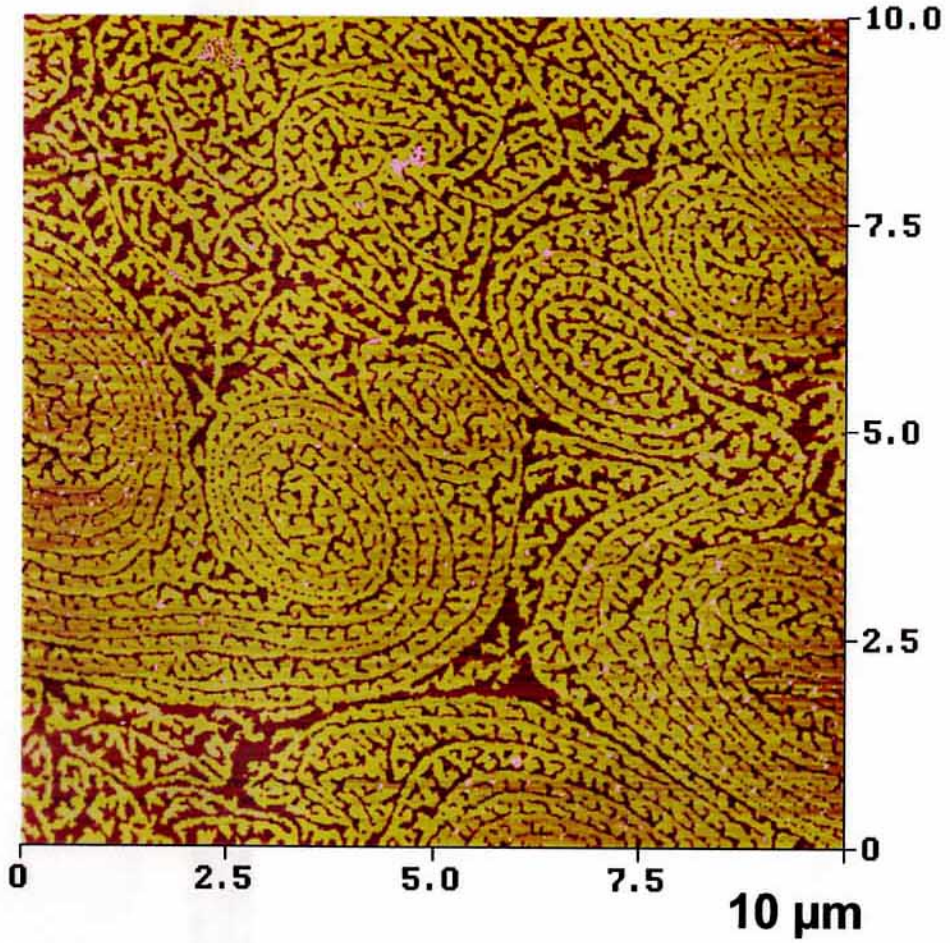

DPPC/P188
π = 22 mN/m

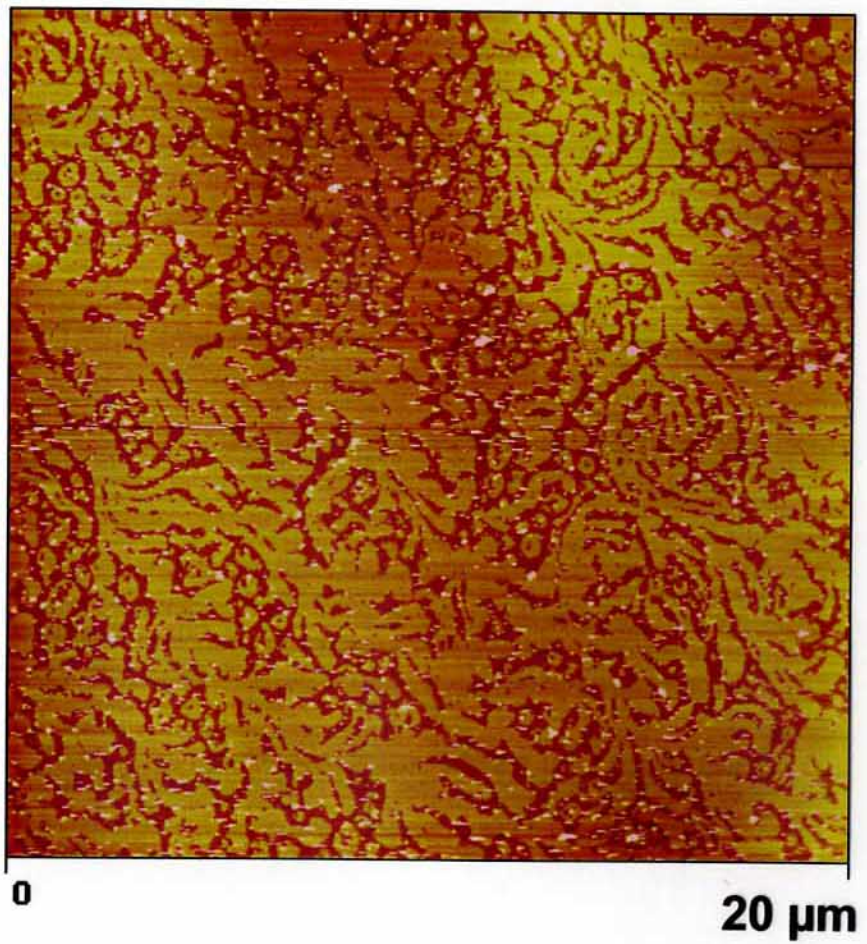

DPPC/P188
π = 20 mN/m

AFM HEIGHT IMAGES OF SUPPORTED P188

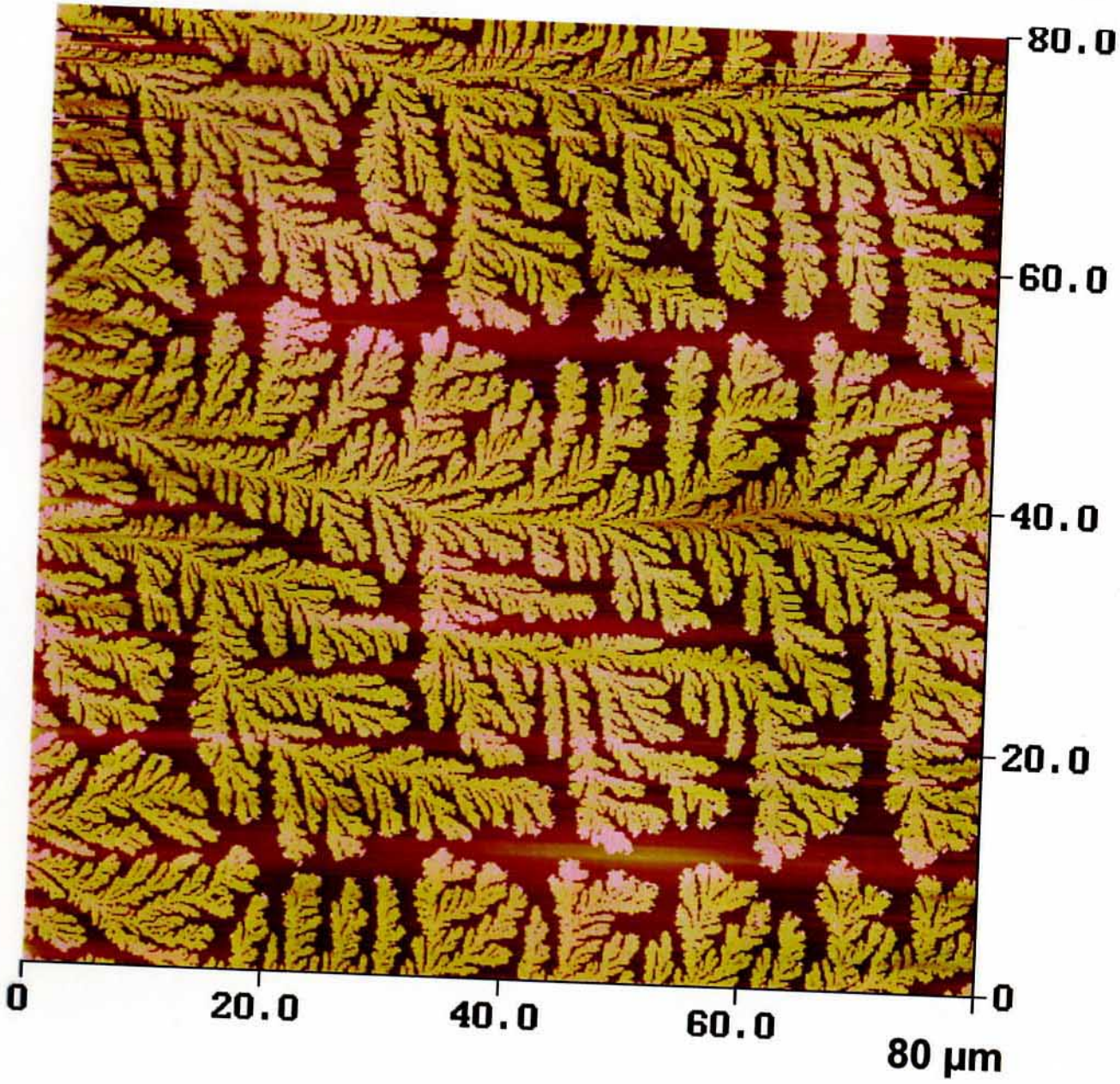

PHASE MODE OF AFM

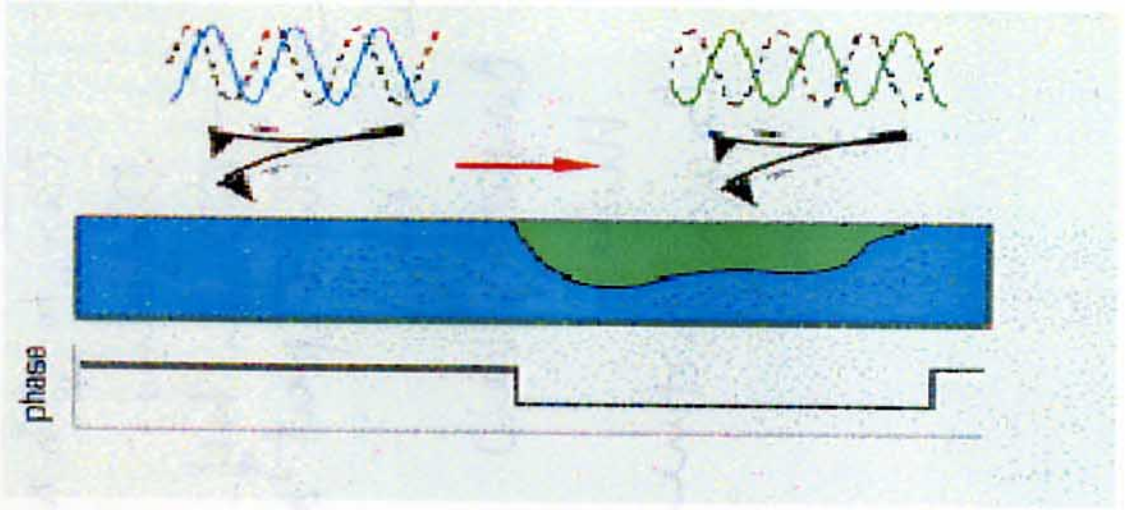

A_o: the amplitude of freely oscillating cantilever
A_{sp}: the set amplitude used for feedback control

Light tapping
(A_o small)

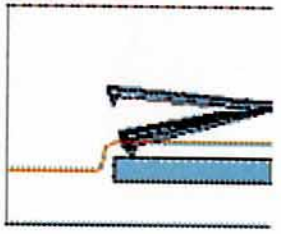

Hard tapping
(A_o large)

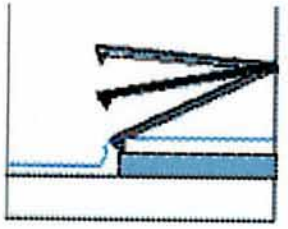

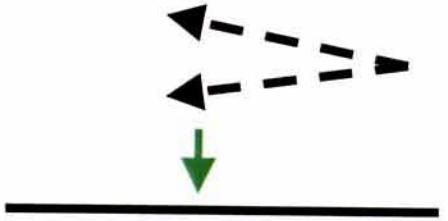

Attractive
Tip-sample interaction

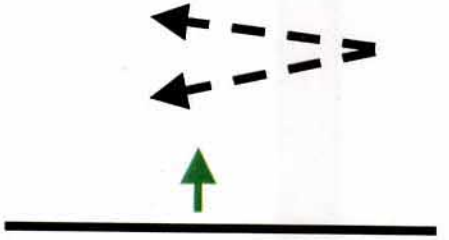

Repulsive
Tip-sample interaction

AFM DEMONSTRATES TWO SPECIES PRESENT ON SUPPORT

Light tapping
(Asp = 14 nm
Ao = 18 nm)

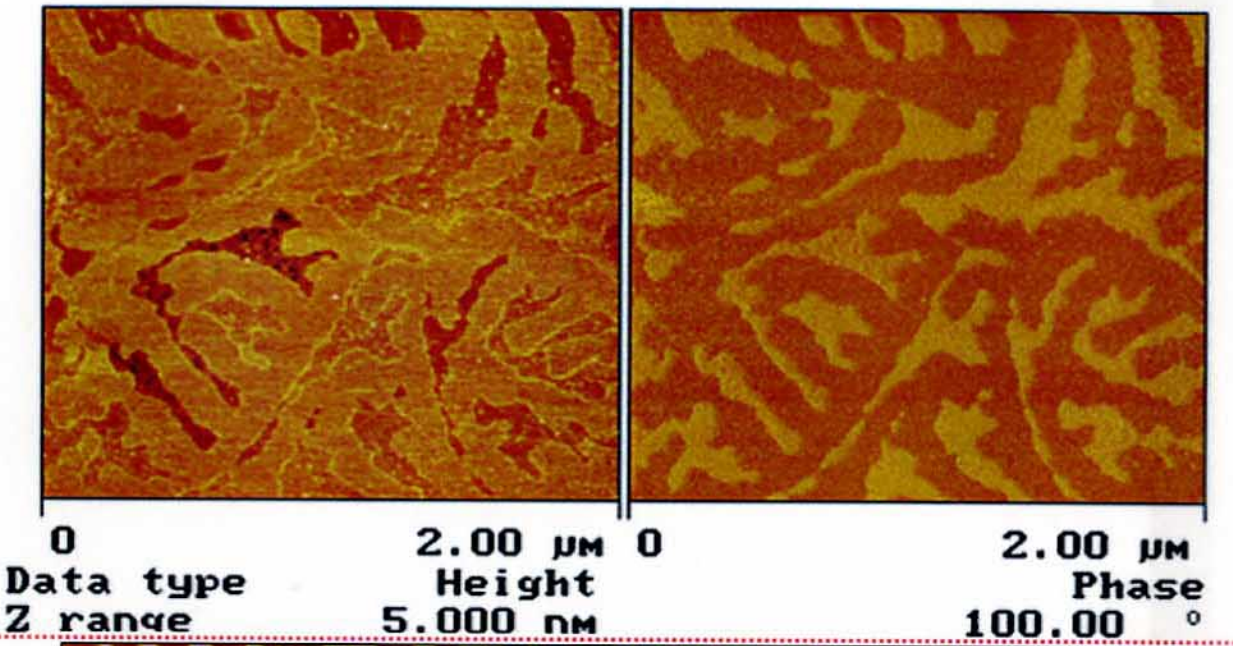

Hard tapping
(Asp = 40 nm
Ao = 53 nm)

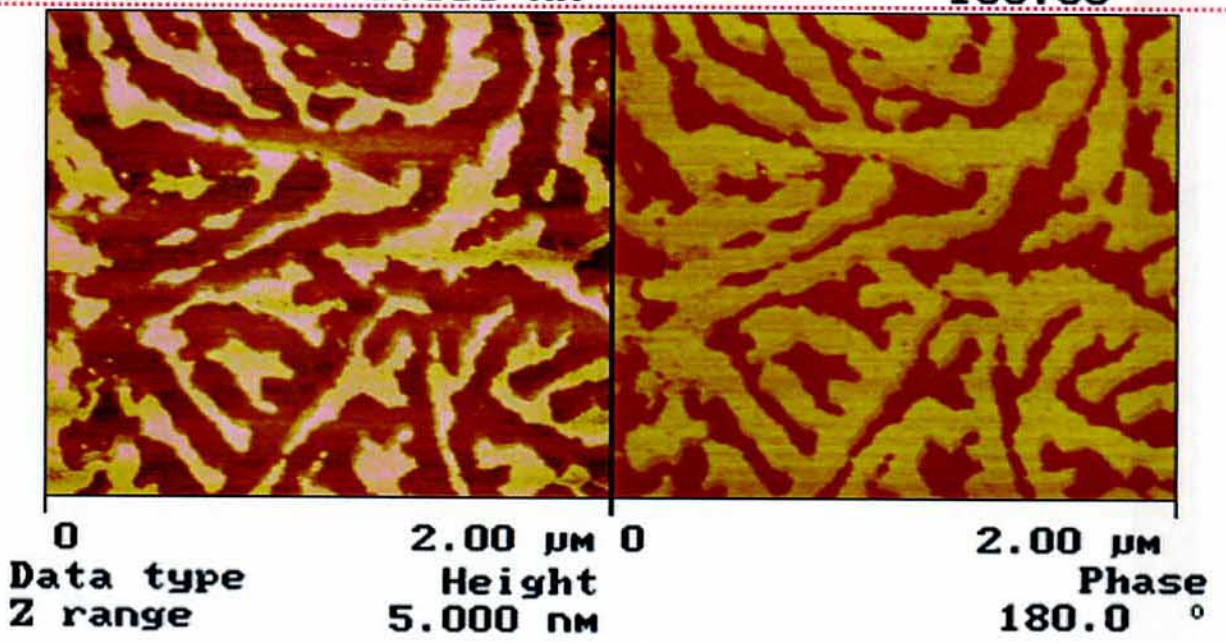

DPPC+P188
@ 20 mN/m, 30°C

CONCLUSIONS

- P188 will only adsorb into damaged regions of cells
- P188 insertion insensitive to headgroup charge
- P188 is "squeezed out" when cell heals
- AFM can identify to location of the polymer
- Insertion of P188 results in interesting morphology

ALZHEIMER'S DISEASE (AD)

- Clinical dementia consistent with AD has long been known

- Bavarian psychiatrist Alois Alzheimer (1906) called attention to

  -> neurofibrillary tanglements
  (altered form of the neuronal microtubule protein, tau)

  -> senile plaques
  (spherical deposits of extracellular amyloid β-protein)

  -> vascular deposits
  (Aβ)

- Sequence

  Glenner & Wong, *Biochem. Biophys. Res. Comm.* (1984) **120**: 885-890
  Masters *et al.*, *Proc. Nat'l. Acad. Sci. USA* (1985) **82**: 4245-4249

- Gene encoding the amyloid precursor protein (βAPP)

  Kang *et al.*, *Nature* (1987) **325**: 733-736

AMYLOID-BETA (Aβ) PROTEIN

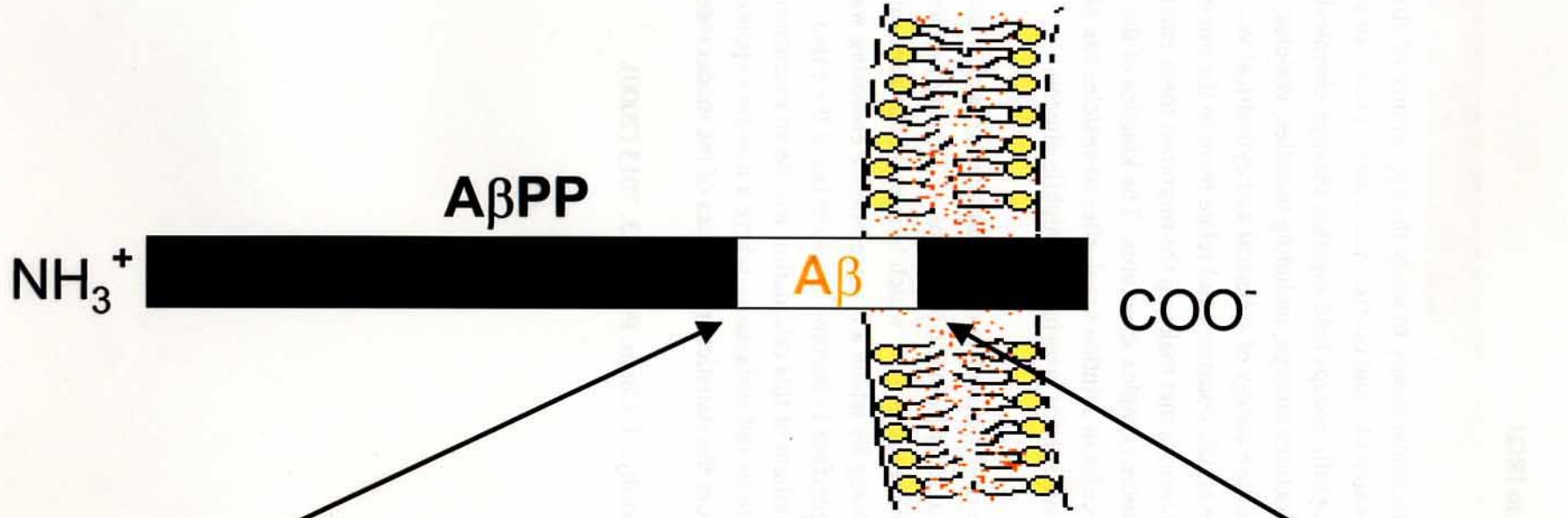

DAEFRHDSGYEVHHQKLVFFAEDVGSNKGAIIGLMVGGVVIA

\- - + + - - + + + - - + blue: charged red: hydrophobic

Self-Perpetuating Change in Protein Conformation

- A mechanism of disease

  Alzheimer's Disease Aβ,
  Huntington's Disease, Parkinson's Disease,
  Systemic Amyloidoses, Prion Diseases (Mad Cows)?

- A mechanism of inheritance

  Yeast Ψ Element, [URE3], Het-S, etc.

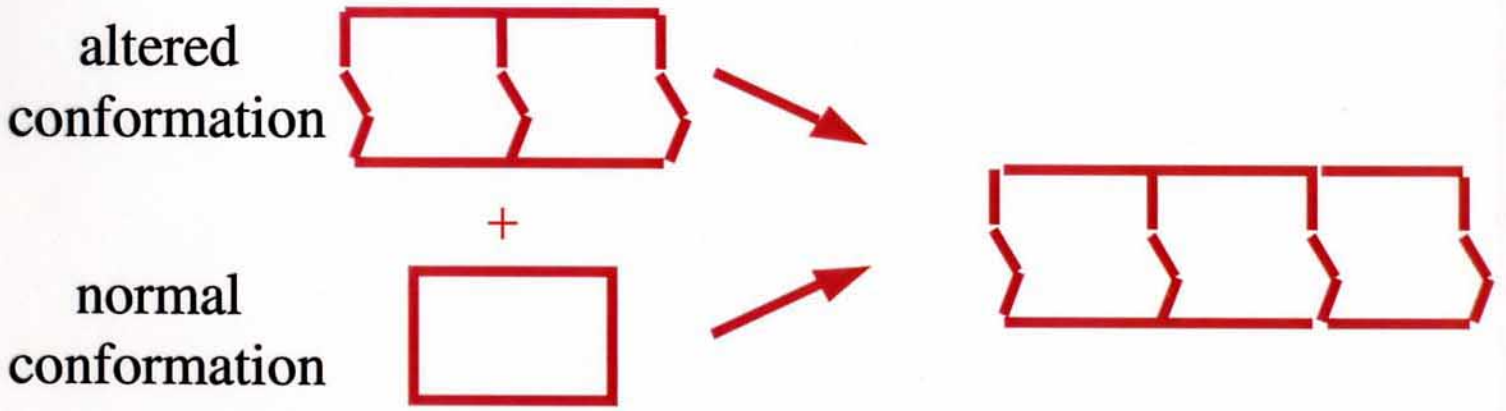

AMYLOID-BETA (Aβ) PROTEIN

- Formed by proteolytic processing
  βAPP -> Aβ
- 39 – 43 amino acid residues
  Aβ 1-42 -> major component in senile plaques
  Aβ 1-40 -> major component in vascular deposits
- Neurotoxicity studies in vitro
  Aβ -> causal agent for cell death
  Yankner *et al.*, *Science* (1989) **245**: 417-420
- For neurotoxic response
  Aβ specimens need to be aged or aggregated
- Aggregation structures and kinetics depend on
  -> pH
  -> ionic strength
  -> peptide concentration
  -> temperature
  -> mixing protocol
  Synder *et al.*, *Biophys. J.* (1994) **67**: 1216-1228

LIPID-INDUCED CONFORMATIONAL CHANGE

- Absence of lipid

  low peptide concentration -> random coil

  high peptide concentration -> β-sheet

- Presence of negatively charged lipid vesicles

  low peptide concentration

  random coil -> β-sheet

- Presence of neutral lipid vesicles

  -> no change in conformation detected at low peptide concentration

- Presence of 0.1 M NaCl and negatively charged lipid vesicles

  -> no change in conformation detected at low peptide concentration

Terzi *et al.*, *Biochemistry* **33** (1994) 7434-7441
Terzi *et al.*, *J. Mol. Biol.* **252** (1995) 633-642
Yanagisawa et al., *Nature Medicine* **1** (1995) 1062-1066
Choo-Smith & Surewicz, *Febs Letters* **402** (1997) 95-98

INSERTION OF Aβ DISSOLVED IN PURE WATER INTO DPPG FILMS

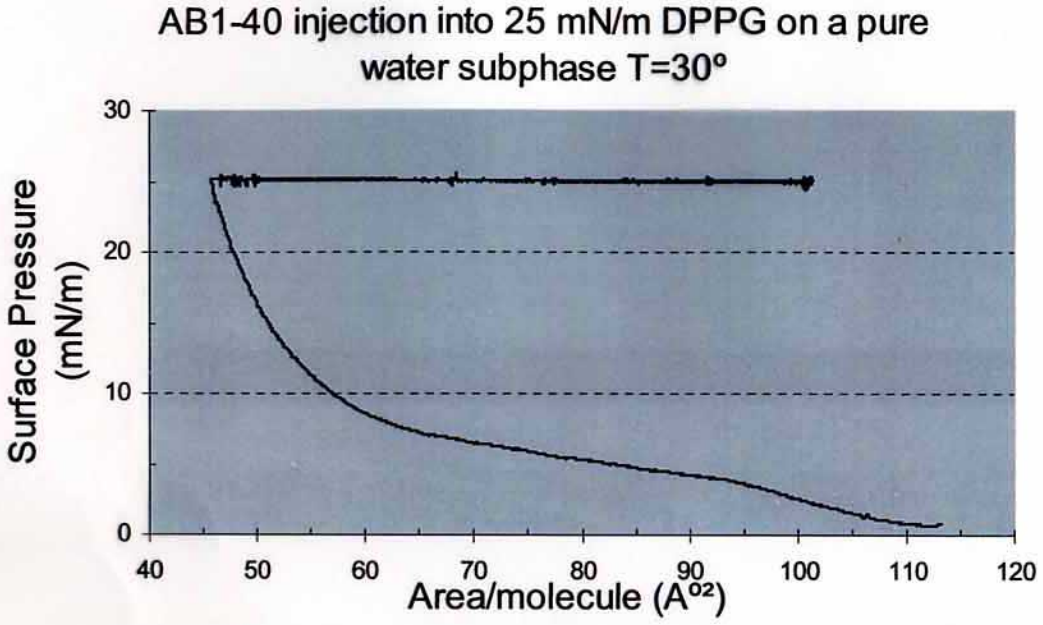

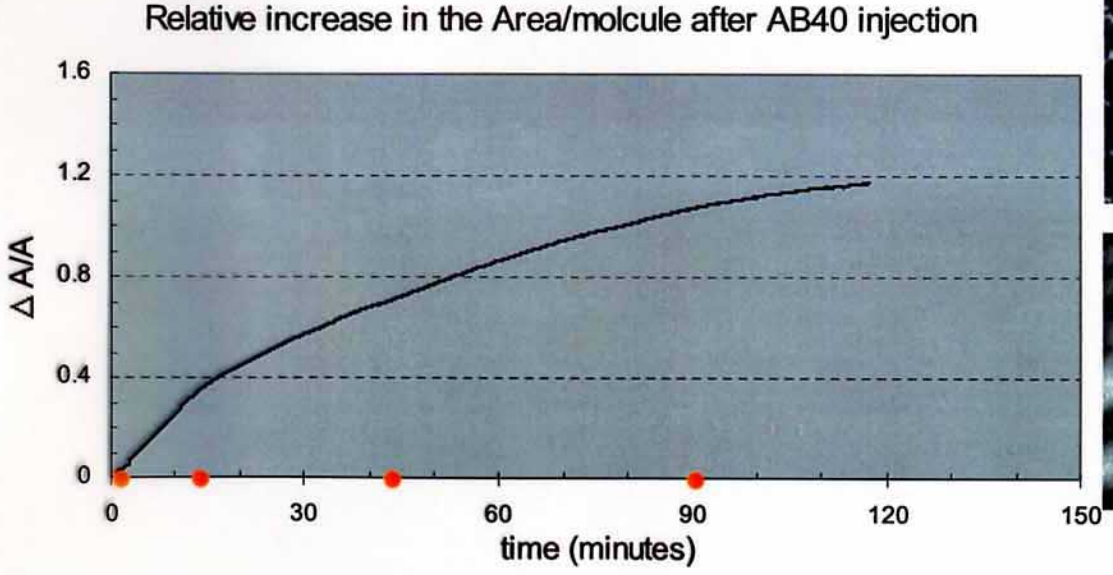

The fluorescence micrographs below shows the change in domain morphology of a DPPG monolayer at 25 mN/m after AB40 is injected into the subphase. The images were taken just before injection, and 15, 45 and 90 minutes after injection of the peptide (in alphabetical order). The corresponding locations are marked on the lower graph.

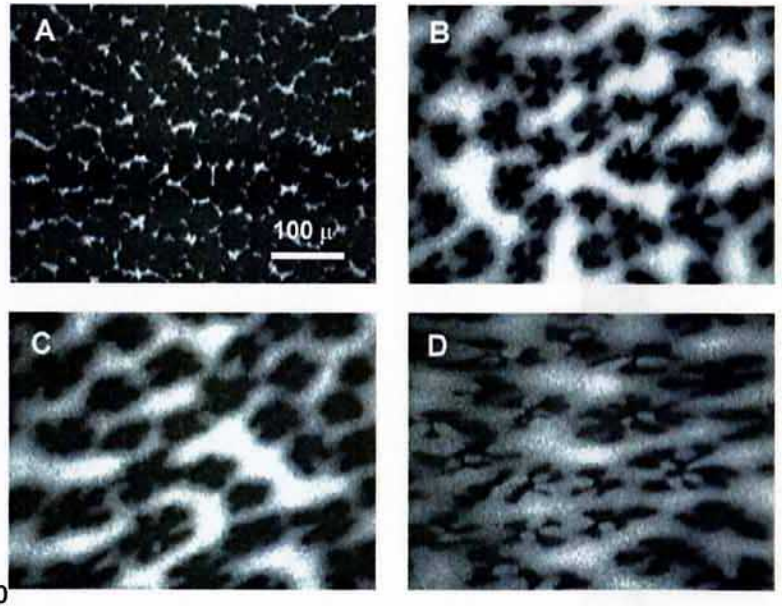

ISOTHERM RESULTS

		Pure Water	Buffer + Salt
DPPG	20 mN/m	200+	52
	23 mN/m		23
	25 mN/m	115	10
	30 mN/m	30	
DPPC	20 mN/m	25	82
	23 mN/m	<3	29
	25 mN/m	0	14
	30 mN/m		2
DPTAP	20 mN/m	88	
	25 mN/m	80	35
	30 mN/m	54	10

		Pure Water	Buffer+Salt
DPPC	15 mN/m	30	
	20 mN/m	25	82
	23 mN/m	<3	29
	25 mN/m	0	14
	30 mN/m		<2
DMPE	15 mN/m	130+	50
	20 mN/m	50+	20
	23 mN/m		12
	25 mN/m	9	

The numbers here are the total percentage change in the area per phospholipid molecule after Aβ40 was injected and the system equilibrated. Aβ40 was dissolved in H_2O prior to injection. The temperature in all the experiments shown here are 30 °C. The subphase is pH=7.4 phosphate buffer with 120mM NaCl where indicated. The peptide concentration in the total subphase volume is 250 nM.

Aβ DISSOLVED IN DMSO: INSERTION RESULTS

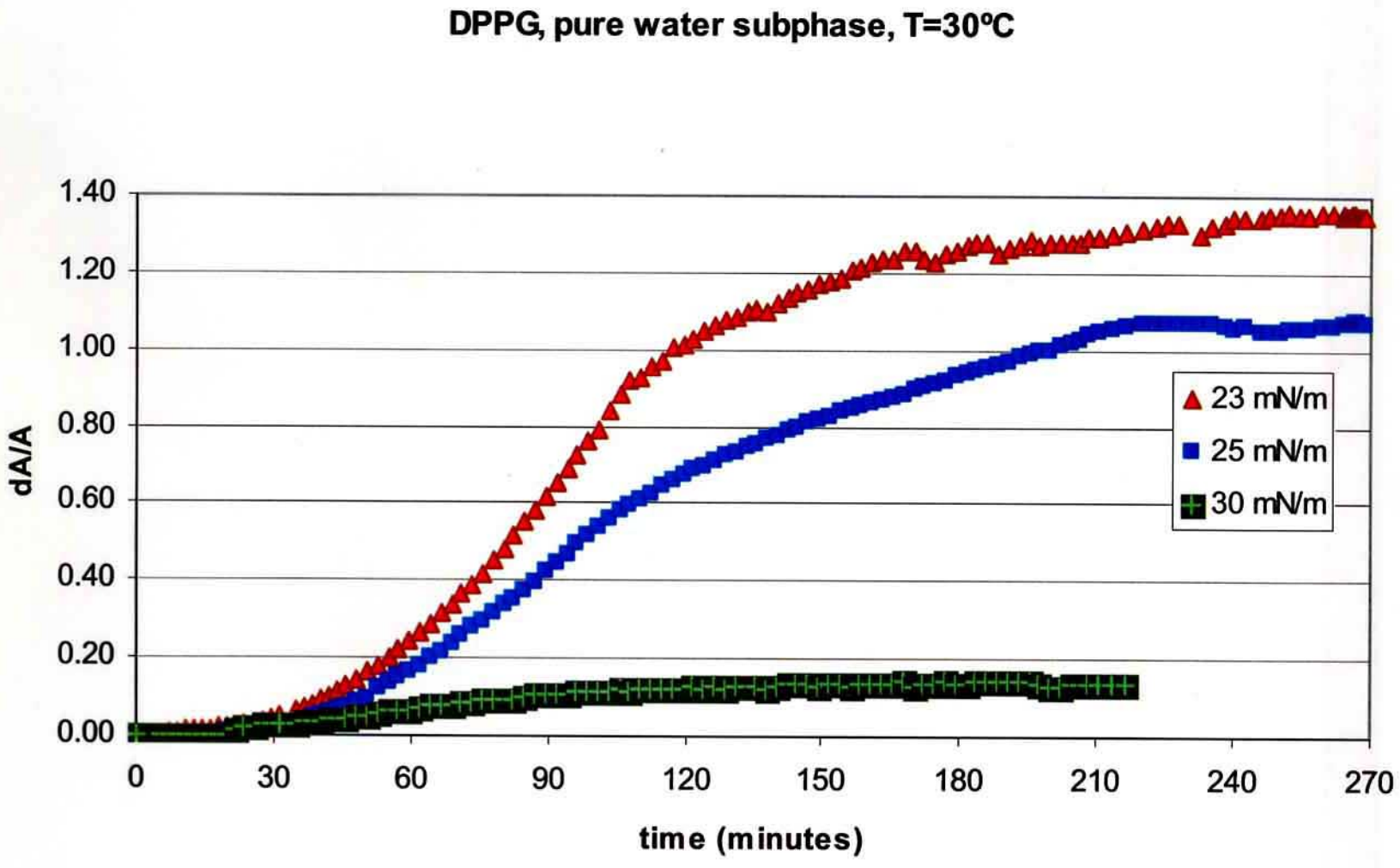

COMPARISON OF DIFFERENT LIPIDS

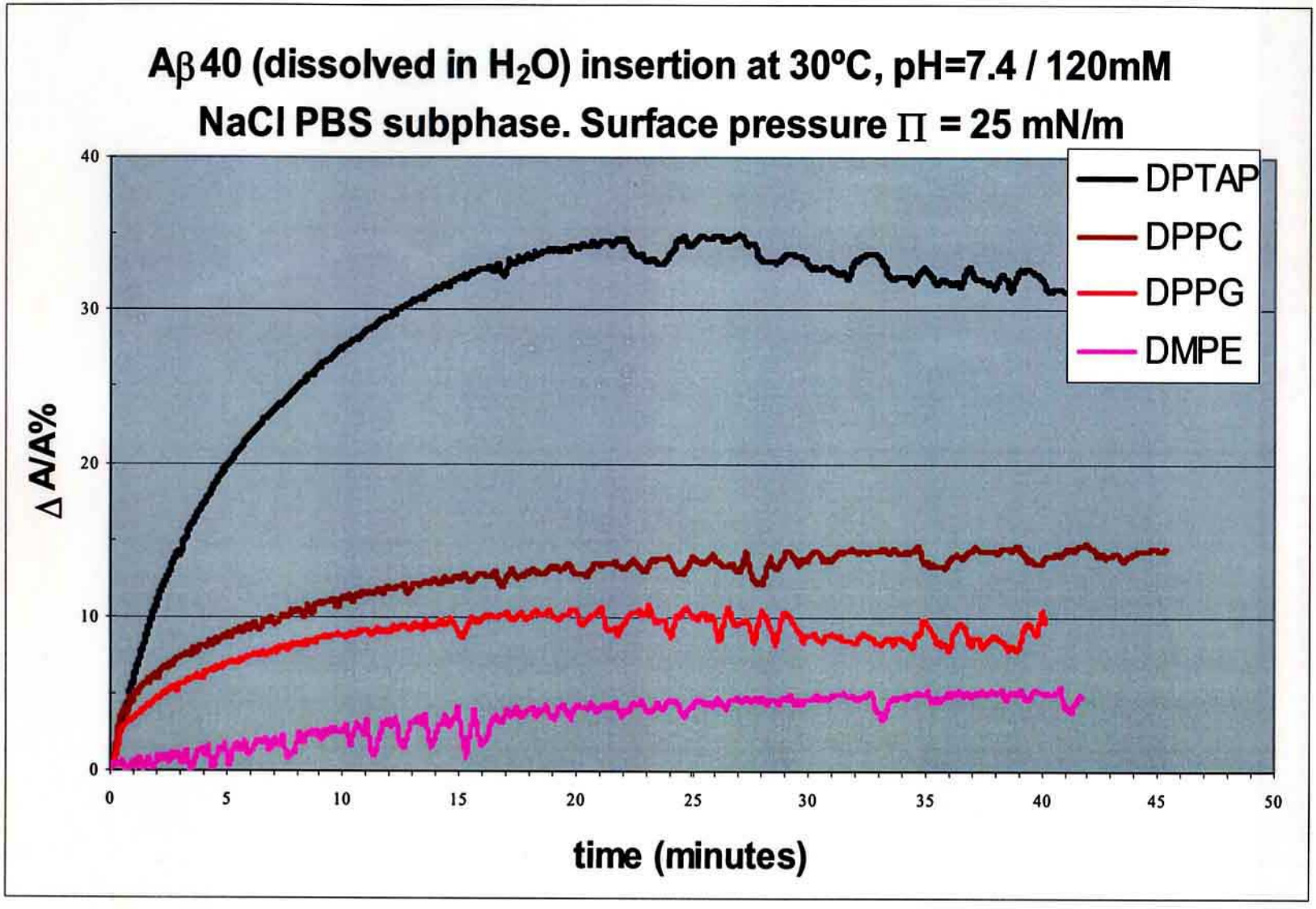

DPTAP-Aβ40 interaction in WATER

DPTAP, T=30 C, Π=30 mN/m

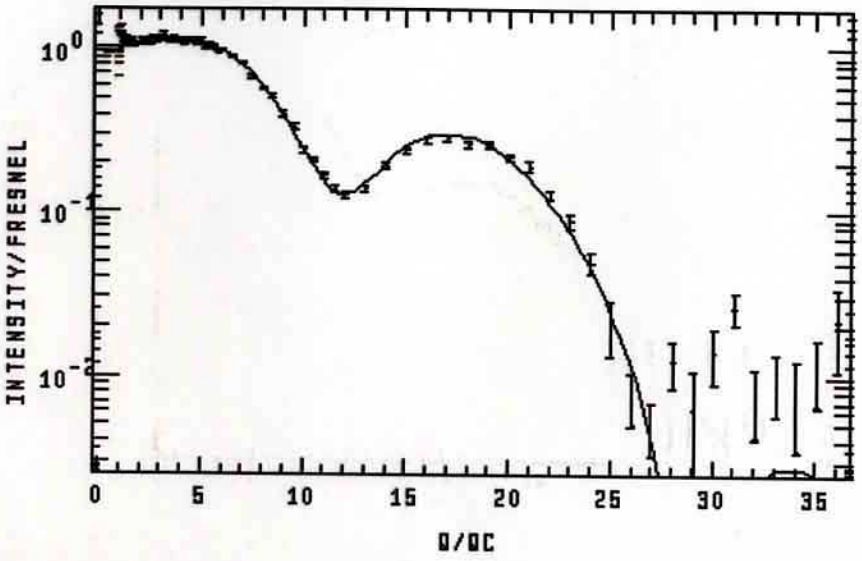

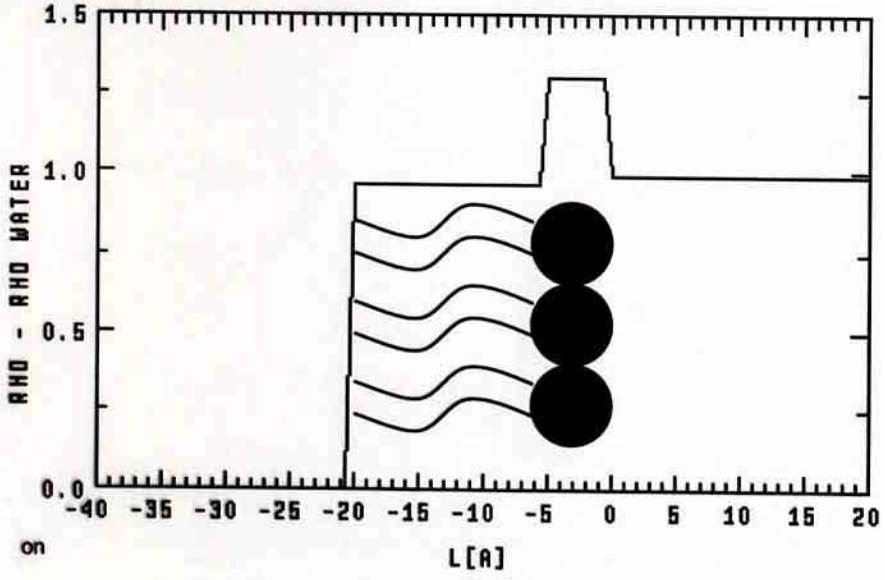

on

DPTAP + Aβ40, T=30 C, Π=30 mN/m

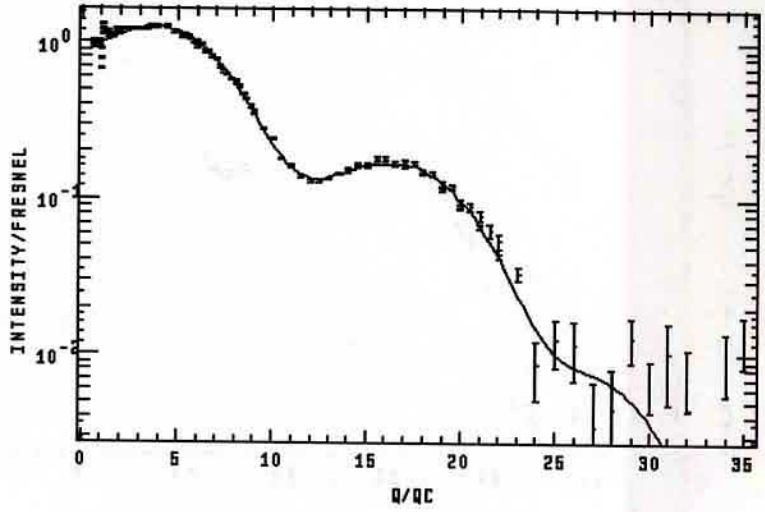

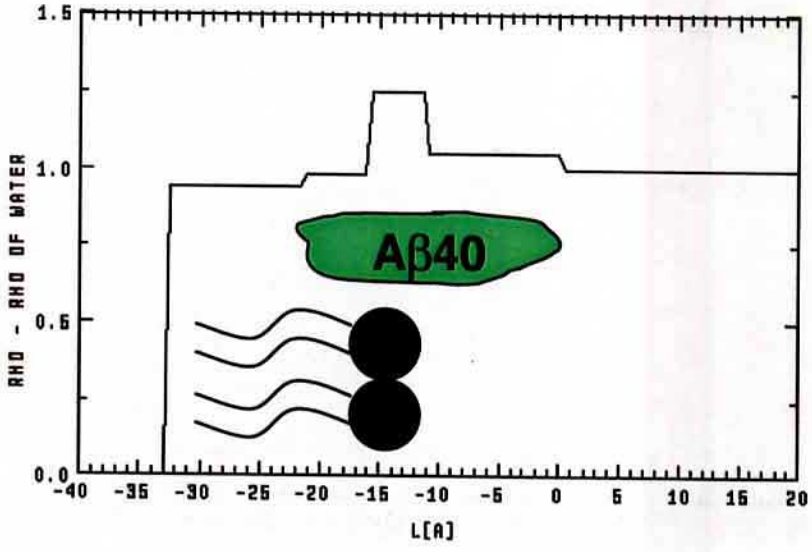

SURFACTANT-LIKE BEHAVIOR

- N-terminus 1-28
  - -> polar extracellular domain
- C-terminus 29-(39 to 42)
  - -> hydrophobic transmembrane region
- Amphipathic in nature
- Behaves like a surfactant
  - -> lowers surface tension
  - -> "critical micelle concentration" exists

  Soreghan *et al.*, *J. Biol. Chem.* (1994) **269**: 28551-28554
- 33 residues or shorter
  - -> no surface response
  - -> transmemebrane portion is necessary

DPTAP-Aβ40 interaction in PBS

DPTAP, T=30 C, Π=30 mN/m

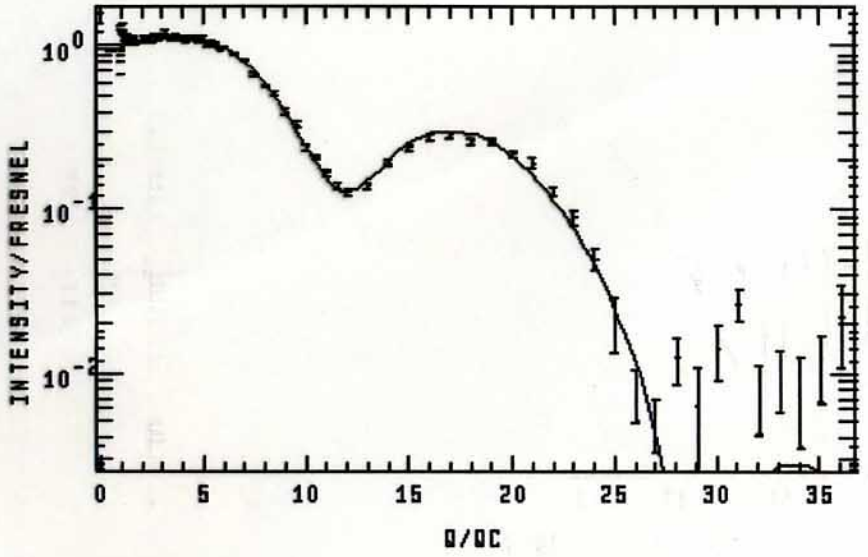

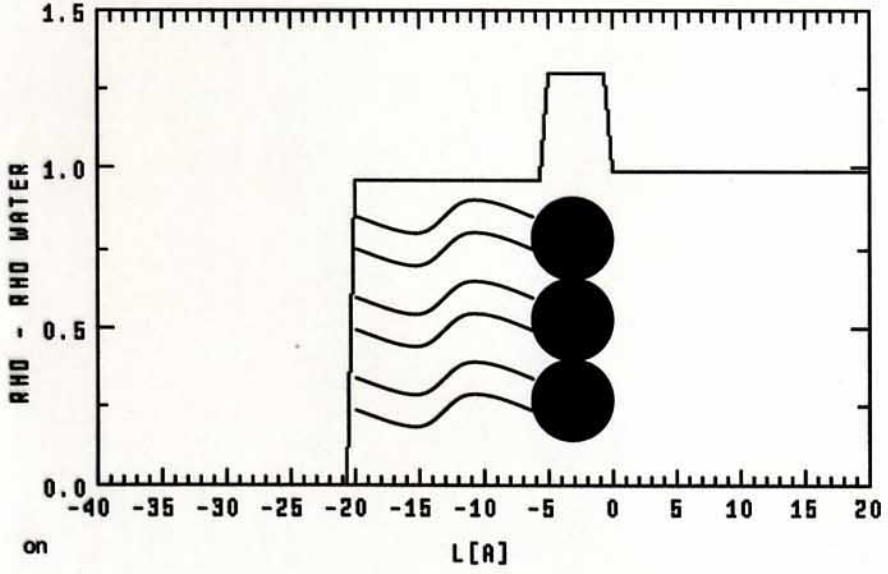

DPTAP + Aβ40, T=30 C, Π=30 mN/m

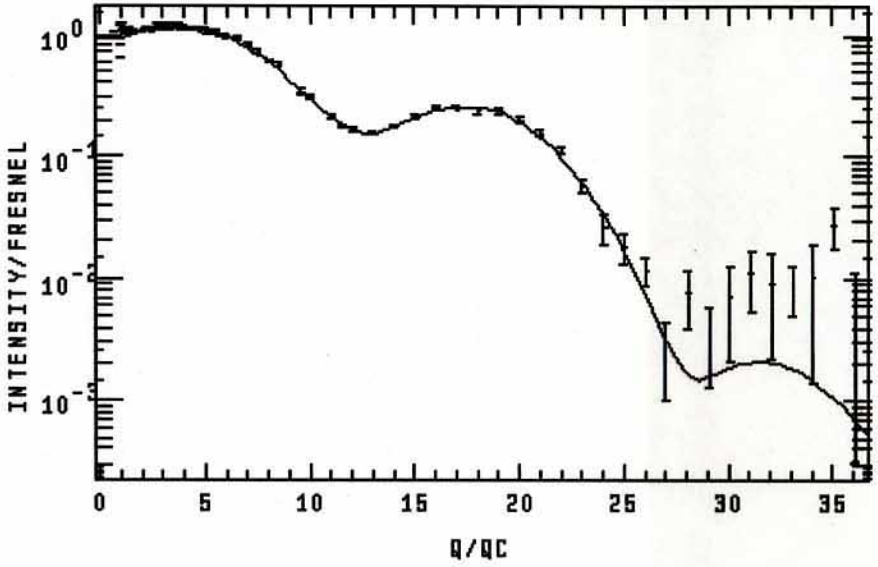

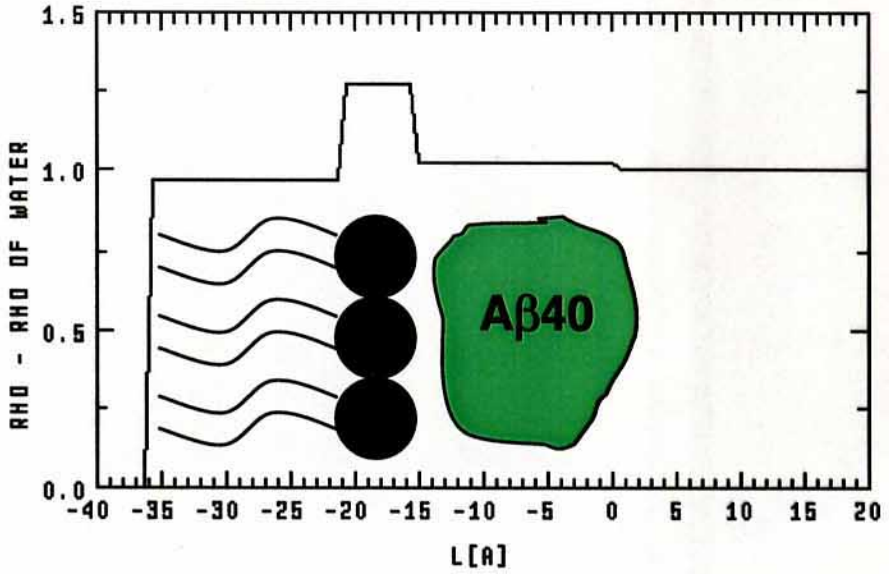

GIXD RESULTS

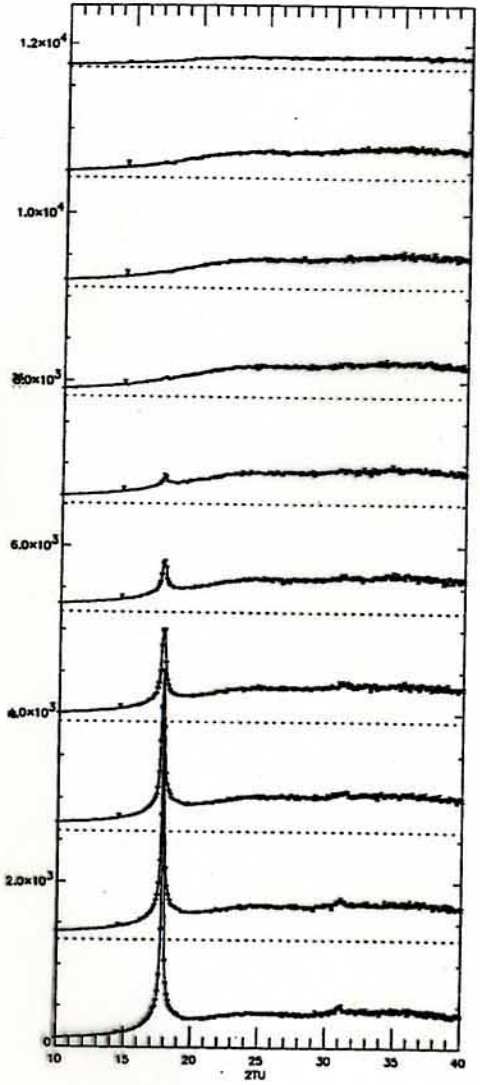

T= 30°C

Π= 30mN/m

intensity has decreased

notice 2nd peak

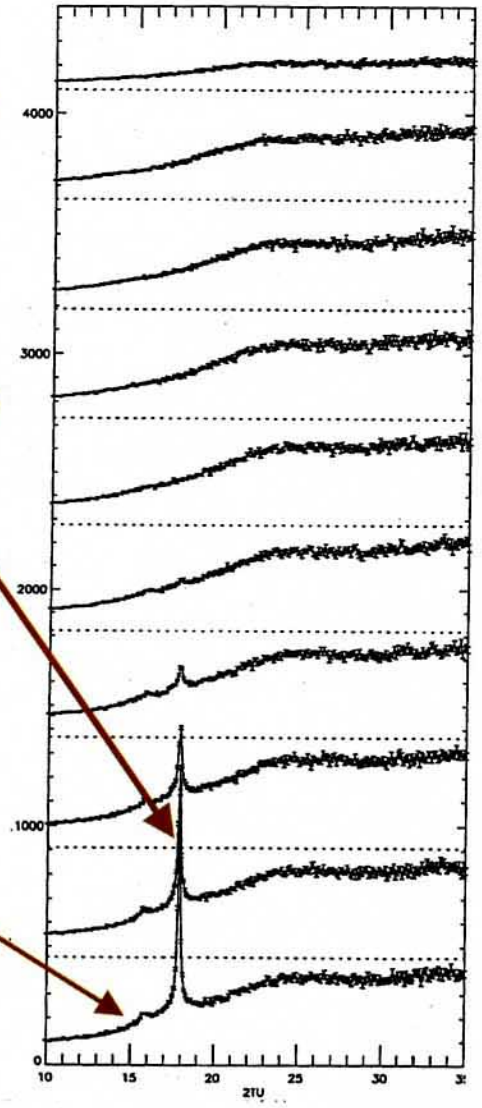

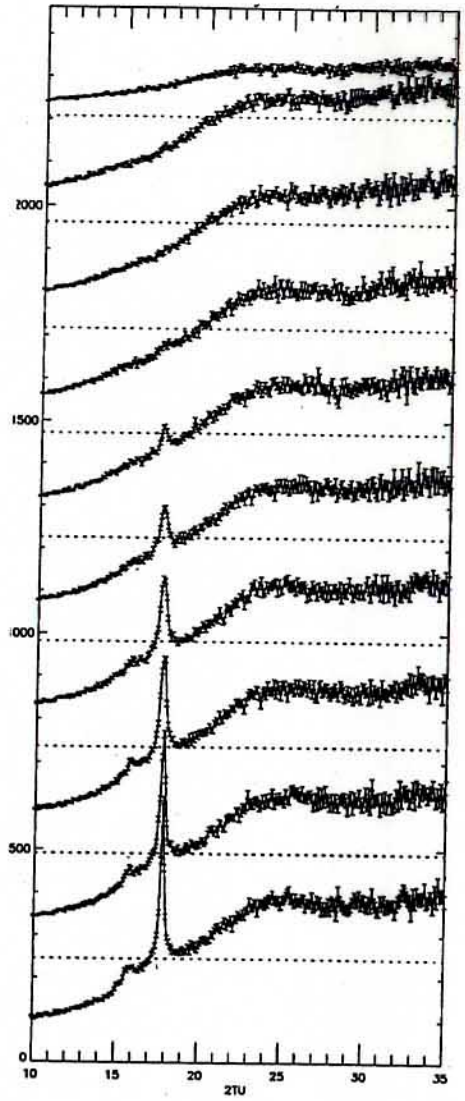

no Aβ40, DPPG only

DPPG with Aβ40

DPPG with Aβ40, 2nd scan

Is the lipid bilayer structured or not?

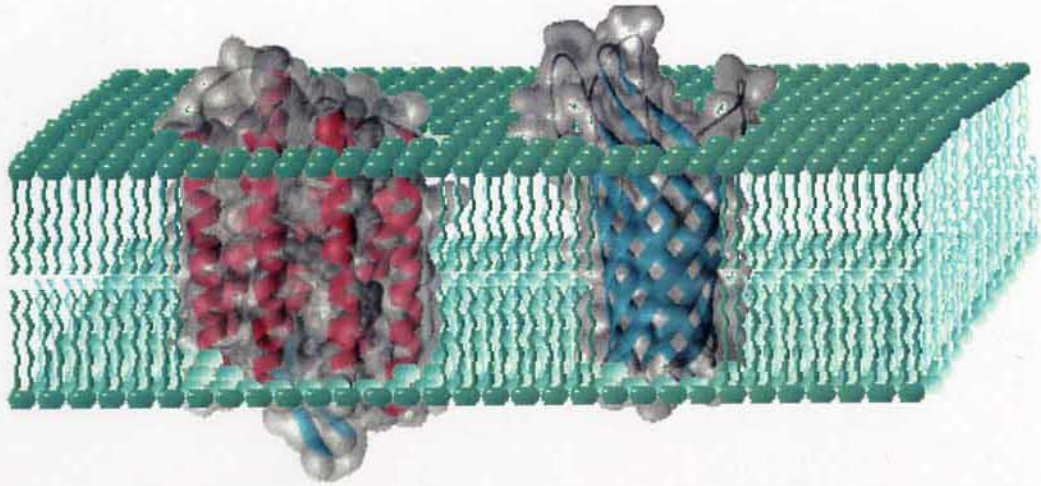

Fluid mosaic model of Nicolson and Singer
Science **1972**, 175, 720; the bilayer is homogenous

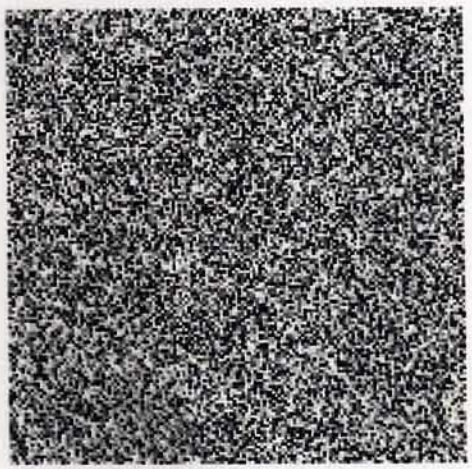

homogenous bilayer

bilayer with lateral heterogeneity

Lateral heterogeneity can be:

- Density fluctuations in a one component bilayer
- Compositional fluctuations in a two component bilayer
- Gel-fluid phase separation pattern

Model membrane composed of a binary mixture

gel phase--low temperatures

hydrocarbons are tightly packed

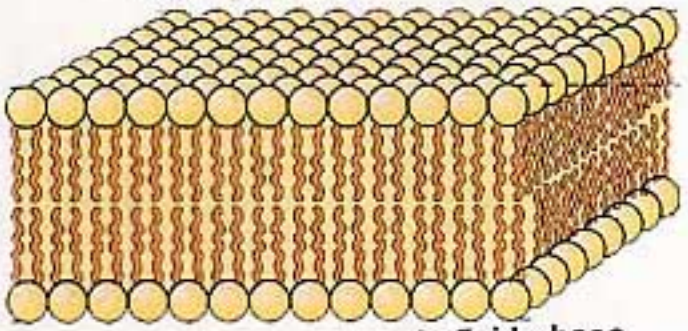

at higher temperatures--moves to fluid phase

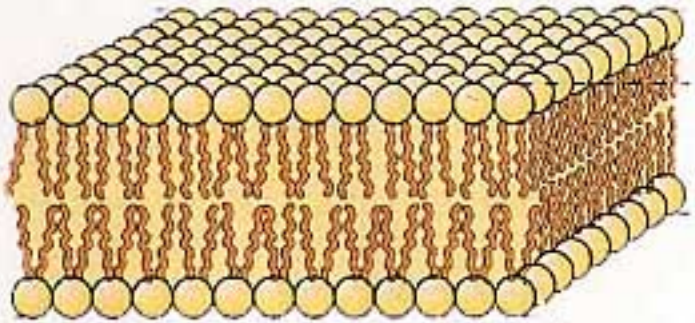

bilayer "melts", movement is allowed

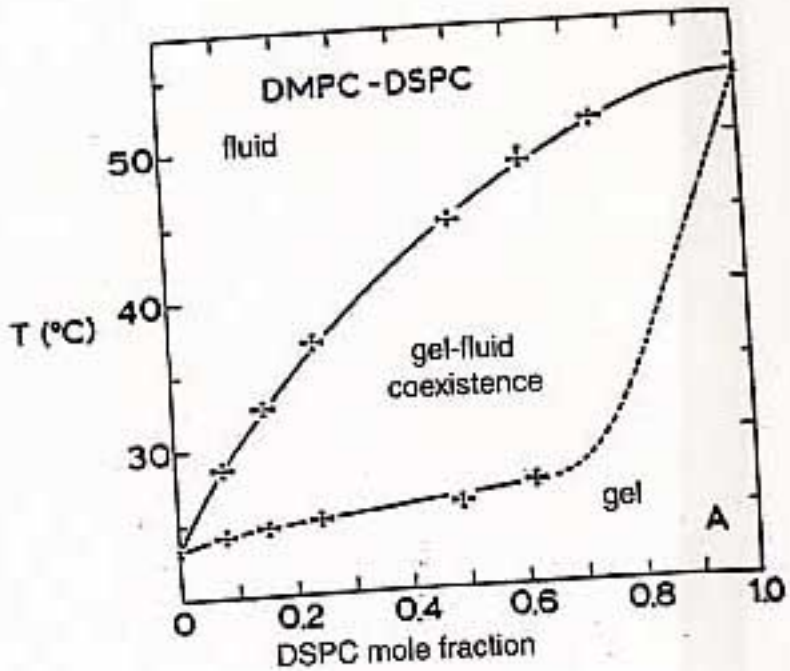

Shimshick, E. J.; McConnell, H. M.
Biochemistry **1973**, *12*, 2351-2360.

Phase diagram of a DSPC/DMPC mixed bilayer

Previous work on lateral phase separation in lipid bilayers

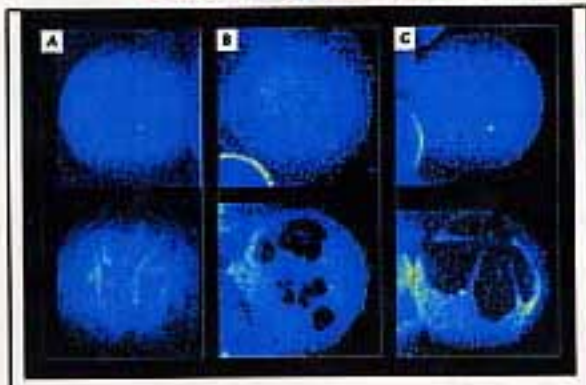

BPJ cover july 2000 DLPC/DPPC (A), DLPC/DSPC (B), DLPC/DAPC (C). Fluid phase top, fluid-gel coexistence bottom. **Fluorescence,** Micron scale

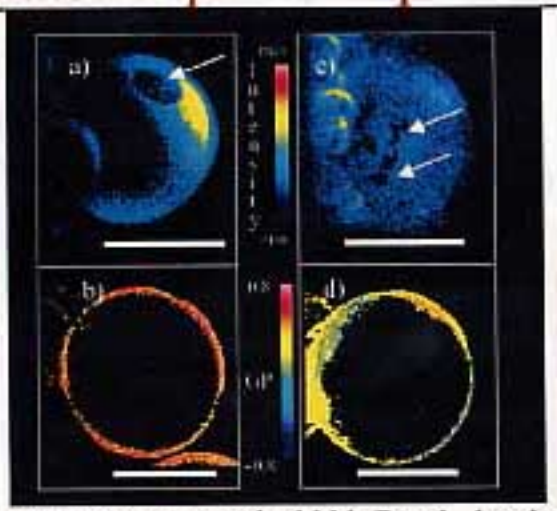

BPJ cover march 2001 Brush border membrane with (a&b) and w/o (c&d) cholesterol.
Fluorescence, Micron scale

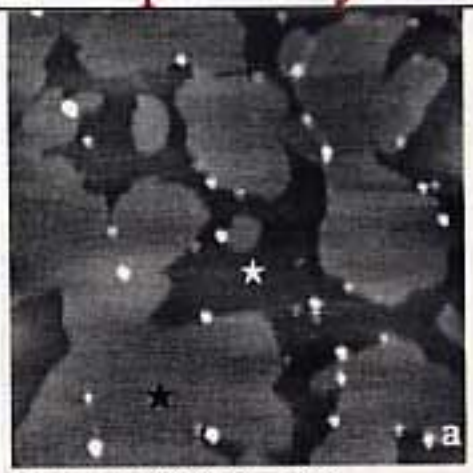

Langmuir 2000, 16, 1473
DPPC/DOPS deposited at room temperature, scan size 2.8 μm.
Atomic force microscopy (AFM)
Micron/Nanometer scale

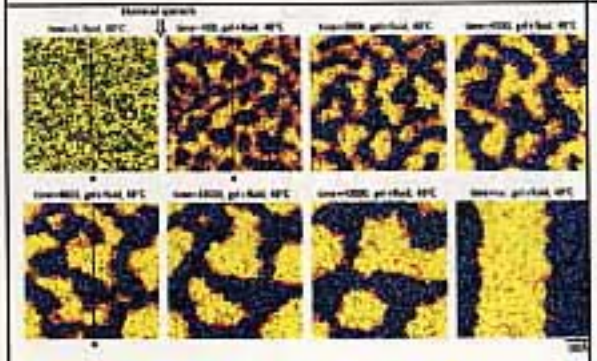

JPC cover dec 14: 2000: Monte Carlo simulations of a DSPC/DMPC bilayer time evolution after quenching. Image size 55nm. **Simulations,** Nanometer scale

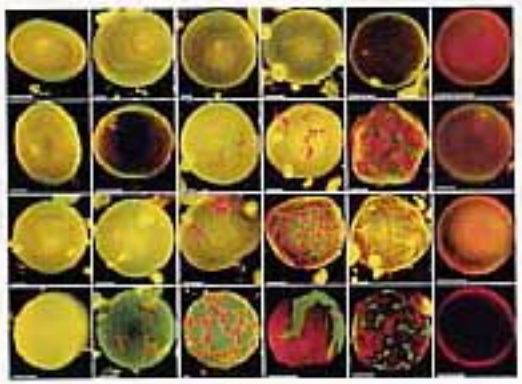

BPJ cover july 2001: DPPC/DLPC/Chol mixture in GUV. Horizontal: DPPC increases. Vertical: cholesterol increases.
Fluorescence, Micron scale

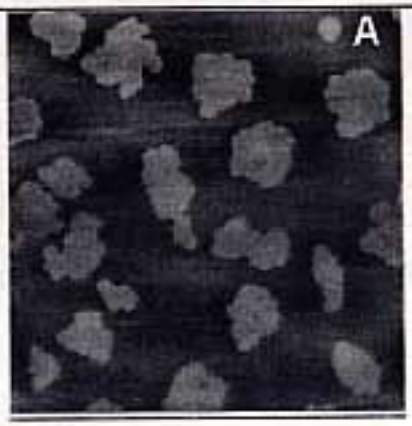

Langmuir, 2001,17, 1653
DPPC/DOPCin PBS quenched to room temperature. Scan size 10 μm **AFM**
Micron scale

Observation of Individual Vesicle Fusion

Egg-PC bilayer domains imaged in fluid using Tapping Mode. The concentration of the vesicle suspension is .3μg/ml diluted in 30mM $MgCl_2$.

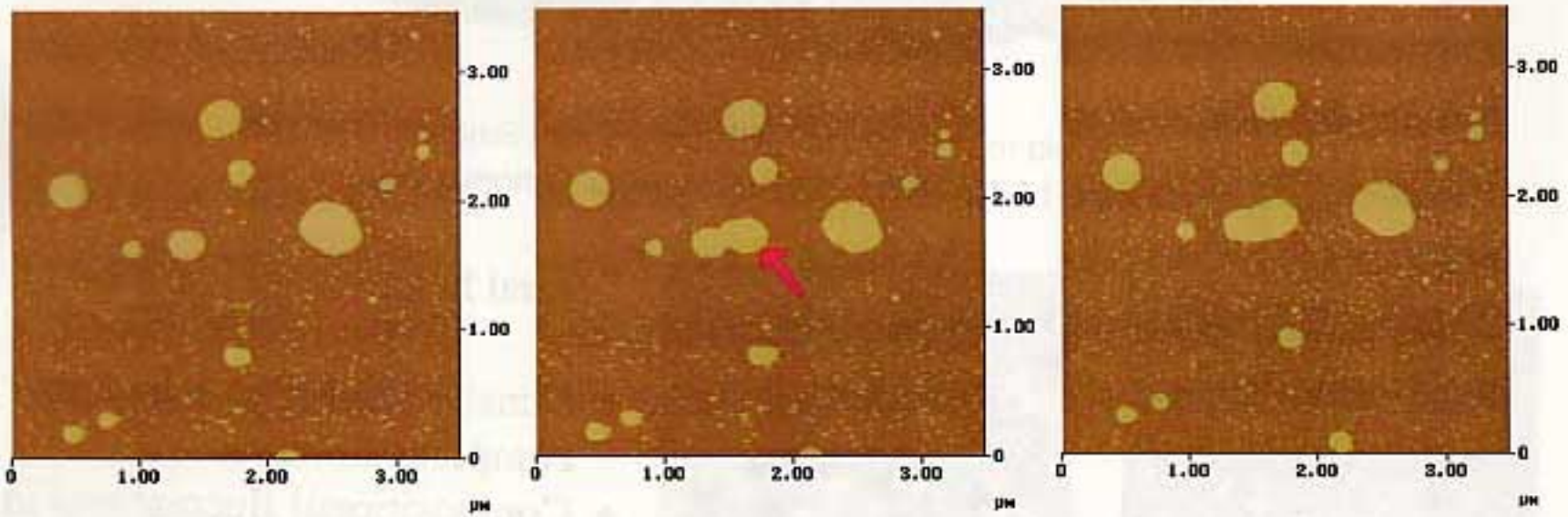

time: 0 minutes 7 minutes 13 minutes

Individual vesicle fuses overlapping with an already adsorbed vesicle (red arrow). The resulting domain decreases perimeter.

Intermediated Fusion Between Bilayer Domains.

Egg-PC bilayer domains imaged in fluid using Tapping Mode. The concentration of the vesicle suspension is .3μg/ml diluted in 30mM $MgCl_2$.

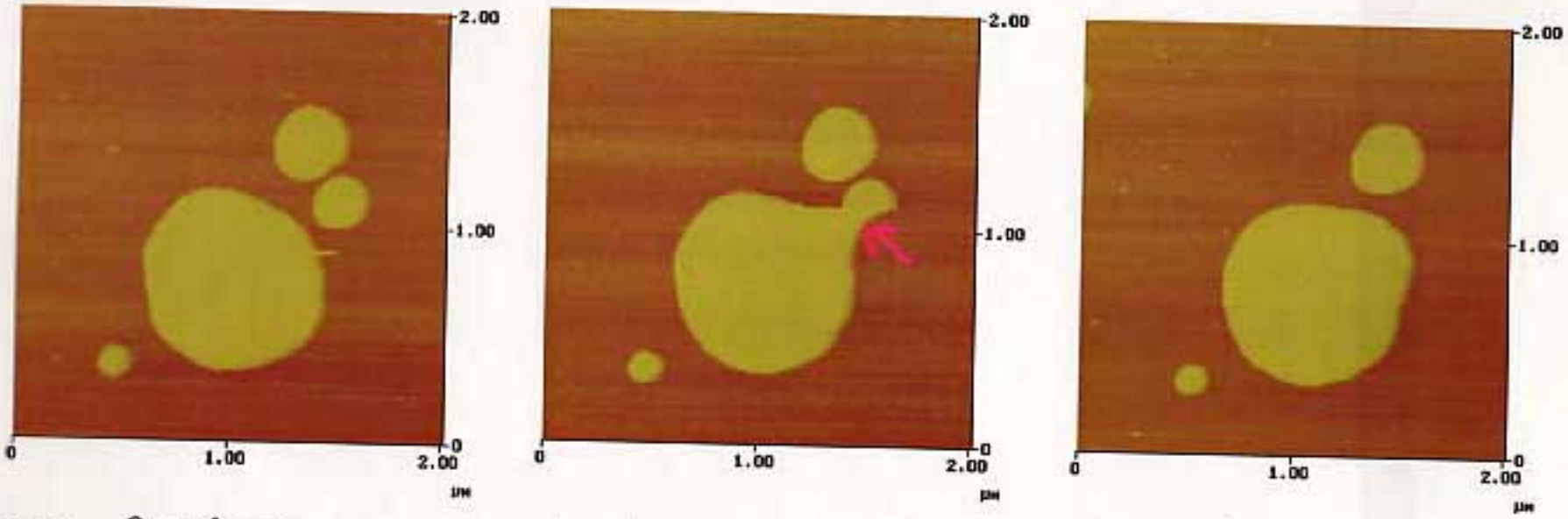

time: 0 minutes 4 minutes 9 minutes

Example of two initially separated bilayer domains that are fused together by a vesicle adsorbing in between (red arrow). The line tension transforms the final bilayer domain shape into a quasi-circular one.

... TO COMPLETE BILAYER COVERAGE

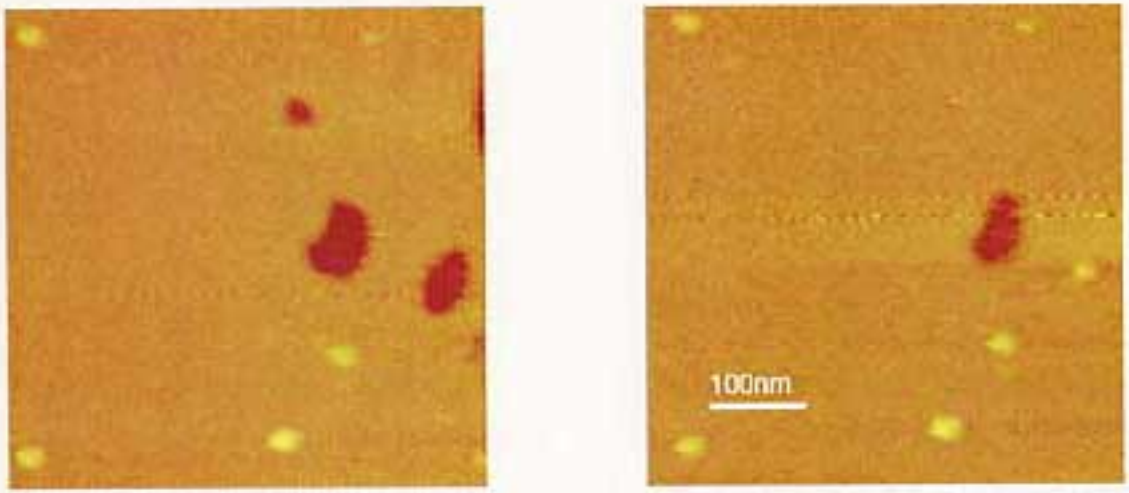

Healing of holes observed at the final stage
of the formation of a continuous lipid bilayer

Muresan and Lee, J. Phys. Chem. B 105 (2001) 852-855

Nanoscale Phase Separation in Supported Bilayers

3:7 DSEPC:DMPC results in compact domains

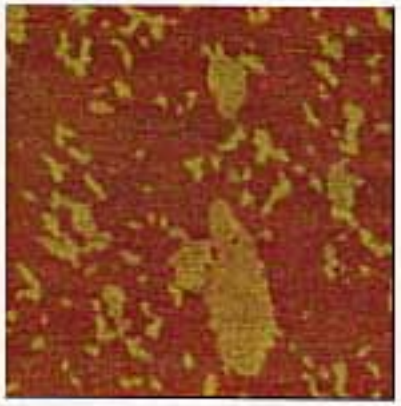

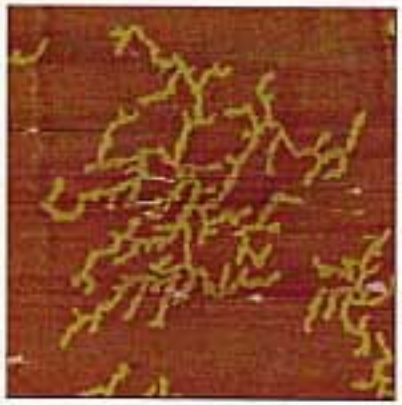

1:1 DSEPC:DMPC results in branched domains

Growth of aggregates in 1:1 mixture

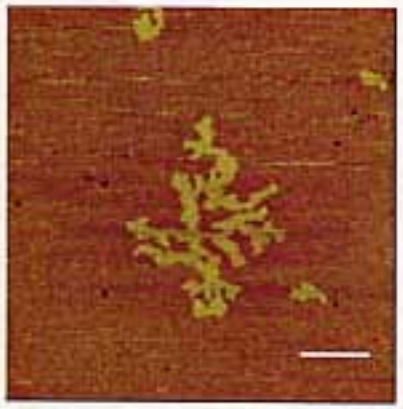

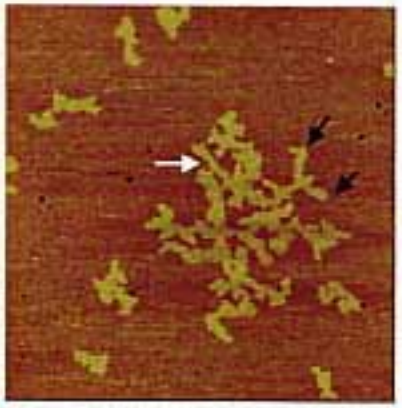

t = 0

t = 1 hour

A.S. Muresan, H. Diamant and K.Y.C. Lee, *JACS* 122 (2001) 6951-6952

Scale bar: 500nm

Formation of Fluid Nanoscale Compartments

3:7 DSEPC:DMPC

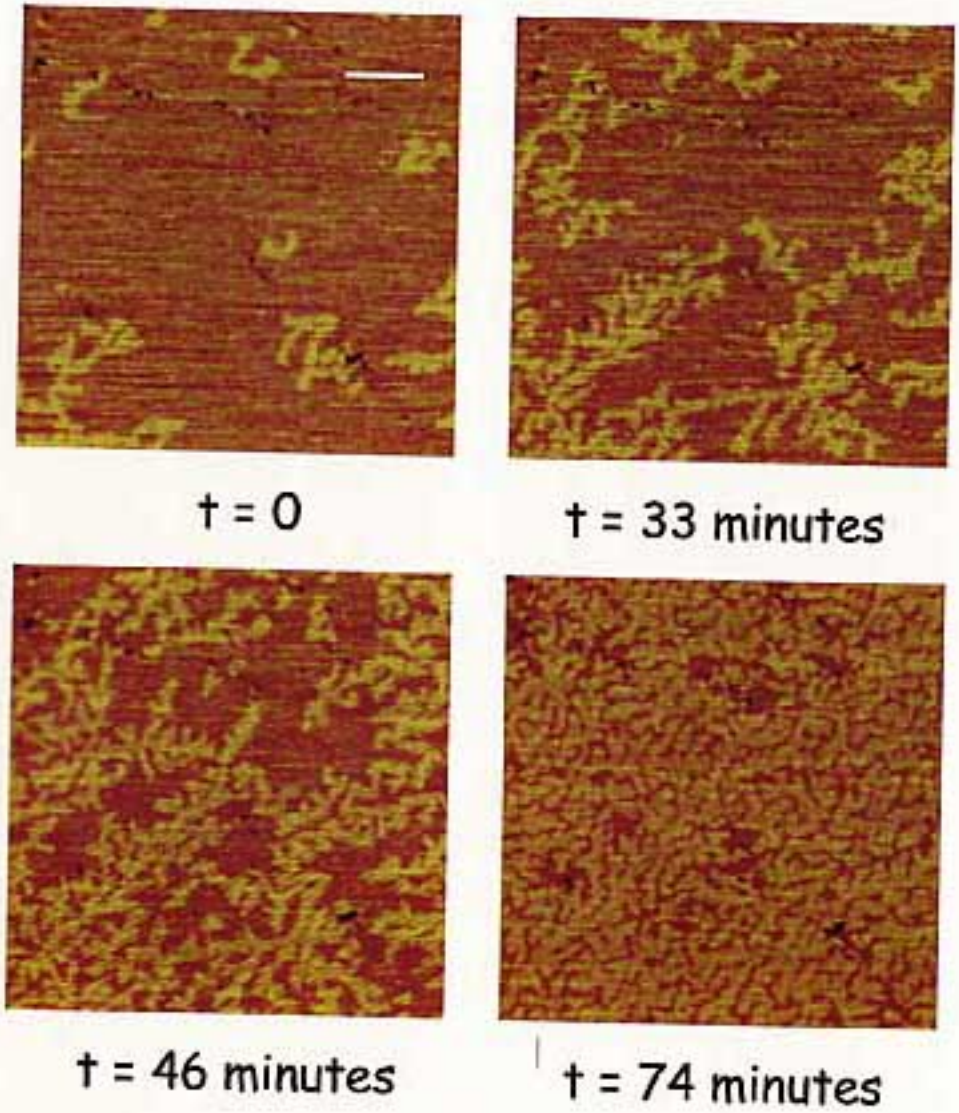

A.S. Muresan, H. Diamant and K.Y.C. Lee, *JACS* 122 (2001) 6951-6952

Scale bar: 500nm

Results

Tapping Mode in air shows bead-like structure for the Aβ fibrils while Tapping Mode in air resolves the helical structure of the fibrils.

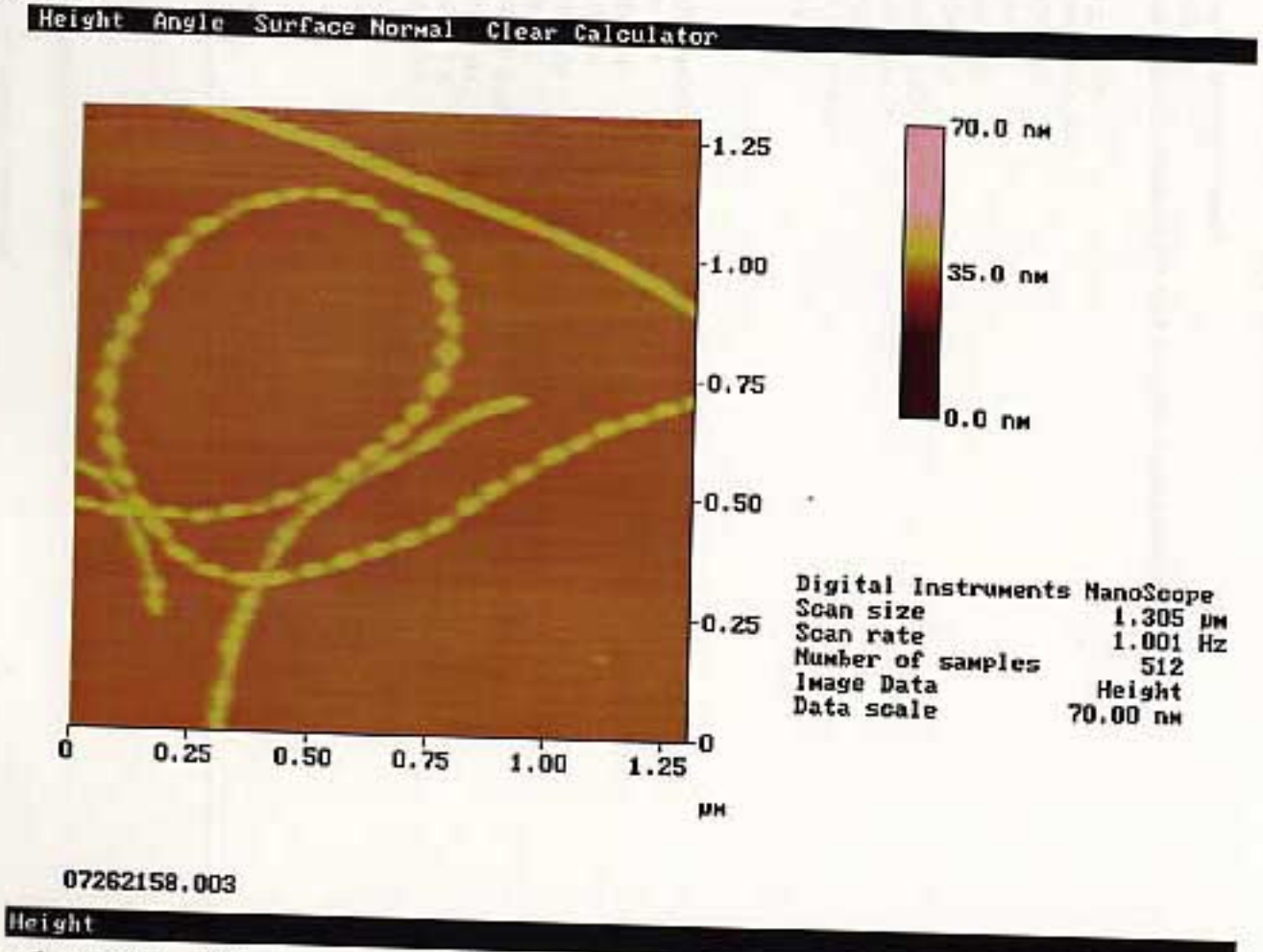

Aged Aβ1-40 imaged in air in TM.

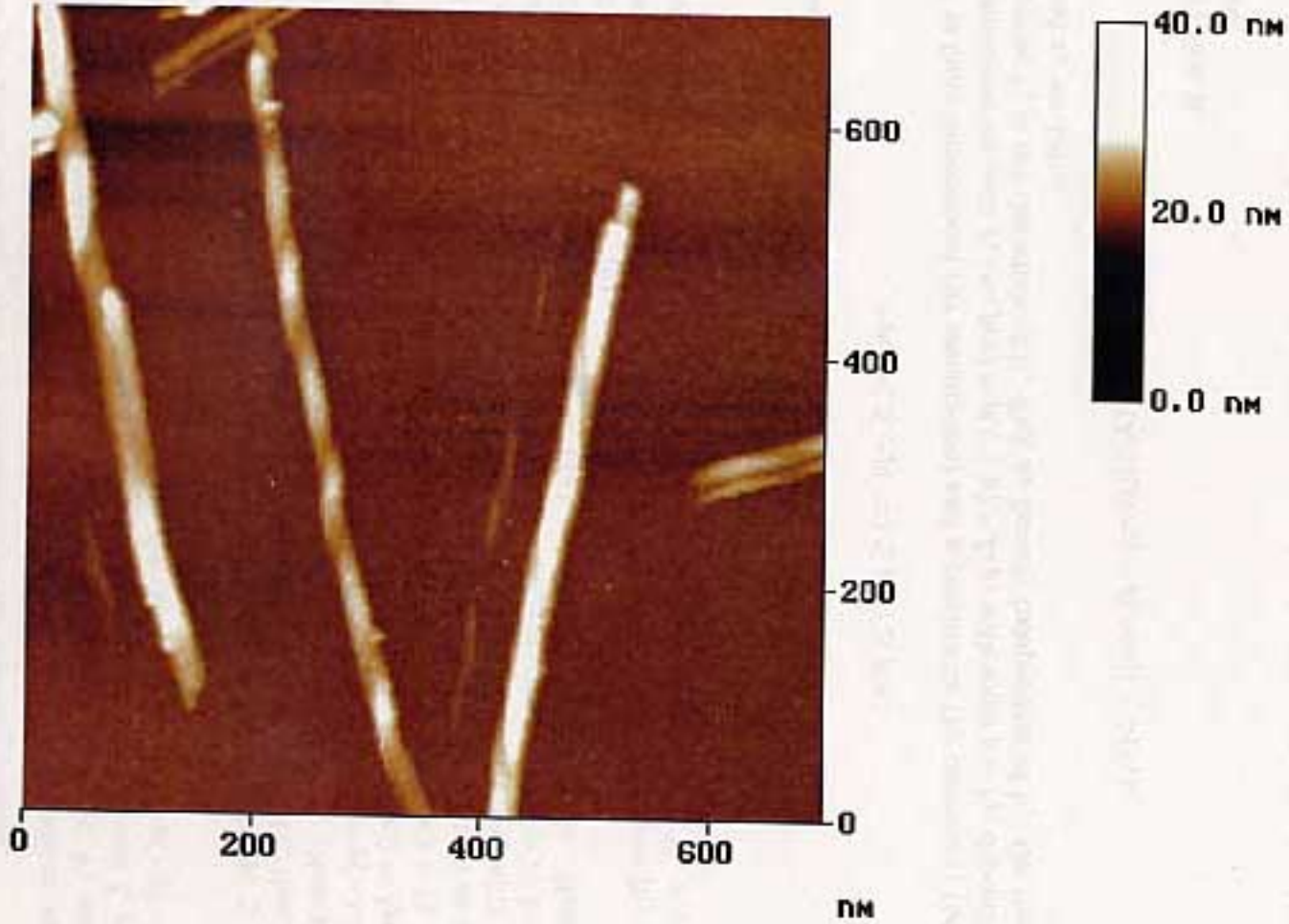

Aβ10-35 fibrils imaged using Tapping Mode in fluid.

PEG does not inhibit fibril formation

but inhibits fibril-fibril association

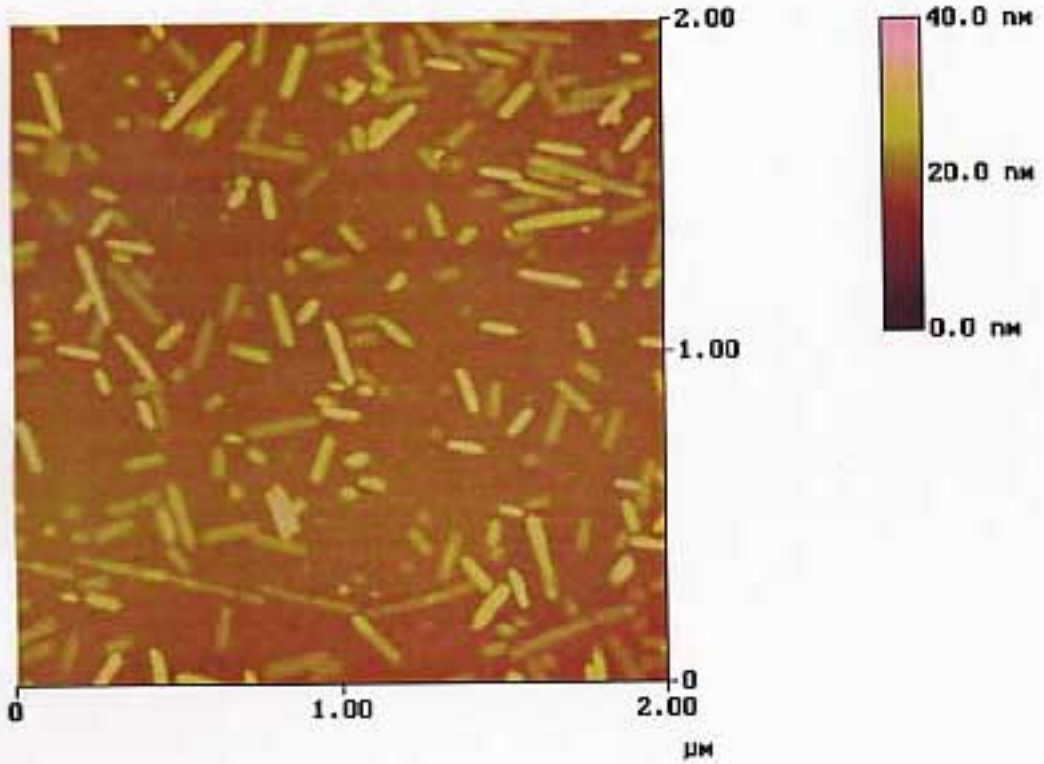

Aβ-PEG fibrils imaged in solution on a graphite surface

Unlike Aβ10-35 fibrils, these fibrils neither overlap nor entangle with one another

No axial periodicity is observed

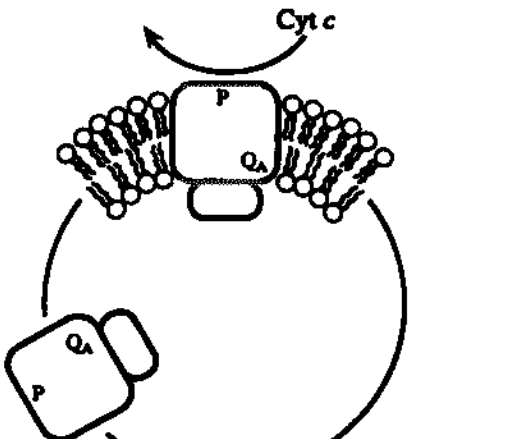

FIGURE 1: Schematic diagram of the bacterial photosynthetic reaction center in a bilayer membrane. The three protein subunits (L, M, and H) and the relevant functional components, the special pair primary electron donor, P, and the primary quinone acceptor, Q_A, are indicated. The RC is depicted in an orientation that is consistent with the results presented and a mechanism in which the vesicles fuse to the glass support by opening out.

membranes (Sui et al., 1988; Plant et al., 1995; Sackmann, 1996), though most of this work does not involve membranes which contain protein.

The RC is the smallest isolatable unit which performs the initial photoinduced charge separation steps in photosynthesis. The three-dimensional structures of RCs from two species of photosynthetic bacteria are known to atomic resolution (Deisenhofer et al., 1995). It is comprised of three subunits, termed L, M, and H, whose total molecular mass is approximately 100 kDa (see Figure 1). Its physiological role is to transduce light energy into a charge separation across the native membrane, which in turn leads to a transmembrane electrochemical potential used by the organism to store energy. The RC accomplishes this charge

EXPERIMENTAL PROCE

Materials. The dye–lipid p
1,2-dihexadecanoyl-*sn*-glycer
ethylammonium salt (Texas R
1,3-diazol-4-yl)-1,2-dihexa
phoethanolamine, triethylam
purchased from Molecular Pr
thiol reductant, tris(carboxyet
RC conjugate, rhodamine X
also purchased from Molecu
biotin, 4-hydroxyazobenzene
and avidin (Immunopure avidi
Chemical Co. Horse heart cy
Chemical Co.

Reaction Centers. RCs we
sphaeroides wild-type or the
methods that are described in
1986). The RCs isolated by t
only the primary quinone, Q
five cysteine residues at posi
and H234. From an examin
the cysteine residue at H156
and the other four are buried
from the surface). *Rhodol*
isolated as described in Tagu
have cysteine residues at pos
and L247, all of which are b
the same three-dimensional s
gous *Rb. sphaeroides* RCs (K
surface cysteine residue was
Rb. capsulatus RC by repl
position M189 to create the
in detail in Boxer et al. (199

RC–Biotin and RC–Rho
sphaeroides RCs. The surfac
be modified using reagents v
groups; this was used to
rhodamine conjugates at the
teine H156 (Debus et al., 198
in 10 mM Tris, pH 8.0, and 0.
to about 75 μM using a Centr
Co.). The RCs were then dia
9.0, and 0.025% LDAO buffe
changes of buffer containing
A 10-fold molar excess of the

Unilamellar Vesicles

- Freeze-thaw extrusion
- lipid (dissolved in chcl3) dried under N_2 stream forming a thin film
- dried overnite under vacuum
- rehydrate & vortex
- 5-10 freeze thaw cycles
- extrusion using desired pore size
  or
  probe sonicate for ~50 nm diam. vesicles.

Proteoliposomes

- protein added to vesicles at certain desired ratio
- run down Sephadex Column previously equilibrated with lipid.

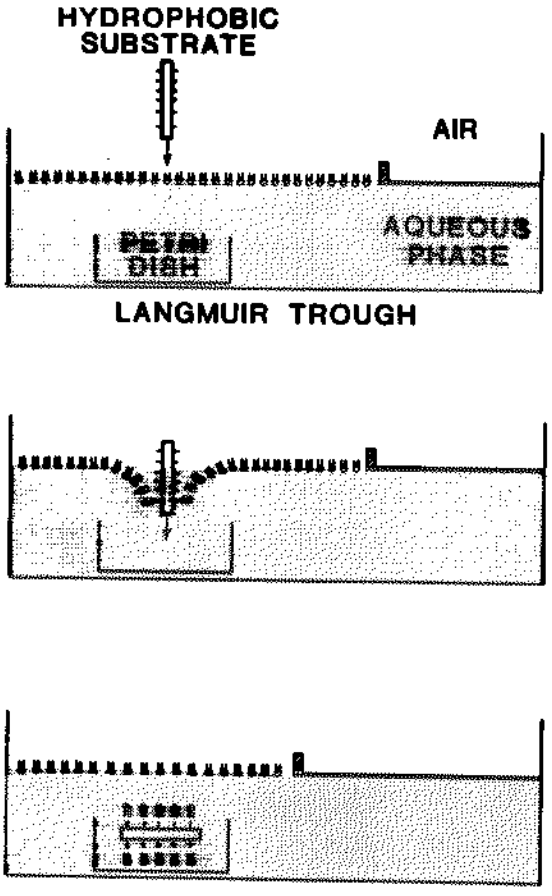

Fig. 1. Transfer of a phospholipid monolayer from the air-water interface to a solid support. The support, which has been alkylated to render it hydrophobic, is lowered vertically through the phospholipid monolayer at the air-water interface in a Langmuir trough. Supported monolayers can also be prepared by lowering the substrate horizontally through the air-water interface (for example, see Ref. 24).

hydrophilic solid supports; again, these can be glass, quartz or single crystal silicon. Fig. 1 shows the transfer of phospholipid monolayers onto an alkylated support. The alkylated support is lowered through the monolayer at the air-water interface in a Langmuir-Blodgett trough. Sometimes the support is kept in a vertical orientation during immersion (as in Fig. 1) and sometimes a 'face-down' (horizontal) immersion is used.

There are at least two methods of preparing supported bilayers. In Fig. 2, a supported bilayer

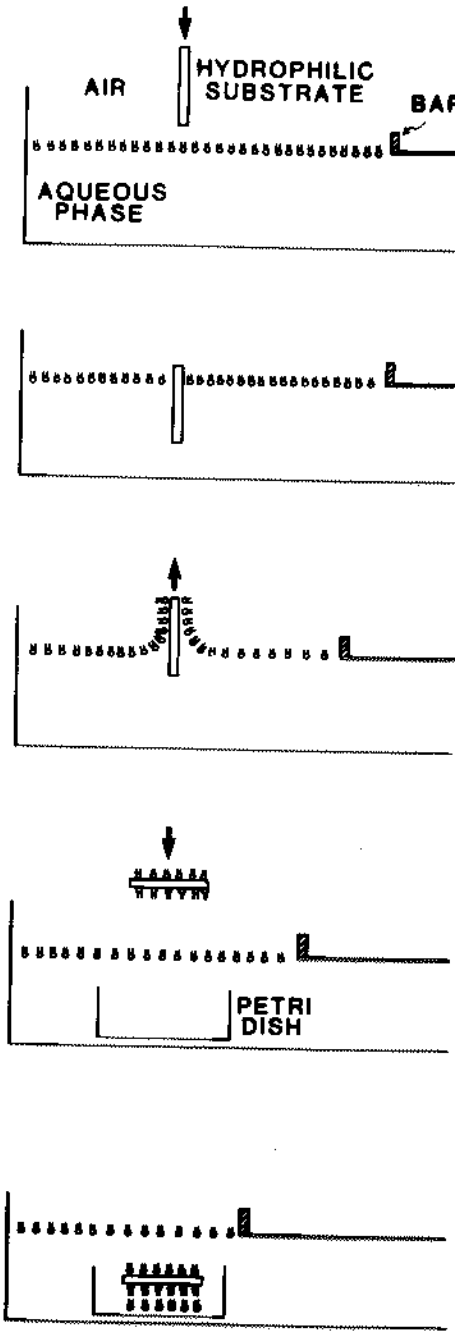

Fig. 2. Preparation of supported
transfer of two monolayers from t
layers are spread at the air-wat
trough. The clean hydrophilic silic
immersed vertically through the m
significant change in surface pres
The substrate is then pulled out
permit water to drain from the sur
surface pressure observed is then c
the area of the trough. The loss in

Formation of Supported Bilayers

① Monolayer transfer by Langmuir-Blodgett techniques
- automatic dep. process
- process can be followed by ellipsometry & epifluorescence
- both layers can be manipulated

② Vesicle Rupture
- reconstitute with proteins in native orientation

③ Monolayer + Vesicle Rupture
- allows the presentation of correct side on each leaflet
- maintains mobility of lower leaflet

Self-Assembly of Supported bilayers

① Integrated bilayers w/ lower leaflet fixed to substrate either covalently or by ion bridges

② Supported bilayer with 2 free leaflets

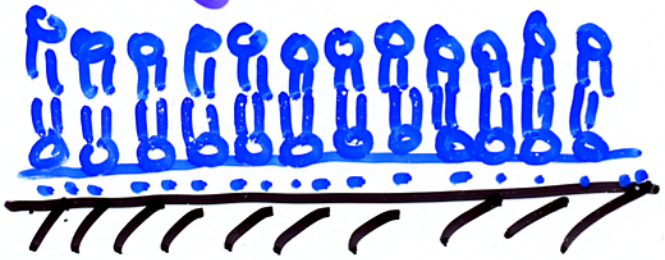

③ Bilayer resting on thin, soft, hydrated polymer film

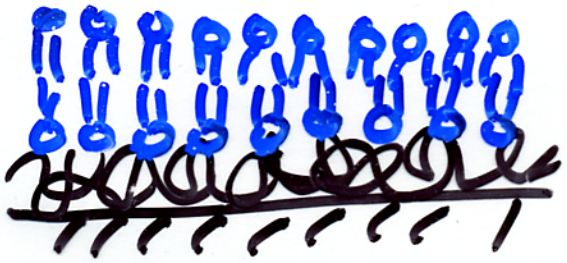

To immobilize monopolar proteins

formed were ultrathin polymer films hydrophobized by coupling of long alkyl chains to hydrophilic polymer backbone

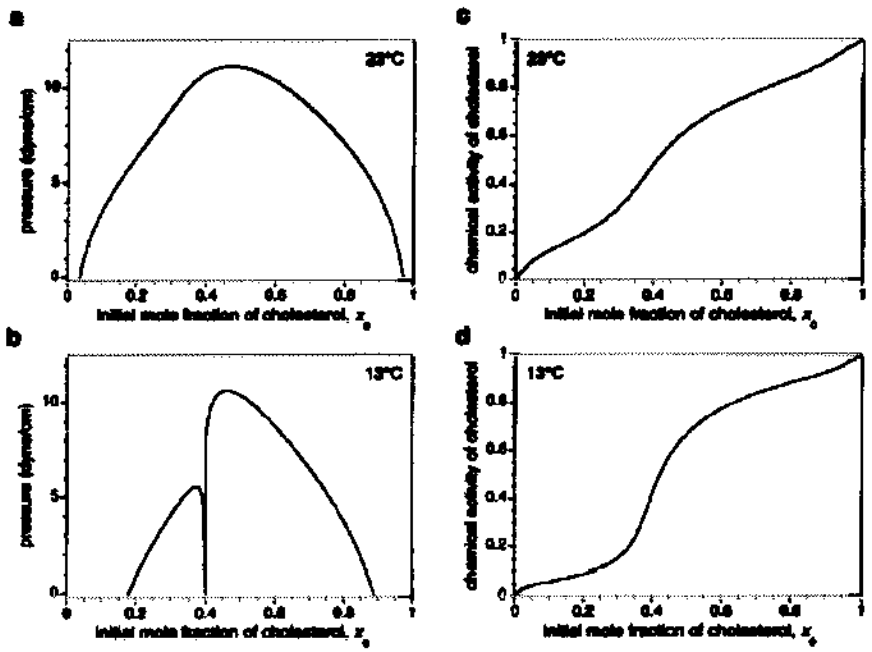

Figure 4. Theoretical phase diagrams and chemical activities. Panels a and b show calculated pressure (π)–composition (x_o) phase diagrams for reactive mixtures containing cholesterol and phospholipid at 23 and 13 °C, respectively. Compositions of coexisting phases were found by the method of double-tangent construction using the free energy of eq 2 and the parameters listed in the text. Panels c and d show calculated chemical activity–composition curves (a_o) for reactive mixtures of cholesterol and phospholipid at a pressure of 20 mN/m and at temperatures of 23 and 13 °C, respectively for the same parameters. The normalized equilibrium constant K^*_{eq} is 0.3, and the cooperativity ω is 2.

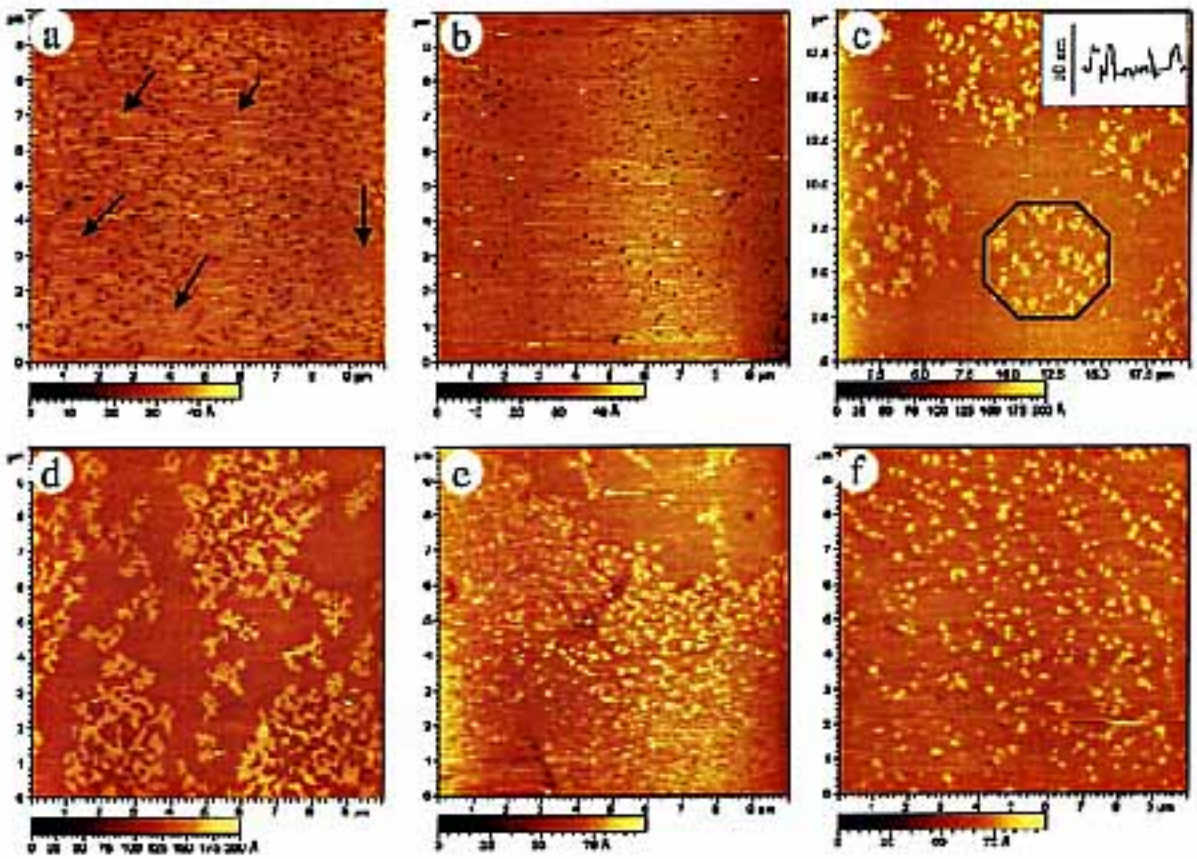

FIGURE 5 AFM images for hybrid bilayers of SPM/DOPC/cholesterol (1:1:1) with and without 5% GM1. (*a* and *b*) SPM/DOPC/cholesterol (1:1:1) bilayers deposited at 10 mN/m (*a*) and 35 mN/m (*b*). The arrows indicate more tightly packed areas of the bilayer. (*c*) SPM/DOPC/cholesterol (1:1:1) bilayer with 1% GM1 deposited at 10 mN/m with one of the large domains containing small GM1-rich microdomains outlined in black; the *x* scale for the section analysis shown in the insert is the same as the image. (*d–f*) SPM/DOPC/cholesterol (1:1:1) bilayers with 5% GM1 deposited at 10 mN/m (*d*), 30 mN/m (*e*), and 35 mN/m (*f*).

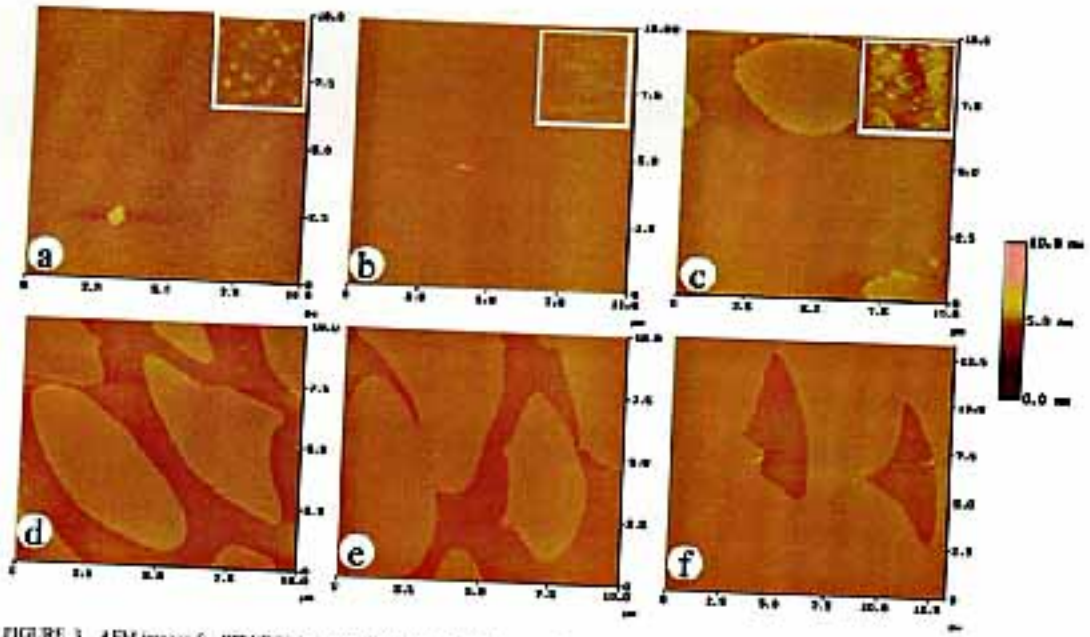

FIGURE 3 AFM images for SPM/DOPC and SPM/DOPC/cholesterol monolayers. (*a*) SPM/DOPC (1:1) monolayer deposited at 7 mN/m. The inset is a small-scale image (500 × 500 nm²). (*b*) SPM/DOPC (1:1) monolayer with 10% cholesterol transferred at 7 mN/m. The inset is a small-scale image (500 × 500 nm²). (*c*) SPM/DOPC (1:1) monolayer with 20% cholesterol at 7 mN/m. The inset is a large-scale image (40 × 40 μm²). (*d*) SPM/DOPC (1:1) monolayer with 33% cholesterol at 7 mN/m. (*e*) SPM/DOPC (1:1) monolayer with 33% cholesterol at 10 mN/m. (*f*) SPM/DOPC (1:1) monolayer with 33% cholesterol at 30 mN/m. The *z* scale is 10 nm for all images (see color bar) except image *a*, which is 5 nm.

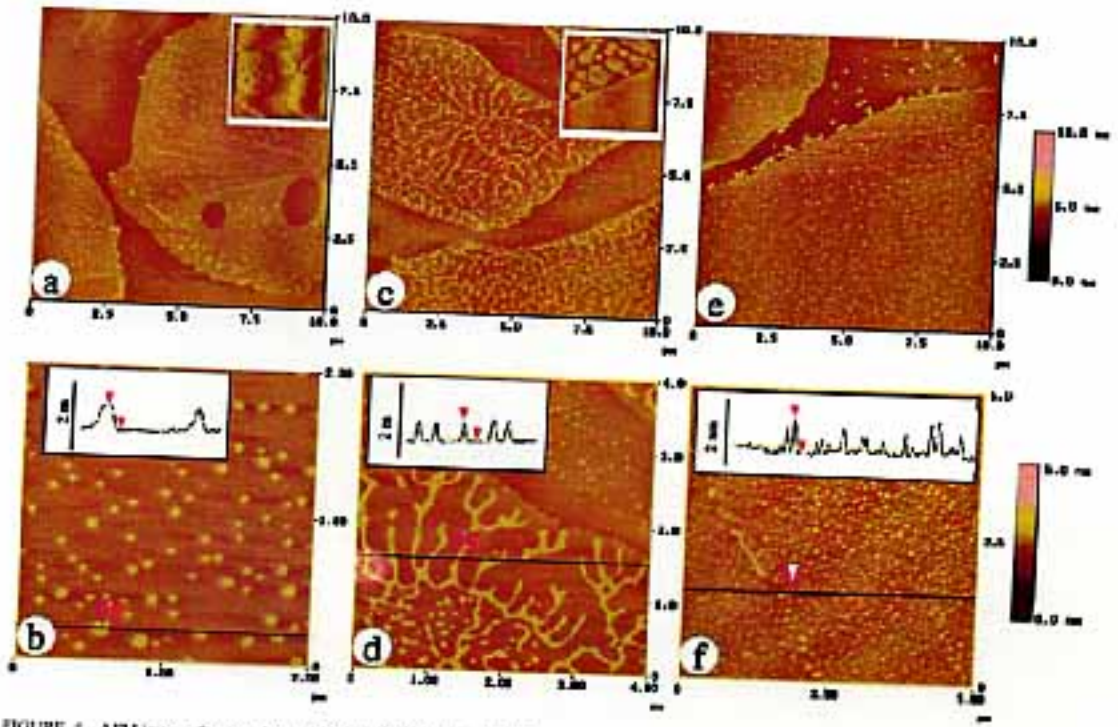

FIGURE 4 AFM images for monolayers of SPM/DOPC/cholesterol (1:1:1) with 1% GM1 (*a*, *b* at 10 mN/m, and *e* at 30 mN/m) and 5% GM1 (*c*, *d* at 10 mN/m, and *f* at 40 mN/m). The insets in *a* and *c* are large-scale images (40 × 40 μm²) for the same sample. The *z* scale (see color bar) is 5 nm for *b*, *d*, and *f* and 10 nm for *a*, *c*, and *e*. Section analyses (for the solid line on the images) are shown as insets in *b*, *d*, and *f*; the *x* scale for the inset is the same as that for the image.

The Size of Lipid Rafts: An Atomic Force Microscopy Study of Ganglioside GM1 Domains in Sphingomyelin/DOPC/Cholesterol Membranes

Chunbo Yuan, Jennifer Furlong, Pierre Burgos, and Linda J. Johnston
Steacie Institute for Molecular Sciences, National Research Council of Canada, Ottawa, Ontario K1A 0R6, Canada

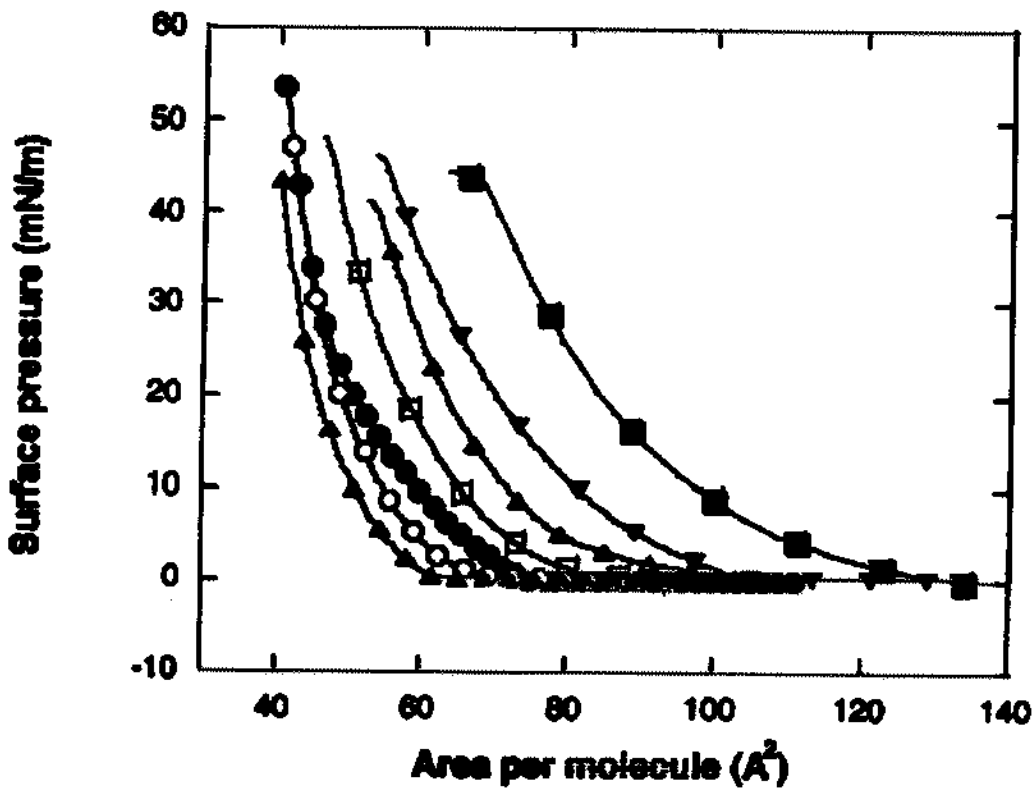

FIGURE 1 Surface pressure-area isotherms for SPM (●), DOPC (■), SPM/DOPC (1:1) (▼), SPM/DOPC (1:1) mixtures with 10% (△), 20% (□), and 33% (○) cholesterol, and a SPM/DOPC/cholesterol (1:1:1) mixture with 5% GM1 (▲).

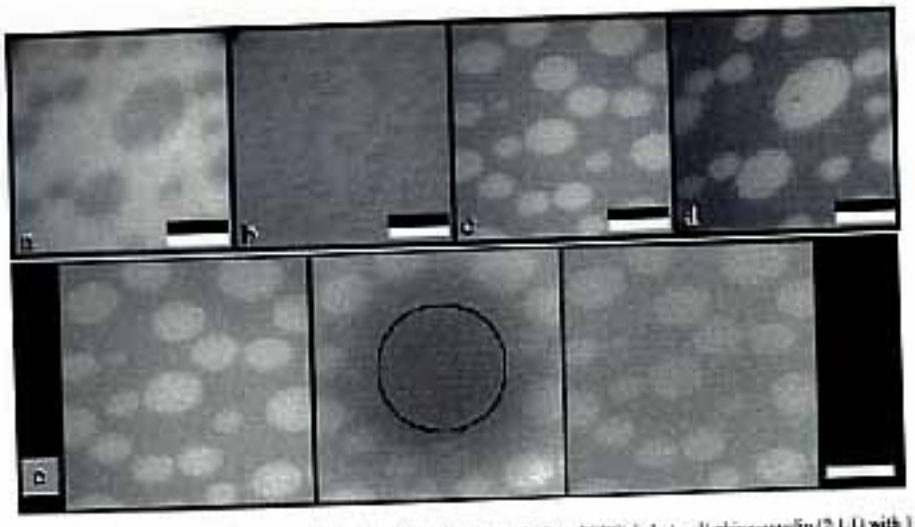

FIGURE 4 Fluorescence micrographs of planar supported phospholipid bilayers made from POPC/cholesterol/sphingomyelin (2:1:1) with 1 mol % GM1 (distal to glass support) and egg PC (proximate to glass support). Only distal lipid layers contain fluorescent lipid dyes. (*a*) 0.1 mol % TR-DHPE; (*b*) 0.5 mol % FL-DPPE; (*c*) 0.5 mol % NBD-DPPE; (*d*) FL-CTB. Note that images *a* and *d* were obtained from the same bilayer preparation, which was double labeled with TR-DHPE and FL-CTB (for 10 min at 1 μg/ml in PBS). Bars, 10 μm. (*e*) Fluorescence from NBD-DPPE equilibrates between liquid-ordered and liquid-disordered regions (*left*) before photobleaching; (*middle*) after 4 min of continuous photobleaching; (*right*) after 4 min of recovery. The circle in the central panel indicates the size of the field stop during the bleaching period. To achieve a significant bleaching rate, neutral density filters in the illumination path of the HBO100 were removed during bleaching. Bar, 10 μm. All images were recorded at room temperature (24°C).

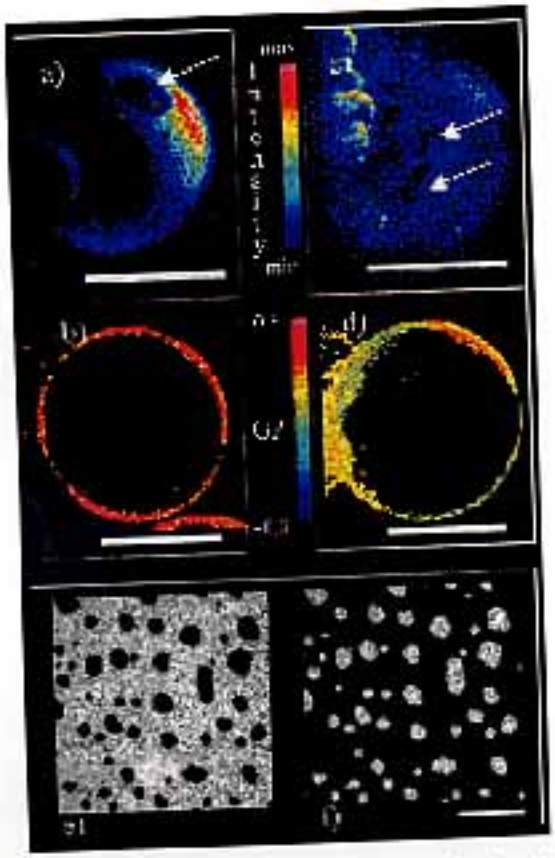

FIGURE 7 Two-photon fluorescence images of polar sections (*a* and *c*) and GP images of equatorial sections (*b* and *d*) of LAURDAN-labeled GUV formed from extracted brush border membrane lipids with cholesterol present (*a* and *b*) at 28°C or with cholesterol extracted (*c* and *d*) at 15°C (see Materials and Methods). Bars, 50 μm. (*e* and *f*) Planar supported BBM monolayer with 0.2 mol % TR-DHPE and 1 mol % GM1 after incubation with FL-CTB (1 μg/ml in PBS for 15 min) as observed in rhodamine channel (*e*) and fluorescein channel (*f*). Bar for planar supported lipid layer is 10 μm.

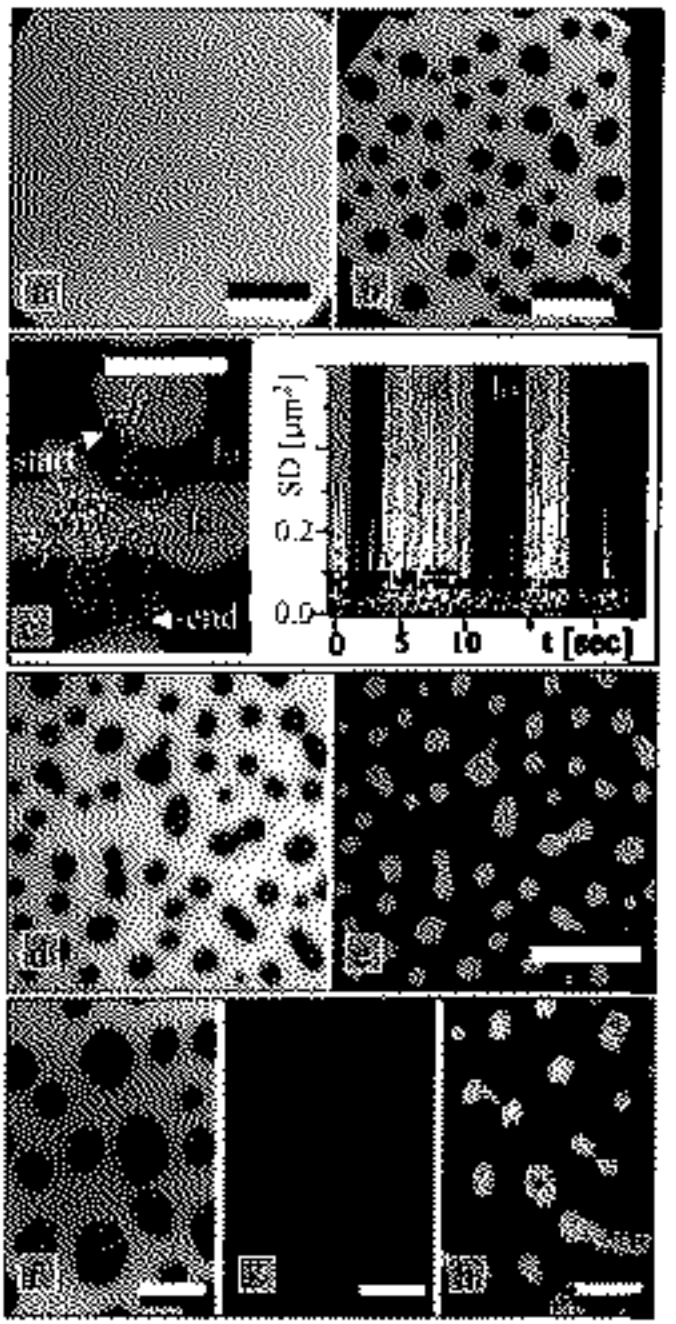

FIGURE 3 Fluorescence micrographs of phospholipid monolayers supported by alkylated glass substrates at room temperature (see Materials and Methods). (*a*) Non-salt mixture (DOPC/cholesterol 2:1); (*b*) Salt-mixture (DOPC/cholesterol/sphingomyelin 2:1:1). Both contain 0.1 mol % FL-DPPE. (*c*, *left panel*) DOPC/cholesterol/sphingomyelin 1:1:1 containing 0.5 mol % FL-DPPE and 1 mol % Cbl1 with overlaid trajectory of gold particle (*D* 40 nm) as visualized by SPT (Sonnen and Joos, 2006). Cbl1 was functionalized to bind specifically to FL-DPPE lipid analogs that are enriched in the liquid-disordered (ld) lipid phase and appear bright in the fluorescence image while being depleted from the liquid-ordered (lo) phase (see text). (*Right panel*) Squared jump distance (SD) between successive video frames ($\Delta t = 33$ ms) for a trajectory. The fluorescence image provided separation between parts of the particle trajectory pertaining to the two different lipid phases. Trajectory analysis (see Materials and Methods) for this particle yielded $D_{ld} = 1.1 \times 10^{-8}$ cm²/s and $D_{lo} = 0.33 \times 10^{-8}$ cm²/s. (*d* and *e*) Double-stained POPC/cholesterol/sphingomyelin (2:1:1) phospholipid monolayer containing 1 mol % Cbl1 and 0.1 mol % TR-DPPE after a 10-min incubation with FL-CTB (1 μg/ml in PBS) as observed in rhodamine channel (*d*) and fluorescein channel (*e*). (*f–h*) DOPC/cholesterol/sphingomyelin (1:1:1) containing 1 mol % Cbl1 with 0.5 mol % FL-DPPE as observed in fluorescein channel, before (*f*) and after (*g*) a 30-min incubation with detergent solution (0.2% Triton X-100 in PBS); *h* shows sample after a post-extraction incubation with FL-CTB (1 μg/ml in PBS for 10 min). With the exception of *c* (3 μm), all scale bars are 10 μm. All experiments were conducted at room temperature (24°C).

Lipid Rafts Reconstituted in Model Membranes

C. Dietrich,* L. A. Bagatolli,[§] Z. N. Volovyk,[‡] N. L. Thompson,[†] M. Levi,[¶] K. Jacobson,*[‡] and E. Gratton[§]

*Department of Cell Biology and Anatomy, [†]Department of Chemistry, and [‡]Lineberger Comprehensive Cancer Center, University of North Carolina at Chapel Hill, Chapel Hill, North Carolina 27599; [§]Laboratory for Fluorescence Dynamics, Department of Physics, University of Illinois at Urbana-Champaign, Urbana, Illinois 61801; and [¶]Department of Medicine, University of Texas Southwestern Medical Center at Dallas and Veterans Administration Medical Center, Dallas, Texas 75216 USA

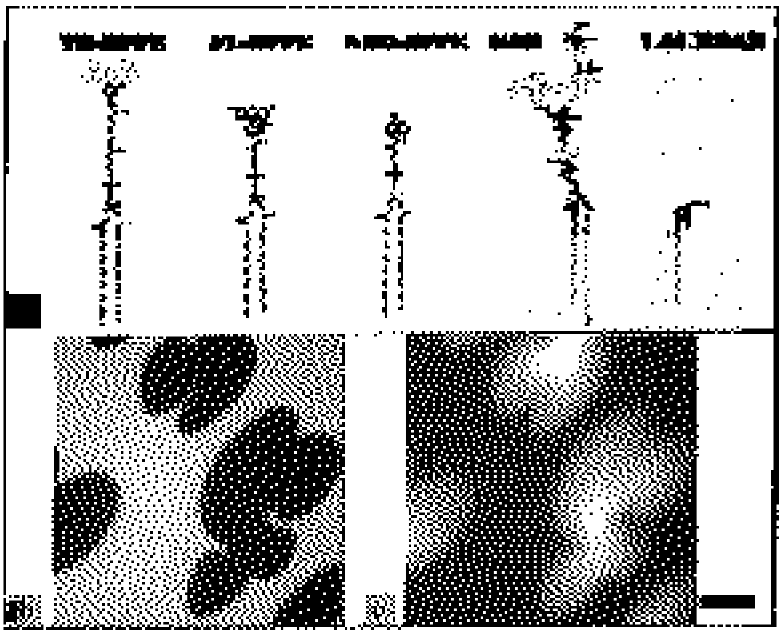

FIGURE 1 [illegible]

CONCLUSIONS

- Aβ40 inserts into lipid membranes under physiologically relevant conditions, and the amount of insertion decreases with increasing surface pressure.
- Monolayer morphology changes drastically after Aβ40 injection even under conditions with no observable trough expansion (apparent insertion).
- Lipid membranes need not be acidic for Aβ insertion: positively charged DPTAP and negatively charged DPPG show similar insertion profiles. Therefore,electrostatics may not be the driving force for peptide insertion.
- Aging the peptide promotes insertion.
- Dissolving Aβ40 in the solvent DMSO causes up to a 40 minute delay in Insertion in pure water at high pressures (>=25 mN/m) and changes the insertion profile.
- Supported bilayers retains their fluidity and can be imaged by AFM.
- Lateral phase separation in bilayers can be detected.
- Aβ fibril shows helicity; modified with PEG do not form cross-mesh.
- Incubation with lipid vesicles leads to formation of protofilament on membrane surface.
- GIXD results confirms the disruption of condensed phase in lipid layer.

INSERTION PROFILE OF AGED Aβ40 INTO A DPPG MONOLAYER

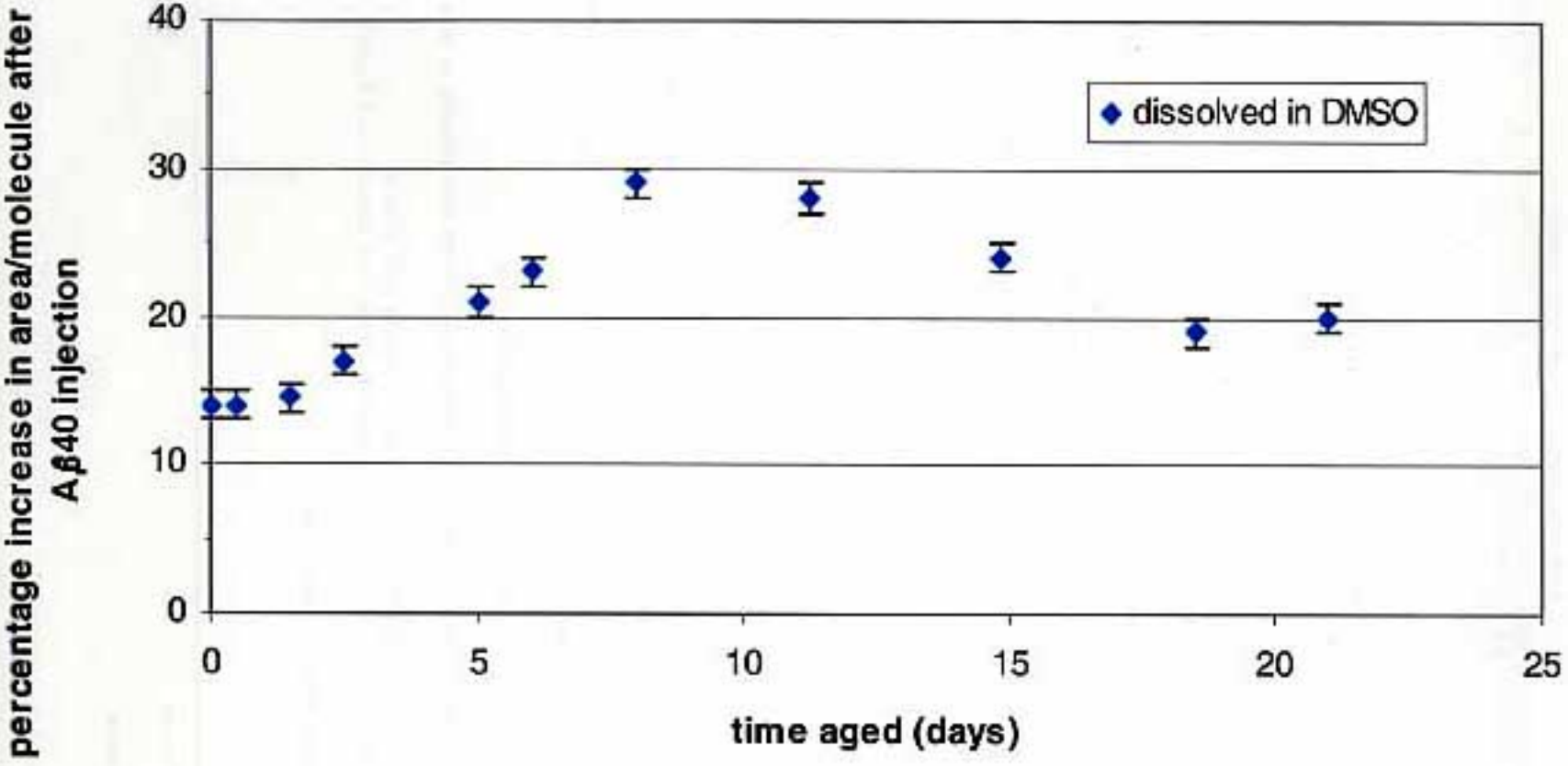

T=30 ºC. Peptide concentration while aging was 12 μM (just below the CMC). Peptide concentration in the subphase *after* injection is 250 nM. Subphase is pure water.

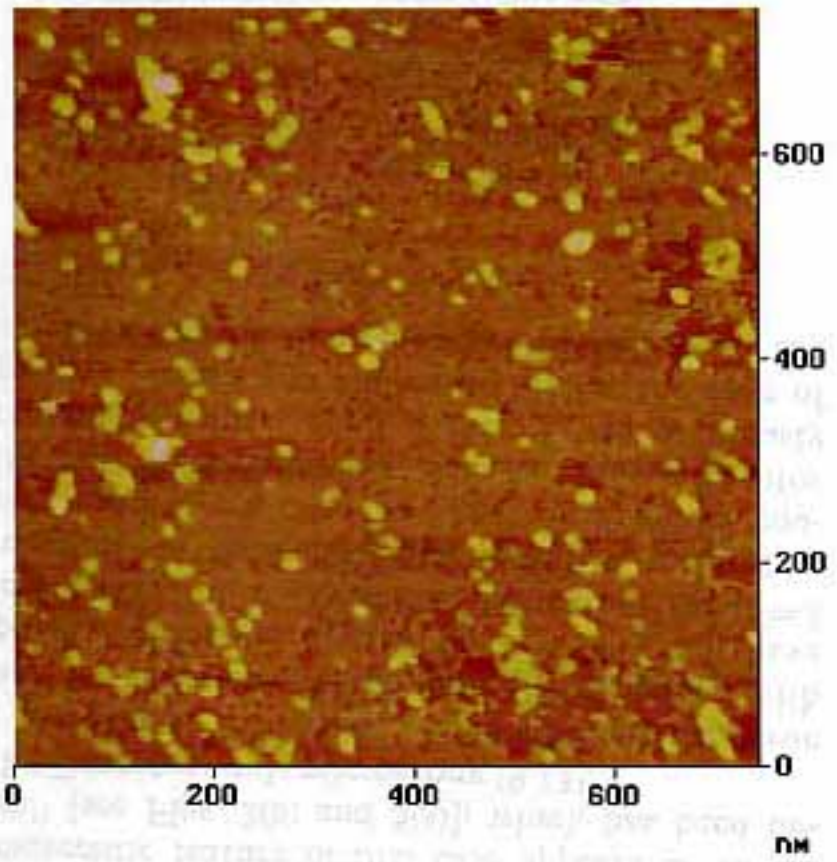

Aβ incubated in a solution of DOPC/GM1/Aβ 9/1/1 molar ratio for one day. Aβ concentration= 60μM. Vesicle concentration Pores on the membrane can be seen together with structures that resemble Aβ protofibrils.

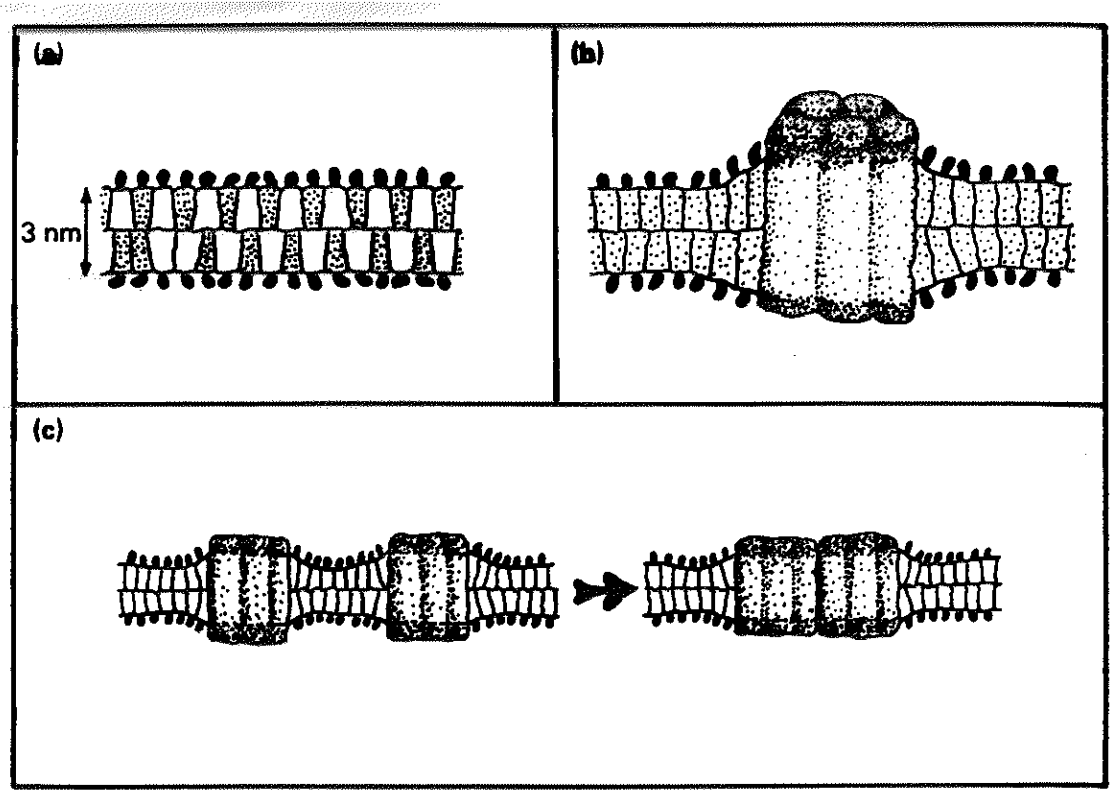

Fig. 17.7. (a) Mixture of two different lipids packing together within a planar membrane. The shaded lipids are cone-shaped ($v/a_0 l_c < 1$); the white lipids are wedge-shaped ($v/a_0 l_c > 1$). (b) Packing constraints induced in the hydrocarbon chain regions of lipids around a protein molecule, which may be relaxed when proteins aggregate, as shown in (c).

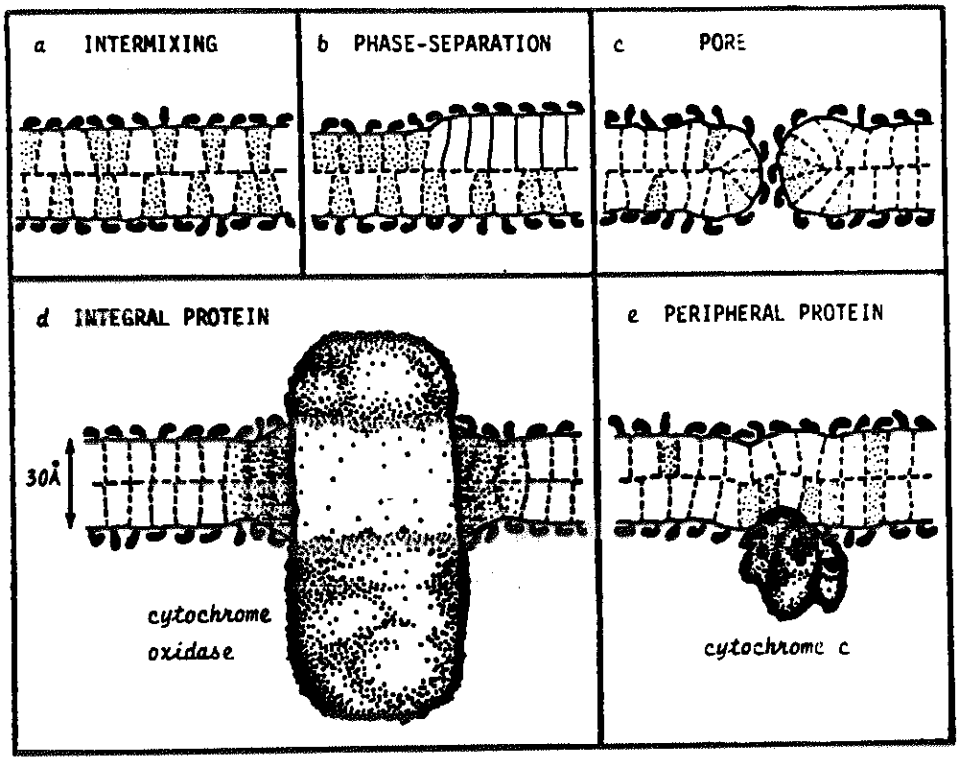

Fig. 17.9. Mean packing conformations of mixed lipid and lipid-protein membranes, showing how local packing stresses may cause clustering of specific lipids and/or non-bilayer shapes (shaded lipid regions). All the figures have been drawn to scale. Note the relatively large size of the cytochrome oxidase protein molecule which protrudes greatly from the bilayer. (From Israelachvili *et al.*, 1980a.)

Fig. 17.8. Schematic figure of a biological membrane. The lipid contents of different membranes vary from as little as 25% up to 80% by weight. At highly curved regions the outer convex face contains mainly cone-shaped lipids while the inner concave face has more wedge-shaped lipids. Note how stressed regions may adopt a locally non-bilayer structure, some of which are shown in more detail in Fig. 17.9

Fig. 17.9. [illegible]
how local
(shaded li
of the cyt
Israelach

may be
exampl
of rhod
can be
Lewis
membr
(Siegel
A bi
protein
Nichol
lipids
for the
a cell
main
lipid
indivi
organ
temp

Supported Bilayers

Dyn. + structural properties studied by

- FTIR
- NMR
- TIRF
- X-ray scattering
- neutron scattering
- lateral diff. measurements
- imaging ellipsometry
- reflection interference contrast microscopy
- SFA

Bilayer on beads → NMR

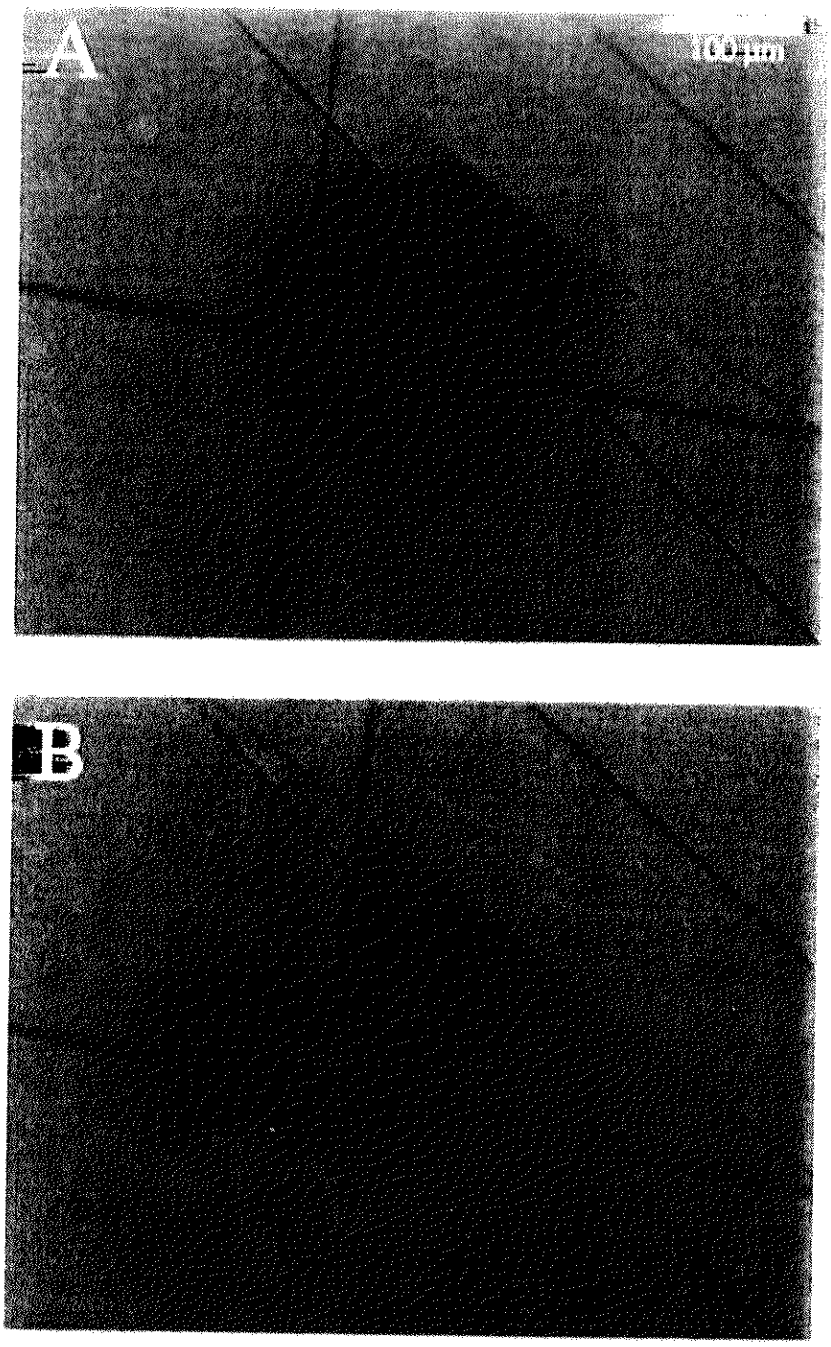

FIGURE 6: (A) Photograph of fluorescence from supported bilayers containing RCs on glass. The mole ratio of RC:lipid in the sample shown is about 1:700. One mole percent of Texas Red DHPE was used as the fluorescent lipid. The sharp dark lines are scratches in the lipid bilayer surface that create physical boundaries to lateral diffusion of the lipids. Prior to being scratched, the surface appeared homogeneous. A circular region of the lipid was shadowed out by the microscope aperture and photobleached with the excitation light. (B) The same field of view 20 min after photobleaching. The photobleached area now fills the central bounded triangular region; other unbounded regions outside the triangle have recovered a substantial amount of fluorescence, as long-range lateral diffusion of fluorescent and photobleached lipid leads to mixing. These results demonstrate that the lipid component is freely diffusing in two

cysteine-reactive fluorescent rh
for imaging the protein compo
These supported bilayers were
PE instead of the Texas red l
the fluorescence spectrum of
of R-492. The fluorescence ir
supported bilayers is uniform
and exactly matches the scrat
dye–lipid probe for a given
fluorescence intensity were r
following bleaching of a rou
Unlike the lipids described abc
diffusion on this time scale. I
protein components in a nat
between 1 and 5 $\mu m^2/s$ (Genn
in the supported bilayers are

An identical experiment v
capsulatus RC mutant (M)18
cent dye R-492. This experir
tigate whether the lack of mol
Rb. sphaeroides RCs might b
the fluorescent label and the
The engineered cysteine is e
surface cysteine (H-156 cy
capsulatus RC) from a consid
of the *Rb. sphaeroides* RC an
with the *Rb. capsulatus* RCs
verified experimentally, as the
has a molar ratio of dye to R
engineered cysteine is situate
c, on the opposite side of the
mobility of these RCs was ot

DISCUSSION

Our goal in this work was
oriented RCs on a solid supp
that RC-containing proteolip
preformed SUVs in a highl
cytochrome *c* binding site faci
with the result reported by Sa
substantiated by the biotin labe
with the cyt *c* binding experim
is genuinely oriented in a tran

The RCs remain oriented ir
cytochrome *c* binding site f

FIGURE 1

A.

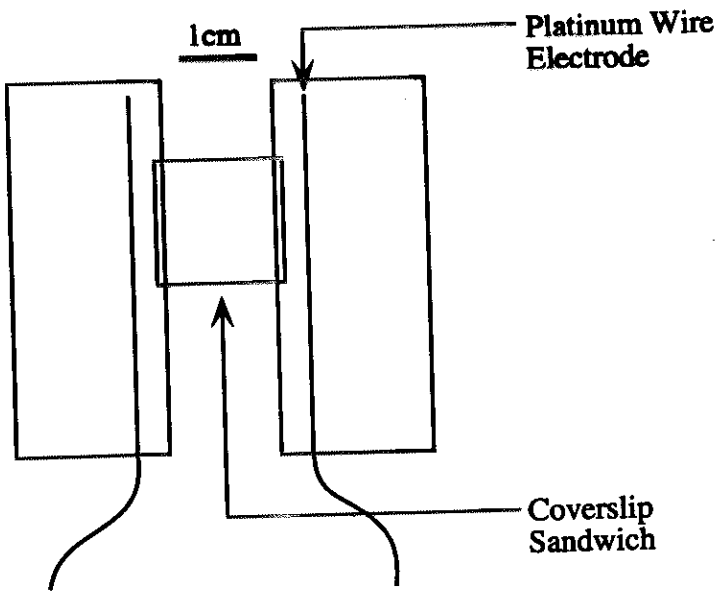
1cm
Platinum Wire Electrode
Coverslip Sandwich

B.

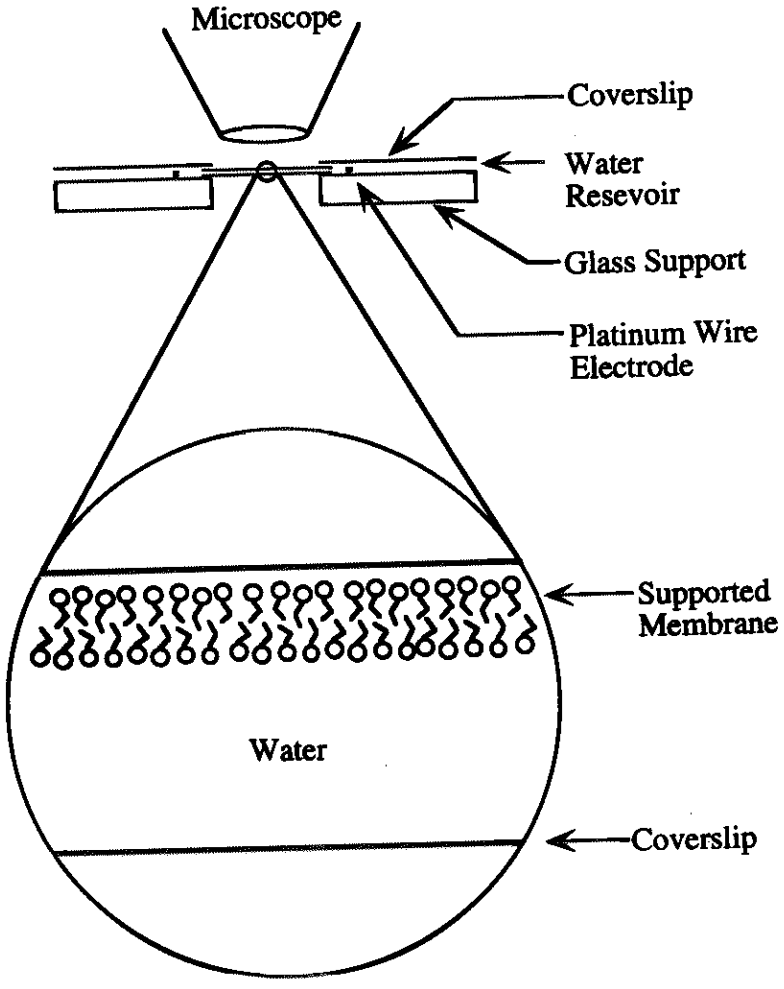
Microscope
Coverslip
Water Resevoir
Glass Support
Platinum Wire Electrode
Supported Membrane
Water
Coverslip

FIGURE 1
Groves et al.

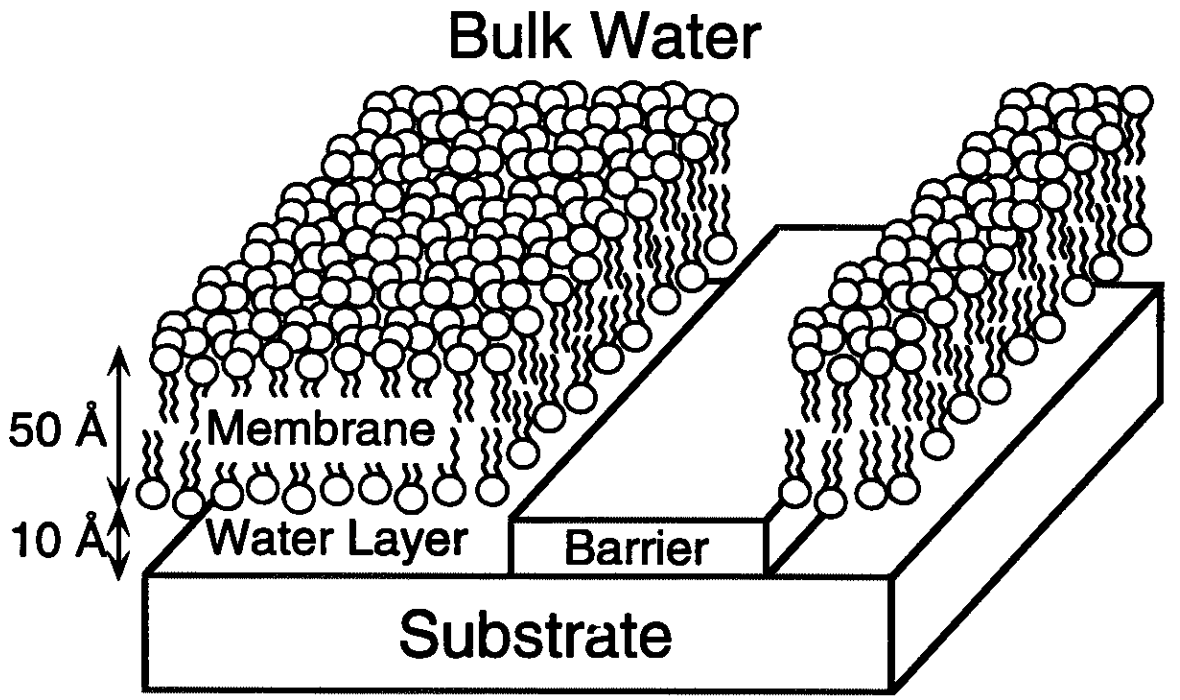

FIGURE 1
Groves et al.

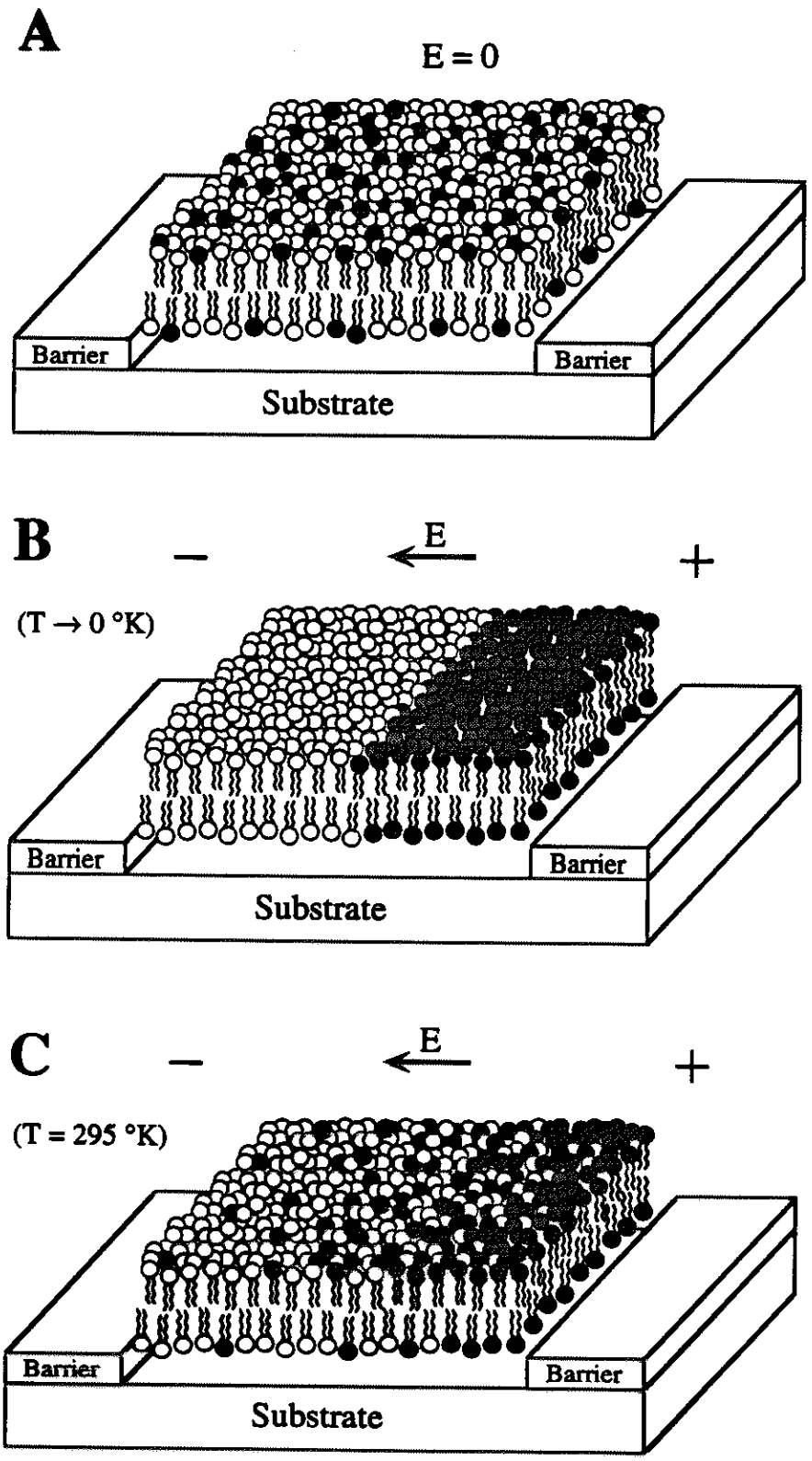

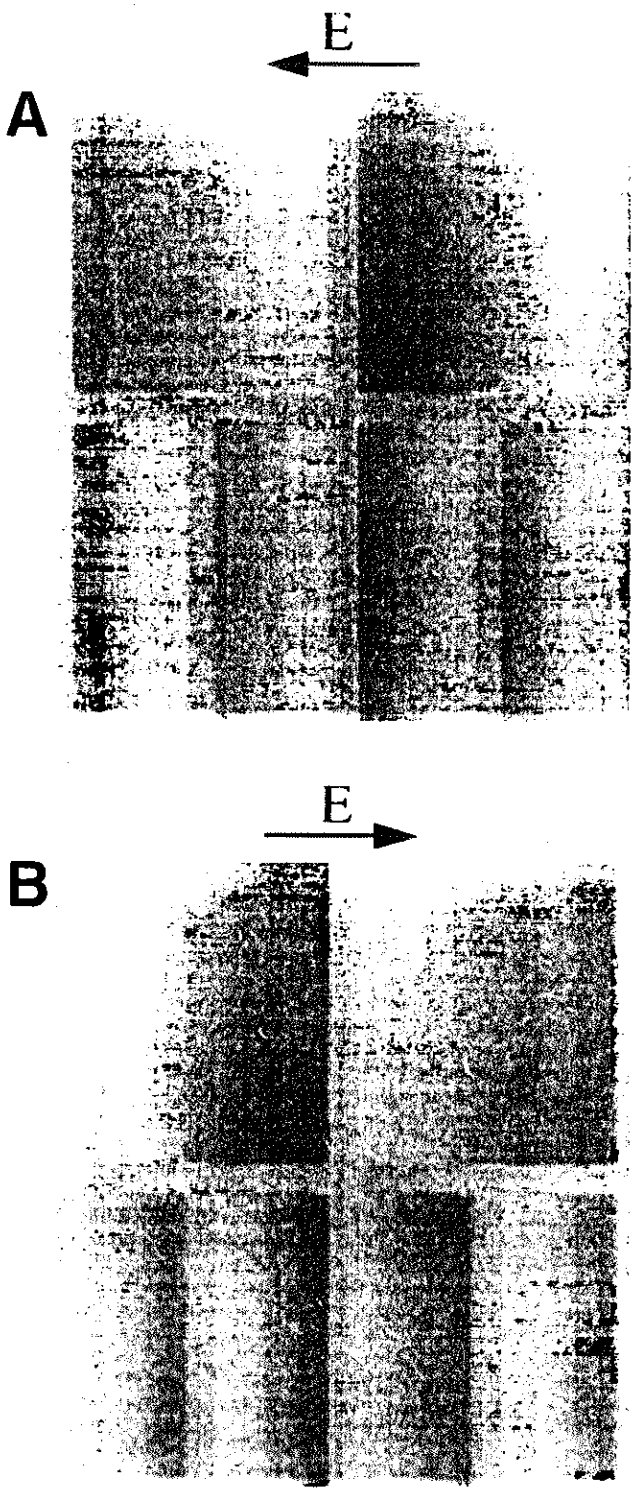
E
A
E
B

Functionalization of Solid Surface

For anchoring polymer

Mixed monolayer of long chain surfactant
exhibiting final head group - binding
& alcohol - non binding

Immobilizat^{n} of protein
Streptavidin - biotin

functionalizing deposited membrane
incorp receptor receptor

Reversible coupling
Chelating lipid
w/ divalent ions : His tag binds
w/out " " : detached occurs
(EDTA)

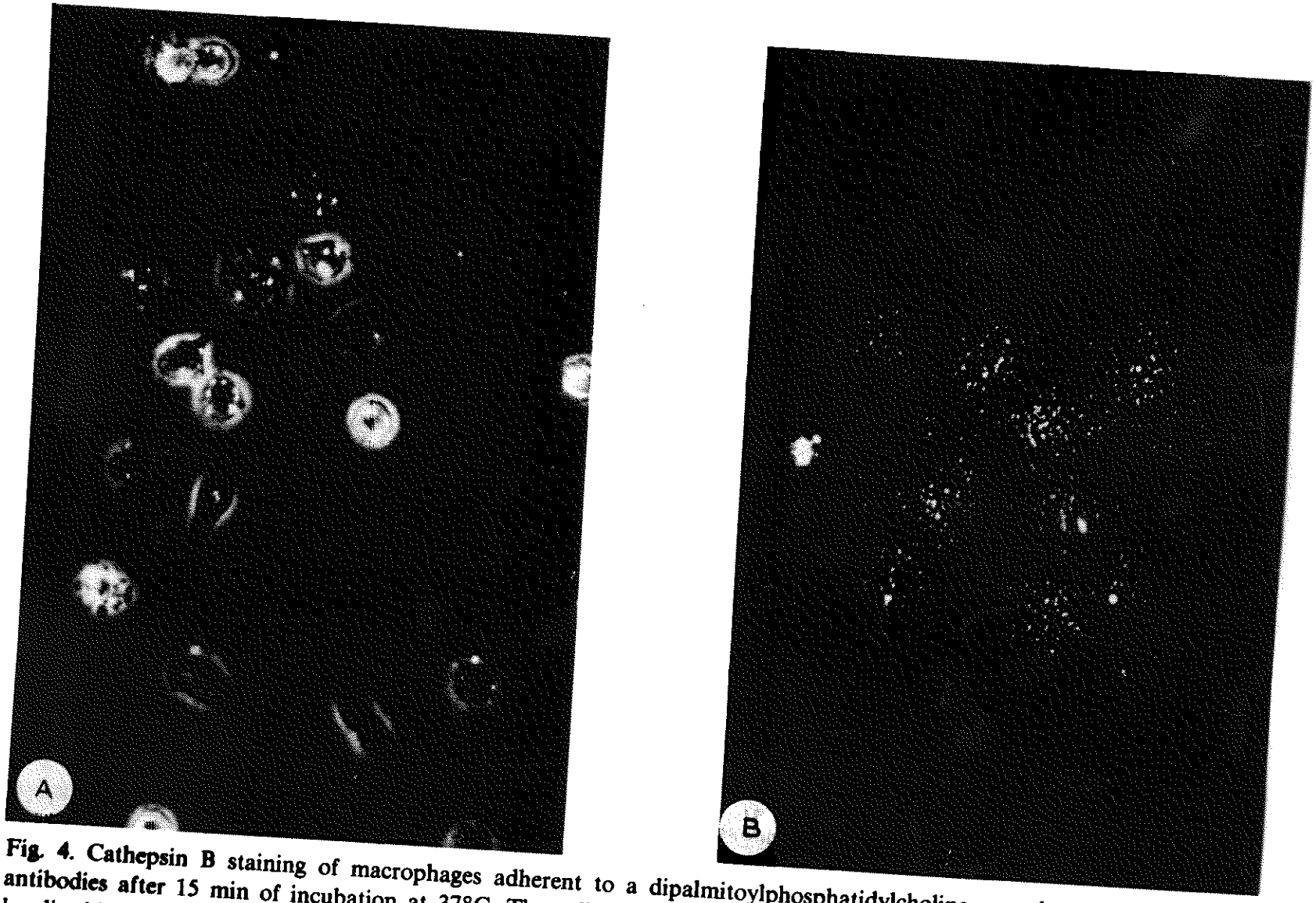

Fig. 4. Cathepsin B staining of macrophages adherent to a dipalmitoylphosphatidylcholine monolayer with lipid-hapten-bound antibodies after 15 min of incubation at 37°C. The yellow-orange granules of fluorescent precipitate formed by the enzyme are localized both inside the cells and outside the cells (associated with the monolayer). (A) Combined phase contrast and epifluorescence photomicrograph taken in the median focal plane of the cells. (B) Epifluorescence photomicrograph taken in a focal plane between the monolayer-coated cover glass and adherent macrophages, showing accumulation of fluorescent precipitate. From Hafeman et al. [29].

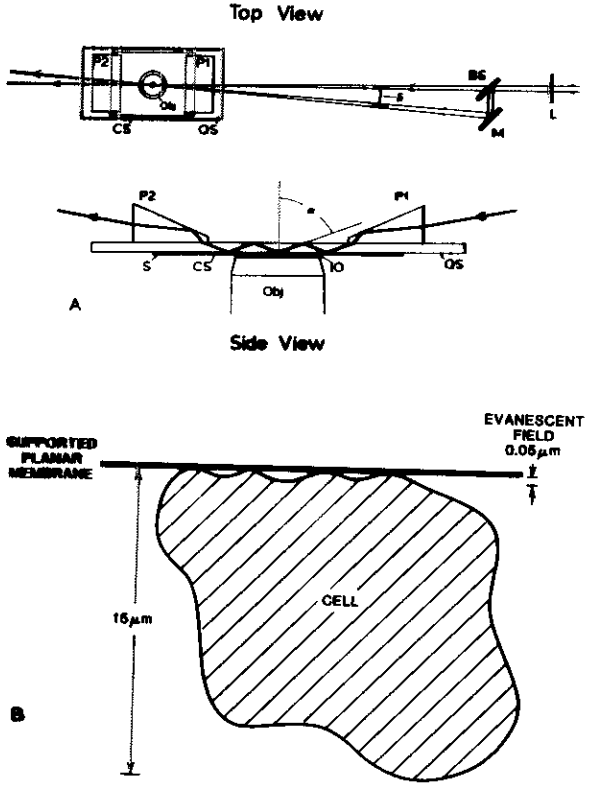

Fig. 5. Evanescent illumination of supported planar membranes. (5A) Apparatus for producing an evanescent radiation field so as to stimulate fluorescence of molecules that are within 100 nm of the lipid monolayer coating the lower surface of the quartz microscope slide (QS). The prisms P1 and P2 are used to introduce and remove the vertically polarized laser beam. Cells are bound to the monolayer on the lower surface of the quartz slide, and are bathed in cell buffer localized between the monolayer and a coverslip (CS). A spacer (S) maintains a fixed distance, 24 microns, between the quartz slide and the coverslip. An objective lens with immersion oil (IO) is used to view cells bound to the monolayer. The top view shows the setup employed to produce an interference pattern in the evanescent wave field; the beam splitter (BS) divides the beam into two beams of equal intensity, and the mirror (M) directs one beam so as to produce an interference pattern over the objective lens of the microscope. Taken from

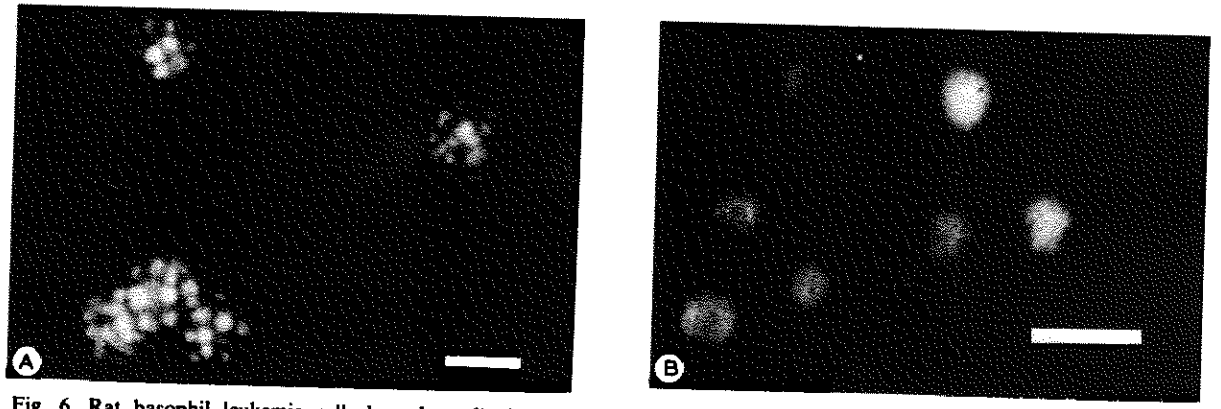

Fig. 6. Rat basophil leukemia cells bound to dipalmitoylphosphatidylcholine monolayers containing two mol% dinitrophenyl lipid-hapten. The scale bars are 25 μm. Before binding to the monolayer membranes, cells were incubated with either fluorescein-labelled monoclonal anti-dinitrophenyl-IgE (6A) or 1 : 1 anti-dinitrophenyl-IgE : fluorescein-labelled rat myeloma IgE (6B). Cells were illuminated by total internal reflection as described in Fig. 5. Monoclonal anti-dinitrophenyl-IgE (clone 26.82, [41]) was obtained from F.T. Liu and D.H. Katz, Scripps Clinic and Research Foundation, La Jolla, CA. Rat myeloma IgE was obtained from Henry Metzger, National Institutes of Health, Bethesda, MD. The rat basophil leukemia cells were incubated with the monolayers in complete cell buffer: 135 mM NaCl/5 mM KCl/1 mM $MgCl_2$/1.8 mM $CaCl_2$/5.6 mM glucose/0.5 mg per ml gelatin/10 mM 4-(2-hydroxyethyl)-1-piperazineethanesulfonic acid at pH 7.2.

would have been very difficult to reach using conventional cell culture techniques.

Supported planar membranes containing H-2K^k, prepared by the method shown in Fig. 3, were more effective in inducing secondary cytotoxic responses in vitro, than the small unilamellar vesicles from which the supported planar membranes were prepared [18]. In addition, through the use of supported planar membranes, in this case made from vesicles containing H-2k^k spread at an air-water interface, it has been possible to show that cloned cytotoxic T cells bind specifically to target membranes containing only purified allo-antigen [37]. The T cell clone used in these studies was derived from conventional mixed lymphocyte culture, and selected on the basis of its cytotoxicity for H-2K^k-bearing target cells.

The phenomenon of recognition of allo-antigen

the generality of this model for allo-recognition follows from the fact that T cells, which were selected only on the basis of their cytotoxicity for target cells bearing the usual assortment of cell-surface proteins, bind planar membranes containing only the allo-antigen.

In general, it has been difficult to stimulate helper T cell responses with small unilamellar vesicles. Curman et al. [16] were able to stimulate a secondary mixed lymphocyte reaction using partially purified I-A in phospholipid vesicles. The only report of an antigen-induced class II restricted T cell response to purified major histocompatibility complex molecules in liposomes is by Walden et al. [17]. In these experiments, antigen was covalently linked at high concentrations to the target liposomes. We have used affinity purified I-A^d and peptide antigen

Polymer-induced forces

- rep. if anchored to membrane/interface.
- if entangle is possible
  - repulsive @ large dist.
  - attractive @ short "

Dynamic membrane roughness

- determined by out-of-plane motions of lipids

  2-3 Å

- thermally excited membrane undulations can create pronounced bending modulations with amplitudes ~ 10 μm

Undulation forces control cell adhesion, flickering - shape fluctuations

- prevents rigidity
- cell aging
- strong undulation ~ 100 nm from surface coupling them specific short-range forces repulsive long range dispersing pressure.

tayered Membranes as Electrooptical Biosensors

Bilayer used as

① a very thin electrical insulator

② a matrix for incorporation of receptor

③ suppression of nonspecific ligand binding

Support: gold on SnO_2/ZnO_2 or metal oxide.
semiconductor (MOSFET)

ligand binding: Capacitance
Current
measurements

Impedance Spectroscopy

C_m: ε
d_m
surface charge
d_s

- SPR (1.3 - 1.8 μm) water + silicon absorpt
- Surface acoustic waves

- lateral distribute of membrane-bound ligands may be organized by 2D electrophoresis
→ separate bounded + free receptors

(ii) as a matrix for the incorporation of receptors (such as lipid-coupled antigens or antibodies), and (iii) for the suppression of nonspecific ligand binding. For electrical monitoring of ligand binding, the supports can consist of gold-covered or SnO_4/InO_4–covered supports or metal-oxide-semiconductor (field-effect transistors; MOSFETs), and ligand binding can be recorded by capacitance or current measurements.

The capacitance C_m of (supported) lipid-protein bilayers depends in a complex way on the dielectric constant and thickness d_m of the layer, the surface charge of the lipid bilayer and integrated proteins, and the distance between bilayer and support. The receptor surface may be characterized in terms of an effective (dielectric) thickness d^{ϵ}_{eff}. Ligand binding leads to a change in dielectric thickness of $\delta d^{\epsilon}_{eff} = \delta C_m/C_m^2$, indicating that very thin insulating layers are required to achieve high sensitivities.

Fortunately, the different contributions to the membrane impedance can be determined by analyzing the frequency dependence of the complex impedance Z_m of the membrane over a large range of frequencies (Fig. 5A). One convenient way is to measure the absolute value of Z_m and the phase shift Φ (Fig. 5B) and to simulate these so called "Bode plots" by assuming various equivalent circuits to decide which contributions C_i and R_i contribute and to deter-

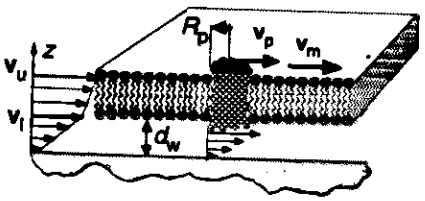

Fig. 4. Velocities and frictional coupling between opposing monolayers of membrane and between the inner monolayer and a rigid wall: $\mathbf{v}_p$, instantaneous velocity of the diffusing particle; $\mathbf{v}_m(z)$, the z-dependent velocity induced within the bilayer by the diffusant [changing from $\mathbf{v}_u$ to $\mathbf{v}_l$ (upper to lower)]; and d_w, thickness of the lubricating film. The velocity gradient in the lubricating film between the inner monolayer and the wall is v_l/d_w. Surface and bulk viscosities of polymer films can be measured by comparison of the diffusion of probes of different head-group structure (*2*, *4*).

$\Theta > 0.97$ (*13*). The sensitivity achieved by electrical detection with such high-quality integrated membranes corresponds to 10^{11} receptors per square centimeter or to a minimum detectable mass of 10^{-9} g/cm^2.

The sensitivity could be improved in various ways. With FET transistors as measuring devices, the active sensor area could be reduced. More-sensitive devices could be used, such as the heterogeneous Si-Ge transistors (*16*), because the conductivity of these 2D electron conductors is extremely sensitive to changes in the surface charge. Another promising strategy is to use interdigitated arrays of microelectrodes with submicrometer electrode distances (*17*). To achieve sensitivities similar to enzyme-linked immunosorbent assays, one would have to develop enzymatic amplification

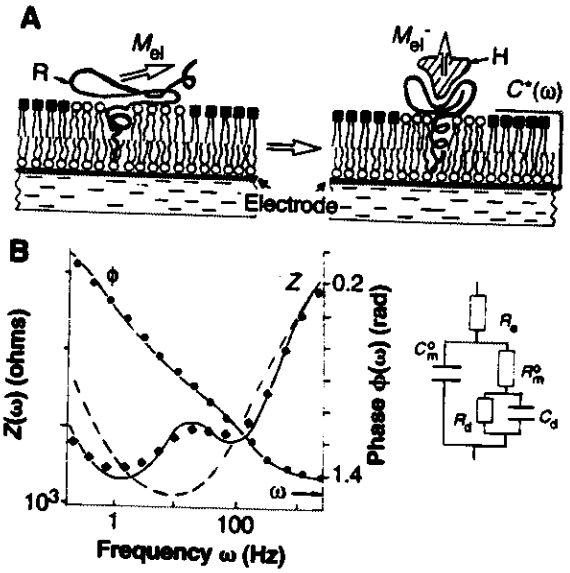

Fig. 5. Supported membranes as biosensors. (**A**) Detection of binding of ligand H to receptor R by complex capacitance (C^*) measurements (impedance spectroscopy). The capacitance C_m of the receptive layer is determined by its average thickness d_m and its dielectric constant ϵ_m, which depends on the electric dipole moment of receptor R (M_{el}, electric dipole moment of the head group of R). An effective electric thickness may be defined as $d^{el}_m/\epsilon_m = \epsilon_0 A/C_m$ (A = area of sensitive layer). (**B**) Evaluation of impedance spectra by equivalent circuits. Bode plots (data points) of frequency dependencies of absolute values of complex impedance Z^* and of the phase shift $\phi(\omega)$ (ω, angular frequency) over a large frequency regime are simulated by equivalent circuits (solid line). Dashed line shows large effect on $Z(\omega)$ if defect capacitance is ignored. R_e, resistance of the electrolyte.

Supported Membranes as Phantom Cells

interplay of specific & universal forces

polymer-induced forces (esp.)

dyn. repulsive forces

- areal density of receptor
  → control lock & key interaction
- cell adhesion in immunological response
  MHC replace antigen presenting cells
  to stimulate T helper cells

Polymer-Lipid Composite Films

- Reconstitute of membrane spanning proteins & the recog. of receptors by 2D electrophoresis
- Study mobility of membrane proteins coupled to macromolecular network
- mimic cytoskeleton & polymer cushions (slightly cross-linked)
  eg. like spectrin-actin network.

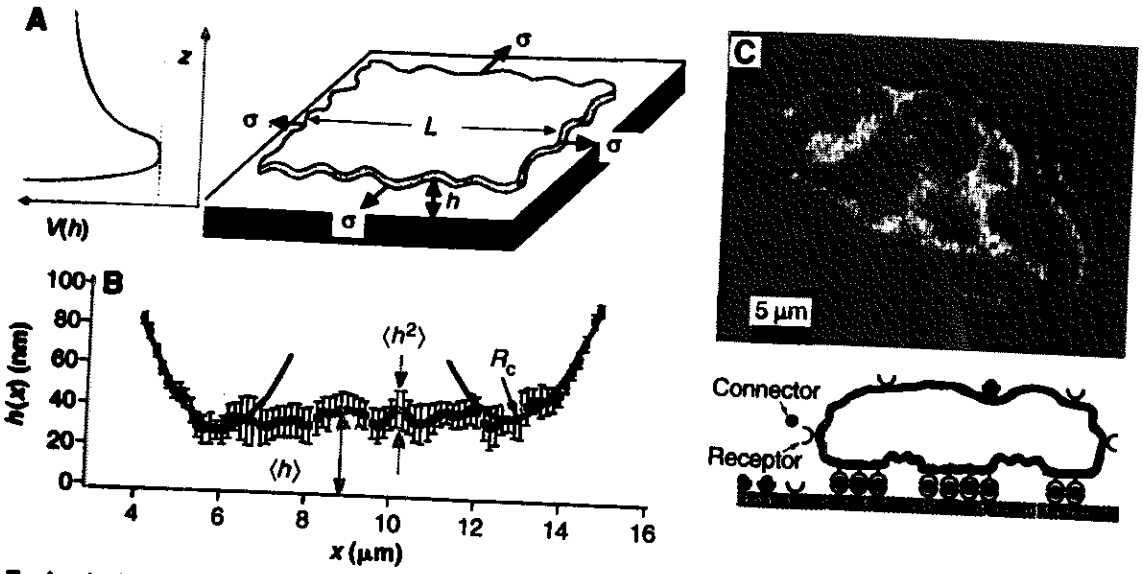

Fig. 7. Analysis of undulation forces between lipid vesicle and rigid wall. (**A**) Schematic view of a dynamically rough piece of membrane of dimensions L by L at distance h above the solid surface with lateral tension σ. The excitations may be decomposed into plane-wave Fourier modes. The effect of the wall is represented by an interfacial potential $V(h)$. (**B**) Representation of parameters characterizing weakly adhering vesicles simultaneously measurable by RICM. These include (i) mean distance $\langle h \rangle$ (~400 Å), (ii) mean square amplitude $\langle h^2 \rangle$ (~20 nm^2), (iii) lateral tension (σ ~ 0.001 mN/m), (iv) force constant of potential $\partial^2 V/\partial Z^2$, (v) contract curvature R_c, and (vi) spatial correlation function of undulation amplitude $u(x)$ (*27*). (**C**) RICM visualization of a dimyristoyl phosphatidylcholine (DMPC) vesicle containing 1 mol % biotin-labeled lipid as the receptor interacting with a surface covered by streptavidin. The formation of adhesion plaques is caused by interplay of the strong attraction between receptors and the repulsive undulation forces.

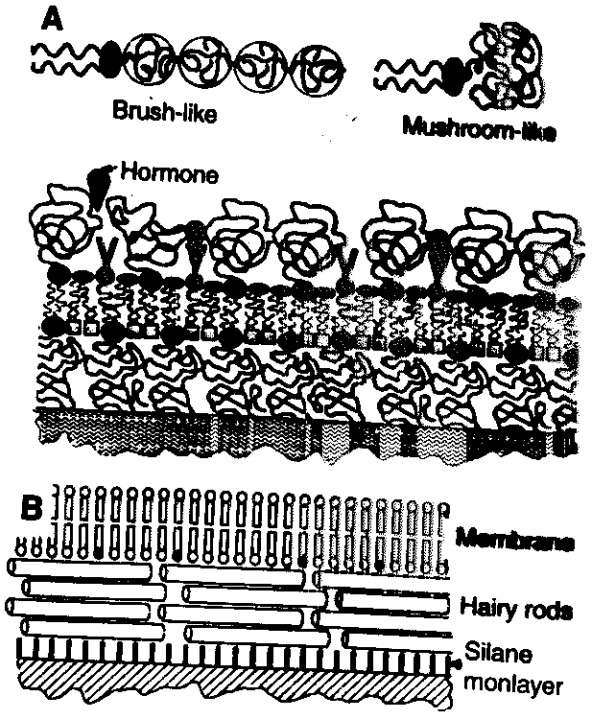

Fig. 8. (**A**) Separation of a bilayer from substrate by stealths formed by (clusters of) polymer brushes (or mushrooms) of hydrophilic polymers (for example, polyethyleneoxide grafted to long-chain lipids). Also shown is the formation of artificial glycocalix on the outer monolayer by the mixing of phospholipids, lipid-coupled receptors, and lipopolymers. (**B**) Membrane deposition on ultrathin layers of hairy rods prepared by the LB technique from hydrophobic hairy rods (cellulose-derivatives), which are hydrophilized by shaving of hydrophobic hairs in HCl vapor.

by increasing the tension, a transition from a weakly to a strongly bound state may occur and one may therefore speak of tension-induced adhesion (*33*). Transitions between free and bound states may arise if swelling is induced in vesicles or cells, leading to an increase of the lateral tension.

The remarkable strength of undulation forces is demonstrated in Fig. 7C. Vesicles containing ~1 mol % biotinylated lipid (as model "receptors") adhere to substrates covered with streptavidin to form tight binding sites. Although the specific attraction is very strong, only adhesive plaques

by 2D electrophoresis (isoelectric focusing), (ii) fundamental studies of the mobility of membrane proteins coupled to macromolecular networks, and (iii) the deposition of self-healing (defect free) membranes to increase the electric resistivity and suppress nonspecific binding (Fig. 5). Composite monolayer-polymer films are also versatile model systems for studies of fluid-fluid wetting by viscous fingering or solitary waves (*14*) as well as dewetting processes. To mimick the physical properties of cytoskeletons beneath cell plasma membranes (such as the spectrin-actin network of erythro-

varied by means of the lateral pressure because the polymer can be switched between the stretched (brush-like) and more expanded (mushroom-like) conformations (*36*). Lipopolymers in the outer monolayer allow one to synthesize artificial glycocalices to study the influence of steric repulsion on cell-substrate interactions or the